studies with use of scattering, spectroscopic, and resonance techniques. Ultimately the combined studies should throw light on crystallization processes in general, including ones involving biological materials.

**Acknowledgment.** We thank S. T. Wilson, R. L. Patton, R. L. Bedard, and E. M. Flanigen for discussion of the results, I. M. Steele for electron microprobe analysis, and N. Weber for manuscript preparation. Financial support was provided by NSF Grants CHE-8618041 and DMR-8519460 (Materials Research Laboratory) and by Union Carbide Corp.

**Supplementary Material Available:** Table of anisotropic displacement parameters (Table IV) (1 page); listing of observed and calculated structure factors (5 pages). Ordering information is given on any current masthead page.

# Molecular Engineering of Solid-State Materials: Organometallic Building Blocks

**Paul J. Fagan,* Michael D. Ward,* and Joseph C. Calabrese**

*Contribution No. 4744 from the Central Research and Development Department, E. I. du Pont de Nemours & Company, Experimental Station, Wilmington, Delaware 19880-0328.*
*Received May 24, 1988*

**Abstract:** The syntheses of the reagents $[Cp^*Ru(CH_3CN)_3]^+(OTf^-)$ (**1**) ($Cp^* = \eta\text{-}C_5(CH_3)_5$; $OTf = CF_3SO_3$) and $[Cp^*Ru(\mu_3\text{-}Cl)]_4$ (**2**) are reported. Reaction of **1** with aromatic hydrocarbons that are used as geometric templates allows the preparation of polycationic complexes with particular shapes and geometries of positive charge. Using [2$_2$]-1,4-cyclophane, the cylindrical rod-like complexes $[(Cp^*Ru)_2(\eta^6,\eta^6\text{-}[2_2]\text{-}1,4\text{-cyclophane})]^{2+}(OTf^-)_2$, $[Cp^*Ru([2_2]\text{-}1,4\text{-cyclophane})CoCp^*]^{3+}(OTf^-)_3$, and $\{[Cp^*Ru(\eta^6,\eta^6\text{-}[2_2]\text{-}1,4\text{-cyclophane})]_2Ru\}^{4+}(OTf^-)_4$ have been synthesized. With triptycene as a template, a triangular trication isolated as the complex $[(Cp^*Ru)_3(\eta^6,\eta^6,\eta^6\text{-triptycene})]^{3+}(OTf^-)_3$ can be prepared. Reaction of **1** with tetraphenylmethane, -silane, -germane, -stannane, and -plumbane results in formation of tetrahedral tetracations isolated as the complexes $\{[Cp^*Ru(\eta\text{-}C_6H_5)]_4E\}^{4+}(OTf^-)_4$ (E = C, Si, Ge, Sn, Pb). The structure of $\{[Cp^*Ru(\eta\text{-}C_6H_5)]_4Ge\}^{4+}(OTf^-)_4$ has been determined by a single-crystal X-ray analysis (monoclinic-*b*, $P2_1/c$ (No. 14); $a$ = 22.633 (3) Å, $b$ = 12.826 (2) Å, $c$ = 24.944 (3) Å, $\beta$ = 93.49 (1)°, $V$ = 7227.6 Å$^3$, $Z$ = 4) and is compared to the structural parameters of the tetracations $\{[Cp^*Ru(\eta\text{-}C_6H_5)]_4E\}^{4+}$ (E = C, Si). Reaction of **1** with hexakis(*p*-methoxyphenoxy)benzene yields $\{[Cp^*Ru(p\text{-}CH_3O\text{-}\eta\text{-}C_6H_4\text{-}O)]_6C_6\}^{6+}(OTf^-)_6$. A single-crystal X-ray analysis of $\{[Cp^*Ru(p\text{-}CH_3O\text{-}\eta\text{-}C_6H_4\text{-}O)]_6C_6\}(OTf)_6\cdot 6CH_3NO_2$ (triclinic, $P\bar{1}$ (No. 2); $a$ = 15.784 (3) Å, $b$ = 16.539 (4) Å, $c$ = 17.817 (3) Å, $\alpha$ = 65.47 (2)°, $\beta$ = 61.82 (2)°, $\gamma$ = 63.86 (3)°, $V$ = 3552.2 Å$^3$, $Z$ = 1) shows that the hexacation contains an octahedral array of ruthenium atoms. With *p*-quaterphenyl and *p*-sexiphenyl, the reaction with **1** leads to formation of the tetracation $[(Cp^*Ru)_4(\eta^6,\eta^6,\eta^6,\eta^6\text{-}p\text{-quaterphenyl})]^{4+}(OTf^-)_4$ and hexacation $[(Cp^*Ru)_6(\eta^6,\eta^6,\eta^6,\eta^6,\eta^6,\eta^6\text{-}p\text{-sexiphenyl})]^{6+}(OTf^-)_6$, respectively. A single-crystal X-ray analysis of the complex $[(Cp^*Ru)_4(\eta^6,\eta^6,\eta^6,\eta^6\text{-}p\text{-quaterphenyl})](OTf)_4$ has been performed (triclinic, $P\bar{1}$ (No. 2); $a$ = 12.897 (3) Å, $b$ = 13.630 (2) Å, $c$ = 11.906 (2) Å, $\alpha$ = 108.31 (1)°, $\beta$ = 107.39 (2)°, $\gamma$ = 100.38 (1)°, $V$ = 1807.3 Å$^3$, $Z$ = 1). The potential use of these complexes for the rational control and preparation of solid-state molecular materials is discussed.

A fundamental problem in the synthesis of all solid-state materials is the difficulty associated with obtaining a desired three-dimensional arrangement of atoms or molecules. Finding methods to control predictably the arrangement of a crystalline material's constituents would greatly aid in the design of solids with desired physical properties. In this paper, we describe the synthesis, structure, and properties of organometallic building blocks with specific geometric shapes and arrangements of charge for the purpose of assembling molecular crystalline solids in a rational manner. In the following paper,[1] we show how these building blocks can be used in the construction of solid charge-transfer complexes.

The most commonly used approach to engineer a solid is to modify a previously determined structure type. For example, in traditional solid-state techniques, once a particular solid is synthesized empirically and its structure determined, the properties can be changed by substituting at a particular atom site with other ions of the appropriate size.[2] Other approaches also benefit from a predetermined lattice type as in the case of intercalation of molecules into layered solids[3] or into zeolite frameworks.[4] For

**Scheme I**

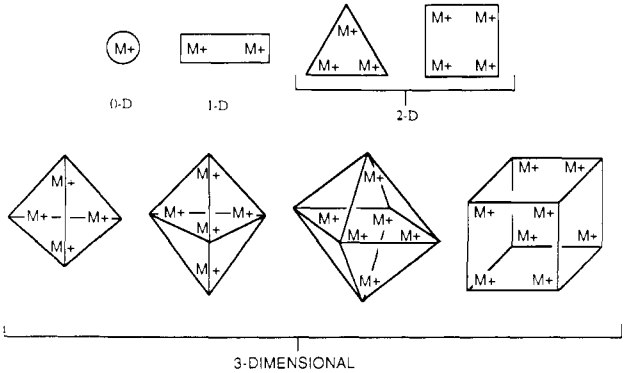


molecular crystalline solids, advantage can be taken of a pre-existing lattice network such as those utilized in the preparation

(1) Ward, M. D.; Fagan, P. J.; Calabrese, J. C.; Johnson, D. C. *J. Am. Chem. Soc.* **1988**, following paper in this journal.

(2) (a) Wells, A. F. *Structural Inorganic Chemistry*; Oxford University Press: Oxford, 1984. (b) West, A. R. *Solid State Chemistry and its Applications*; John Wiley & Sons: New York, 1984.

(3) (a) *Intercalation Layered Materials, NATO ASI Ser., Ser. B* **1986**, *148*. (b) Schöllhorn, R. *Inclusion Compd.* **1984**, *1*, 249-349. (c) *Intercalation Chemistry*; Whittingham, M. S., Jacobson, A. J., Eds.; Academic Press: New York, 1982.

(4) See for example: (a) Schowchow, F.; Puppe, L. *Angew. Chem.* **1975**, *87*, 659-667 and references therein. (b) Randas, S.; Thomas, J. M.; Betteridge, P. W.; Cheetham, A. K.; Davies, E. K. *Angew Chem.* **1984**, *96*, 629-637 and references therein.

0002-7863/89/1511-1698$01.50/0 

**Scheme II**

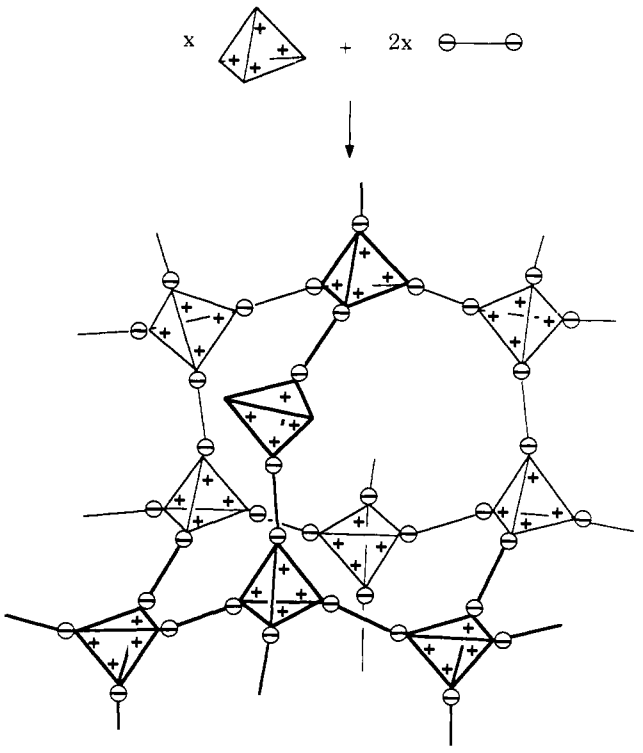

of molecular inclusion compounds (e.g., cyclodextrins).[5,6] Research in the area of the so-called "one-dimensional" molecular solids has been the most successful in cases where the stacking of flat molecules allows at least some rational control of solid-state properties,[7] as in the case of covalently linked phthalocyanines.[8] Still in many cases, crystallization of a particular solid-state phase is fortuitous in nature.

This problem has prompted us to consider an alternative approach for constructing three-dimensional molecular solid networks. A potential means of predictably controlling the lattice architecture of crystalline materials is first to synthesize molecules with particular geometric shapes and distributions of localized charges such as the cations shown in Scheme I. Condensation of these cations with appropriately chosen anions would then limit the number of possible geometries obtainable by a crystalline lattice. For example, if a diamond-like lattice structure were to be constructed, the condensation of a tetrahedral tetracation with a rod-like dianion could be expected to lead to the three-dimensional adamantane-like framework illustrated in Scheme II. This lattice is diamond-like in the sense that the tetrahedral tetracations replace the carbon atoms, and the dianionic rods represent the connecting C–C bonds of the diamond lattice. The solid can be viewed as being held together by the electrostatic attraction between the localized charges at the ends of the molecules. Thus the geometry of the charges within the molecular constituents is envisioned as controlling the eventual three-dimensional framework geometry. In the previous example, filling in the void space with neutral molecules during crystallization could form the basis for preparing new inclusion hosts.

Several considerations went into preparing the molecules with which to test the above hypothesis. The charges within the molecules should be rigidly held in place and be localized as much as possible. A flexible molecule with charge delocalized over its framework would translate to the least predictable behavior upon crystallization. The charges should not be "buried" too deeply within the molecule and be shielded from the localized charges of the counterions. Another desirable feature for a geometric class of compounds would be the ability to adjust sequentially the spacing between charges within the particular molecular framework. If a particular solid lattice were obtained, the dimensions (and physical properties) could thus be varied systematically by substituting closely related molecules with small adjustments in the distance between charges.

The ability of the $Cp'M^+$ ($Cp' = \eta$-$C_5H_5$ or $\eta$-$C_5(CH_3)_5$; M = Fe, Ru) fragment to form adducts with arenes has been known for some time.[9,10] In particular, we had noted a very strong interaction of the $Cp^*Ru^+$ fragment with aromatic hydrocarbons. Here we report a convenient synthesis of the reagent $[Cp^*Ru(CH_3CN)_3^+]OTf^-$ (**1**: OTf = $O_3SCF_3$) which reacts with aromatic hydrocarbons to form arene complexes in high yield under relatively mild conditions, and which is tolerant of a variety of functional groups. With use of aromatic hydrocarbons as geometric templates, reaction with **1** allows the preparation of cationic complexes with some of the overall shapes and charge distributions shown in Scheme I. A number of other novel multimetallated aromatic hydrocarbons can also be prepared with this reagent. In the following paper,[1] we demonstrate the use of these species in the preparation of charge-transfer compounds wherein the charge geometry of the cations reported here is used to control the solid state packing motif of flat cyanohydrocarbon anions.

## Results

**A. Synthesis of Monocationic Ruthenium–Arene Complexes.** The reagents $CpRu(CH_3CN)_3^+PF_6^-$ and $Cp^*Ru(CH_3CN)_3^+PF_6^-$ have been reported previously and are known to react with arenes.[10] The latter complex had been prepared by Mann and co-workers by reaction of $Cp^*Sn(CH_3)_3$ with $(\eta$-$C_6H_6)RuCl_2$ followed by metathesis with $PF_6^-$ to form the benzene complex $Cp^*Ru(\eta$-$C_6H_6)^+PF_6^-$.[10a-c] Photolysis of the benzene complex in acetonitrile led to formation of the acetonitrile complex. We have developed a convenient thermal route to the triflate salt **1**. Reduction of $Cp^*RuCl_2$[11] with 1 equiv of triethylborohydride in THF precipitates the crystalline orange derivative $[Cp^*Ru(\mu_3$-$Cl)]_4$ (**2**), which was isolated in 79% yield (eq 1). The molecularity of **2** was determined from a single-crystal X-ray analysis and this complex

$$Cp^*RuCl_2 + (C_2H_5)_3BH^-Li^+ \xrightarrow[-LiCl]{-1/2H_2} {}^1/_4[Cp^*Ru(\mu_3\text{-}Cl)]_4 \quad (1)$$
$$\mathbf{2}$$

(5) (a) Pagington, J. S. *Chem. Br.* **1987**, *23*, 455–458. (b) Breslow, R. *Inclusion Compd.* **1984**, *3*, 473–508. (c) Tabushi, I. *Inclusion Compd.* **1984**, *3*, 445–471. (d) Saenger, W. *Inclusion Compd.* **1984**, *2*, 231–259. (e) Saenger, W. *Angew. Chem.* **1980**, *92*, 343–361.

(6) (a) Eaton, D. F. *Tetrahedron* **1987**, *43*, 1551–1570. (b) Eaton, D. F.; Anderson, A. G.; Tam, W.; Wang, Y. *J. Am. Chem. Soc.* **1987**, *109*, 1886–1888. (c) Eaton, D. F.; Tam, W.; Wang, Y. *Polym. Mater. Sci. Eng.* **1986**, *55*, 527–531. (d) Wang, Y.; Eaton, D. F. *Chem. Phys. Lett.* **1985**, *120*, 441–444. (e) Stoddart, J. F. *Annu. Rep. Prog. Chem., Sect. B.* **1984**, *80*, 353–378.

(7) (a) Miller, J. S.; Epstein, A. J. *Angew. Chem.* **1987**, *99*, 332–339. (b) *Extended Linear Chain Compounds*; Miller, J. S., Ed.; Plenum Press: New York; Vol. 1–3.

(8) (a) Gaudiello, J. G.; Almeida, M.; Marks, T. J.; McCarthy, W. J.; Butler, J. C.; Kannewurf, C. R. *J. Phys. Chem.* **1986**, *90*, 4917–4920. (b) Inabe, T.; Gaudiello, J. G.; Moguel, M. K.; Lyding, J. W.; Burton, R. L.; McCarthy, W. J.; Kannewurf, C. R.; Marks, T. J. *J. Am. Chem. Soc.* **1986**, *108*, 7595–7608. (c) Hale, P. D.; Pietro, W. J.; Ratner, M. A.; Ellis, D. E.; Marks, T. J. *J. Am. Chem. Soc.* **1987**, *109*, 5943–5947. (d) Gaudiello, J. G.; Marcy, H. O.; McCarthy, W. J.; Moguel, M. K.; Kannewurf, C. R.; Marks, T. J. *Synth. Met.* **1986**, *15*, 115–128.

(9) (a) Lacoste, M.; Varret, F.; Toupet, L.; Astruc, D. *J. Am. Chem. Soc.* **1987**, *109*, 6504–6506. (b) Geurchais, V.; Astruc, D. *J. Organomet. Chem.* **1986**, *312*, 97–111. (c) Sutherland, R. G.; Iqbal, M.; Piorko, A. *J. Organomet. Chem.* **1986**, *302*, 307–341. (d) Robertson, I. W.; Stephenson, T. A.; Tocher, D. A. *J. Organomet. Chem.* **1982**, *228*, 171–177 and references therein. (e) Hamon, J.-R.; Astruc, D. *Organometallics* **1988**, *7*, 1036–1046.

(10) (a) Schrenk, J. L.; McNair, A. M.; McCormick, F. B.; Mann, K. R. *Inorg. Chem.* **1986**, *25*, 3501–3504. (b) McNair, A. M.; Mann, K. R. *Inorg. Chem.* **1986**, *25*, 2519–2527. (c) McNair, A. M.; Schrenck, J. L.; Mann, K. R. *Inorg. Chem.* **1984**, *23*, 2633. (d) Gill, T. P.; Mann, K. R. *Organometallics* **1982**, *1*, 485–488. (e) Kaganovich, V. S.; Kudinov, A. R.; Rybinskaya, M. I. *Izv. Akad. Nauk SSSR, Ser. Khim.* **1986**, 492–493. (f) Segal, J. A. *J. Chem. Soc., Chem. Commun.* **1985**, 1338–1339. (g) Vol'kenau, N. A.; Bolesova, I. N.; Shul'pina, L. S.; Kitaigorodskii, A. N.; Kravtsov, D. N. *J. Organomet. Chem.* **1985**, *288*, 341–348. (h) Vol'kenau, N. A.; Bolesova, I. N.; Shul'pina, L. S.; Kitaigorodskii, A. N. *J. Organomet. Chem.* **1984**, *267*, 313–321. (i) Moriarty, R. M.; Ku, Y.-Y.; Gill, U. S. *Organometallics* **1988**, *7*, 660–665.

(11) (a) Tilley, T. D.; Grubbs, R. H.; Bercaw, J. E. *Organometallics* **1984**, *3*, 274–278. (b) Oshima, N.; Suzuki, H.; Moro-oka, Y. *Chem. Lett.* **1984**, 1161–1164.

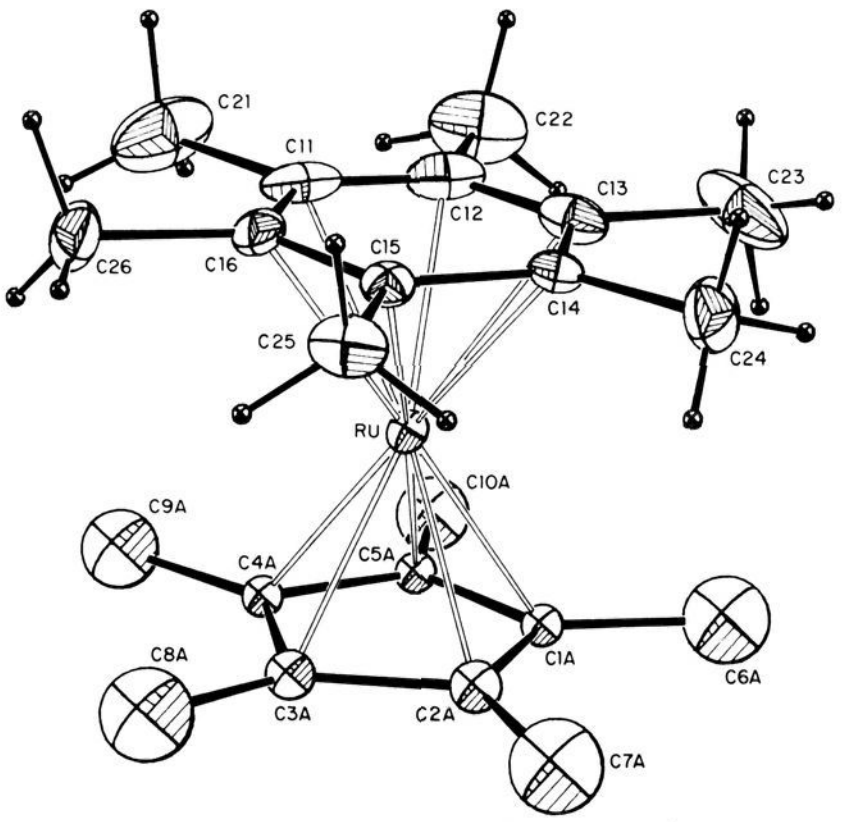


**Figure 1.** ORTEP drawing and numbering scheme for the cation $Cp^*Ru[\eta\text{-}C_6(CH_3)_6]^+$.

serves as a useful starting material for a host of Ru(II) complexes. These results will be described in more detail elsewhere.[12] Refluxing **2** in acetonitrile followed by addition of AgOTf yields a solution of **1**, which upon workup gave **1** as an orange-yellow crystalline solid in 95% yield (eq 2). Complex **1** is soluble in THF, $CH_2Cl_2$, and other polar solvents but is insoluble in diethyl ether. Due to its air-sensitivity, all reactions with this complex were carried out under nitrogen.

$$\tfrac{1}{4}[Cp^*Ru(\mu_3\text{-}Cl)]_4 \xrightarrow[\text{(2) AgOTf}]{\text{(1) }\Delta,\ CH_3CN} \underset{\mathbf{1}}{Cp^*Ru(CH_3CN)_3{}^+OTf^-} \quad (2)$$

Reaction of **1** with benzene, toluene, mesitylene, hexamethylbenzene, styrene, or benzaldehyde at room temperature in THF or $CH_2Cl_2$ leads to formation of the corresponding arene complexes **3a–f** that can be isolated in high yield as colorless crystalline solids (eq 3). The arene salts once formed are thermally stable and air-stable (as is typical of all the arene complexes prepared in this study). In general, we have found **1** to be highly specific for reaction with arene rings in the presence of a variety of functional groups, forming the arene complexes in high yield in the majority of cases.

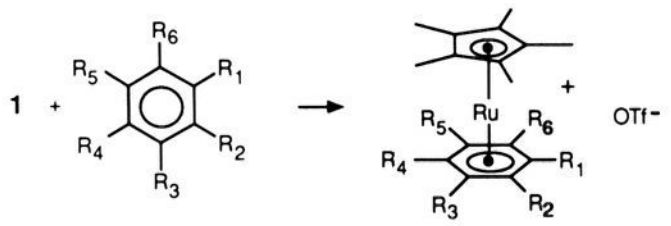


(3)

**3a**, $R_1$-$R_6$ = H
**3b**, $R_1$ = $CH_3$, $R_2$-$R_6$ = H
**3c**, $R_1$, $R_3$, $R_5$ = $CH_3$; $R_2$, $R_4$, $R_6$ = H
**3d**, $R_1$-$R_6$ = $CH_3$
**3e**, $R_1$ = HC=O; $R_2$-$R_6$ = H
**3f**, $R_1$ = HC=$CH_2$; $R_2$-$R_6$ = H

Tables I and II list the NMR spectral parameters for **3a–f**. In all cases, a characteristic upfield shift is observed for the arene protons in the $^1H$ NMR spectra upon coordination to ruthenium as has been reported previously.[10] Similarly, the resonances of the arene carbons coordinated to ruthenium are shifted upfield in the $^{13}C$ NMR spectra.

The structure of the cation $[Cp^*Ru(\eta\text{-}C_6Me_6)]^+$ has been determined from a single-crystal X-ray structure of the salt $[Cp^*Ru(\eta\text{-}C_6Me_6)][TCNQ]$ reported in the accompanying paper

(12) Fagan, P. J., manuscript in preparation.

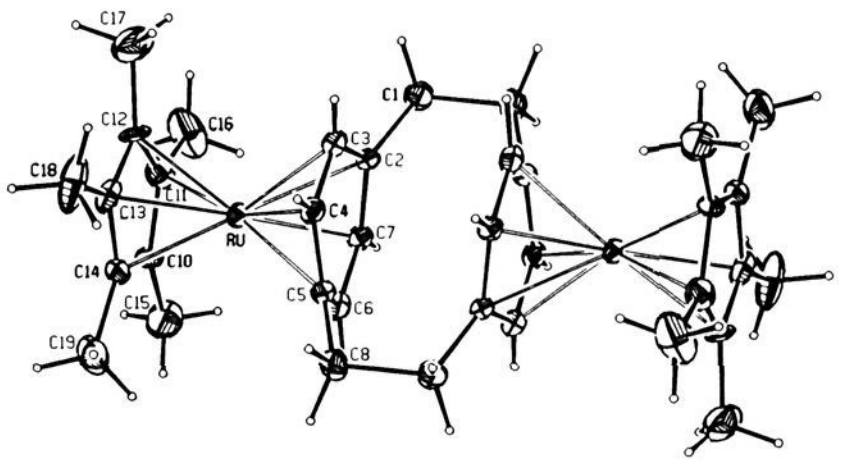


**Figure 2.** ORTEP drawing and numbering scheme for the dication $[(Cp^*Ru)_2(\eta^6,\eta^6\text{-}[2_2]\text{-}1,4\text{-cyclophane})]^{2+}$.

(TCNQ = tetracyanoquinodimethane).[1] Here we report only the structural features of the ruthenium cation. The bond lengths and bond angles for the $[Cp^*Ru(\eta\text{-}C_6Me_6)]^+$ cation (Figure 1) are given in Tables III and IV, respectively. The structure consists of a Cp* ligand and a hexamethylbenzene ligand bound to ruthenium in a $\eta^5$ and $\eta^6$ fashion, respectively. The average C–C (ring) and the C–Me distances of the $\eta\text{-}C_5Me_5$ ligand are 1.50 (1) and 1.54 (1) Å, respectively. There is a disorder that prevents a more precise determination of these bond distances. The average C–C (ring) and C–Me distances of the $\eta\text{-}C_6Me_6$ ligand are 1.374 (9) and 1.52 (2) Å, in reasonable agreement with the values reported for hexamethylbenzene (1.39 (2) and 1.53 (2) Å, respectively).[13] However, the ring bond distances are shorter than those found for $[(\eta\text{-}C_6Me_6)_2Ru]^{2+}$ (1.426 (6) Å).[14] The planes of the two ring ligands are essentially parallel with a 3.55-Å interplanar separation. The Ru–centroid distance for the $\eta\text{-}C_6Me_6$ ligand is 1.753 (10) Å, and the Ru–Cp*(centroid) distance is 1.80 (2) Å. The angle formed with the ring centroids and the ruthenium atom is 178.8 (9)°. A related iron hexamethylbenzene complex $[(\eta\text{-}C_5H_5)Fe(\eta\text{-}C_6Me_6)][TCNQ]_2$ has been structurally characterized previously.[15]

**B. Synthesis of a Linear Dication and Other Complexes with Charges in a Linear Array.** The reaction of 2 equiv of **1** with $[2_2]$-1,4-cyclophane in THF at room temperature leads to formation of the colorless, air-stable, crystalline complex $[(Cp^*Ru)_2(\eta^6,\eta^6\text{-}[2_2]\text{-}1,4\text{-cyclophane})]^{2+}(OTf^-)_2$, which can be isolated in 91% yield (eq 4) (Tables I and II). The complex is soluble in $CH_2Cl_2$, $CH_3CN$, and $CH_3NO_2$ but is insoluble in THF

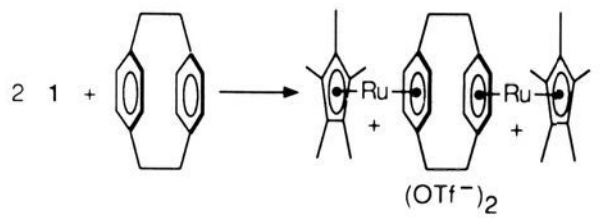


(4)

and diethyl ether. Many other cyclophane complexes have previously been prepared by Boekelheide and co-workers,[16,19c] and

(13) Brockway, L. O.; Robertson, J. M. *J. Chem. Soc.* **1939**, 1324–1332.
(14) Ward, M. D.; Johnson, D. C. *Inorg. Chem.* **1987**, *26*, 4213–4227.
(15) Lequan, R.-M.; Lequan, M.; Jaouen, G.; Ouahab, L.; Batail, P.; Padiou, J.; Sutherland, R. G. *J. Chem. Soc., Chem. Commun.* **1985**, 116–118.
(16) (a) Plitzko, K. D.; Boekelheide, V. *Angew. Chem.* **1987**, *99*, 715–717. (b) Boekelheide, V. *Pure Appl. Chem.* **1986**, *58*, 1–6. (c) Voegeli, R. H.; Kang, H. C.; Finke, R. G.; Boekelheide, V. *J. Am. Chem. Soc.* **1986**, *108*, 7010–7016. (d) Swann, R. T.; Hanson, A. W.; Boekelheide, V. *J. Am. Chem. Soc.* **1986**, *108*, 3324–3334. (e) Swann, R. T.; Boekelheide, V. *Tetrahedron Lett.* **1984**, *25*, 899–900. (f) Swann, R. T.; Hanson, A. W.; Boekelheide, V. *J. Am. Chem. Soc.* **1984**, *106*, 818–819. (g) Garbe, J. E.; Boekelheide, V. *J. Am. Chem. Soc.* **1983**, *105*, 7384–7388. (h) Rohrbach, W. D.; Boekelheide, V. *J. Org. Chem.* **1983**, *48*, 3673–3678. (i) Finke, R. G.; Voegeli, R. H.; Laganis, E. D.; Boekelheide, V. *Organometallics* **1983**, *2*, 347–350. (j) Laganis, E. D.; Voegeli, R. H.; Swann, R. T.; Finke, R. G.; Hopf, H.; Boekelheide, V. *Organometallics* **1982**, *1*, 1415–1420. (k) Schrich, P. F. T.; Boekelheide, V. *J. Am. Chem. Soc.* **1981**, *103*, 6873–6878. (l) Laganis, E. D.; Finke, R. G.; Boekelheide, V. *Tetrahedron Lett.* **1980**, *21*, 4405–4408.
(17) (a) Elzinga, J.; Rosenblum, M. *Organometallics* **1983**, *2*, 1214–1219. (b) Hanson, A. W. *Cryst. Struct. Commun.* **1982**, *11*, 901–906. (c) Elzinga, J.; Rosenblum, M. *Tetrahedron Lett.* **1982**, *23*, 1535–1536. (d) Koray, A. R. *J. Organomet. Chem.* **1981**, *212*, 233–236. (e) Laganis, E. D.; Finke, R. G.; Boekelheide, V. *Proc. Natl. Acad. Sci. U.S.A.* **1981**, *78*, 2657–2658.

**Table I.** $^1$H NMR Data for Arene Complexes[a]

| complex | Cp* | M-C(arene)-H | other |
|---|---|---|---|
| $[Cp^*Ru(\eta\text{-}C_6H_6)]^+(OTf^-)$ | 2.04 (s, 15 H) | 5.85 (s, 6 H) | |
| $\{Cp^*Ru[(\eta\text{-}C_6H_5)CH_3]\}^+(OTf^-)$ | 2.00 (s, 15 H) | 5.76 (m, 5 H) | 2.23 (s, 3 H, $CH_3$) |
| $[Cp^*Ru(\eta\text{-}C_6(CH_3)_3H_3)]^+(OTf^-)$ | 1.90 (s, 15 H) | 5.56 (s, 3 H) | 2.18 (s, 9 H, $CH_3$) |
| $\{Cp^*Ru[\eta\text{-}C_6(CH_3)_6]\}^+(OTf^-)$[b] | 1.64 (s, 15 H) | | 2.08 (s, 18 H, $CH_3$) |
| $\{Cp^*Ru[(\eta\text{-}C_6H_5)CH{=}O]\}^+(OTf^-)$ | 1.99 (s, 15 H) | 6.16 (m, 3 H) | 9.90 (s, 1 H, HC=O) |
| | | 6.36 (m, 2 H) | |
| $\{Cp^*Ru[(\eta\text{-}C_6H_5)CH_a{=}CH_bH_c]\}^+(OTf^-)$ | 1.95 (s, 15 H) | 5.91 (m, 3 H) | 5.71 (d, 1 H, 10.8 Hz, $H_b$) |
| | | 5.98 (m, 2 H) | 5.94 (d, 1 H, 17.5 Hz, $H_c$, overlapping phenyl) |
| | | | 6.41 (dd, 1 H, 10.8 and 17.5 Hz, $H_a$) |
| $[(Cp^*Ru)_2(\eta^6,\eta^6\text{-}[2_2]\text{-}1,4\text{-cyclophane})]^{2+}(OTf^-)_2$[b] | 1.83 (s, 30 H) | 5.47 (s, 8 H) | 3.03 (s, 8 H, $CH_2$) |
| $[Cp^*Co(\eta^6\text{-}[2_2]\text{-}1,4\text{-cyclophane})]^{2+}(OTf^-)_2$ | 2.00 (s, 15 H) | 6.86 (s, 4 H) | 3.37 (m, 8 H, $CH_2$) |
| | | | 6.52 (s, 4 H, arene) |
| $[Cp^*Ru(\eta^6,\eta^6\text{-}[2_2]\text{-}1,4\text{-cyclophane})CoCp^*]^{3+}(OTf^-)_3$ | 1.86 (s, 15 H) | 5.43 (s, 4 H) | 3.28 (AA′BB′, 4 H, $CH_2$) |
| | 2.04 (s, 15 H) | 6.90 (s, 4 H) | 3.55 (AA′BB′, 4 H, $CH_2$) |
| $[(\eta^6\text{-}[2_2]\text{-}1,4\text{-cyclophane})_2Ru]^{2+}(OTf^-)_2$ | | 5.91 (s, 8 H) | 3.04 (AA′BB′, $CH_2$) |
| | | 6.93 (s, 8 H) | 3.34 (AA′BB′, $CH_2$) |
| $\{[Cp^*Ru(\eta^6,\eta^6\text{-}[2_2]\text{-}1,4\text{-cyclophane})]_2Ru\}^{4+}(OTf^-)_4$ | 1.86 (s, 30 H) | 5.55 (s, 8 H) | |
| | | 6.35 (s, 8 H) | |
| $[Cp^*Ru(\eta^6\text{-triptycene})]^+(OTf^-)$ | 1.63 (s, 15 H) | 5.59 (AA′BB′, 2 H) | 5.55 (s, 2 H, bridgehead H) |
| | | 6.21 (AA′BB′, 2 H) | 7.00 (AA′BB′, 2 H, arene) |
| | | | 7.24 (AA′BB′, 2 H, arene) |
| | | | 7.42 (AA′BB′, 2 H, arene) |
| | | | 7.61 (AA′BB′, 2 H, arene) |
| $[syn\text{-}(Cp^*Ru)_2(\eta^6,\eta^6\text{-triptycene})]^{2+}(OTf^-)_2$ | 1.60 (s, 30 H) | 5.58 (AA′BB′, 4 H) | 5.52 (s, 2 H, bridgehead H) |
| | | 6.16 (AA′BB′, 4 H) | 7.55 (AA′BB′, 2 H, arene) |
| | | | 7.81 (AA′BB′, 2 H, arene) |
| $[anti\text{-}(Cp^*Ru)_2(\eta^6,\eta^6\text{-triptycene})]^{2+}(OTf^-)_2$ | 1.61 (s, 15 H) | 5.58 (AA′BB′, 2 H) | 5.56 (s, 2 H, bridgehead H) |
| | 1.72 (s, 15 H) | 5.88 (AA′BB′, 2 H) | 7.21 (AA′BB′, 2 H, arene) |
| | | 6.11 (AA′BB′, 2 H) | 7.57 (AA′BB′, 2 H, arene)[d] |
| | | 6.52 (AA′BB′, 2 H) | |
| $[(Cp^*Ru)_3(\eta^6,\eta^6,\eta^6\text{-triptycene})]^{3+}(OTf^-)_3$ | 1.74 (s, 45 H) | 5.88 (AA′BB′, 6 H) | 5.68 (s, 2 H, bridgehead H) |
| | | 6.47 (AA′BB′, 6 H) | |
| $\{[Cp^*Ru(\eta\text{-}C_6H_5)]_4C\}^{4+}(OTf^-)_4$ | 1.98 (s, 60 H) | 5.41 (m, 4 H) | |
| | | 6.21 (m, 8 H) | |
| | | 6.52 (m, 4 H) | |
| | | 6.88 (m, 4 H) | |
| $\{[Cp^*Ru(\eta\text{-}C_6H_5)]_4Si\}^{4+}(OTf^-)_4$ | 1.98 (s, 60 H) | 5.90 (d, 8 H, 5.8 Hz, ortho) | |
| | | 6.25 (t, 4 H, 5.8 Hz, para) | |
| | | 6.32 (t, 8 H, 5.8 Hz, meta) | |
| $\{[Cp^*Ru(\eta\text{-}C_6H_5)]_4Ge\}^{4+}(OTf^-)_4$ | 1.95 (s, 60 H) | 6.02 (d, 8 H, 5.8 Hz, ortho) | |
| | | 6.22 (t, 4 H, 5.8 Hz, para) | |
| | | 6.29 (t, 8 H, 5.8 Hz, meta) | |
| $\{[Cp^*Ru(\eta\text{-}C_6H_5)]_4Sn\}^{4+}(OTf^-)_4$ | 1.94 (s, 60 H) | 6.08 (d, 8 H, 5.5 Hz, ortho) | |
| | | 6.20 (m, 12 H, meta and para) | |
| $\{[Cp^*Ru(\eta\text{-}C_6H_5)]_4Pb\}^{4+}(OTf^-)_4$ | 1.94 (s, 60 H) | 6.17 (m, 20 H) | |
| $\{[Cp^*Ru(\eta\text{-}C_6H_5)]_3(C_6H_5)Sb\}^{4+}(OTf^-)_4$ | 1.91 (s, 45 H) | 6.40 (m, 9 H, meta and para) | 7.99 (m, 3 H, meta and para) |
| | | 6.59 (d, 6 H, ortho) | 8.17 (m, 2 H, ortho) |
| $\{[Cp^*Ru(\eta\text{-}C_6H_5)]_4B\}^{3+}(OTf^-)_3$ | 1.92 (s, 60 H) | 5.08 (br m, 4 H) | |
| | | 5.79 (br m, 8 H, t overlap br m) | |
| | | 6.04 (br m, 4 H) | |
| | | 6.31 (br m, 4 H) | |
| $\{[Cp^*Ru(p\text{-}CH_3O\text{-}\eta\text{-}C_6H_4O)]_6C_6\}^{6+}(OTf^-)_6$ | 2.03 (s, 90 Hz) | 5.94 (s, 24 H) | 3.88 (s, 18 H, $OCH_3$) |
| $[(Cp^*Ru)_4(\eta^6,\eta^6,\eta^6,\eta^6\text{-}p\text{-quaterphenyl})]^{4+}(OTf^-)_4$ | 1.78 (s, 30 H) | 6.23 (m, 6 H) | |
| | 1.94 (s, 30 H) | 6.57 (d, 4 H) | |
| | | 6.86 (AB q, 8 H) | |
| $[(Cp^*Ru)_6(\eta^6,\eta^6,\eta^6,\eta^6,\eta^6,\eta^6\text{-}p\text{-sexiphenyl})]^{6+}(OTf^-)_6$ | 1.79 (s, 30 H) | 6.24 (m, 6 H) | |
| | 1.84 (s, 30 H) | 6.55 (d, 4 H, 5.8 Hz) | |
| | 1.94 (s, 30 H) | 6.86 (AB q, 8 H) | |
| | | 6.95 (s, 8 H) | |

[a] Reported in ppm from tetramethylsilane (300 MHz at 25 °C) in $CD_3NO_2$ unless indicated otherwise (s = singlet, d = doublet, t = triplet, q = quartet, m = multiplet, br = broad). [b] Spectrum obtained in $CD_2Cl_2$. [c] Overlap with 5.58 resonance of syn isomer. [d] Overlap with 7.55 resonance of syn isomer.

the related complexes $[(\eta\text{-}C_5H_5)M(\eta^6,\eta^6\text{-}[2_2]\text{-}1,4\text{-cyclophane})M(\eta\text{-}C_5H_5)](PF_6)_2$ (M = Fe, Ru) are also known.[16h,17]

As detailed in the accompanying paper,[1] the structure of the dication $[(Cp^*Ru)_2(\eta^6,\eta^6\text{-}[2_2]\text{-}1,4\text{-cyclophane})]^{2+}$ has been determined from a single-crystal X-ray analysis of the salt $[(Cp^*Ru)_2(\eta^6,\eta^6\text{-}[2_2]\text{-}1,4\text{-cyclophane})]^{2+}(TCNQ^-)_2$ and is described here. An ORTEP drawing of the dication is shown in Figure 2, and a van der Waals space filling model is shown in Figure 3. The van der Waals space filling model reveals the rod-like cylindrical shape of the dication.

The bond distances and angles of the dication are given in Tables V and VI, respectively. The cation is composed of two $\eta\text{-}C_5Me_5$ rings bound to two ruthenium centers that in turn are bound to and separated by the $[2_2]$-1,4-cyclophane ligand. The average Cp* C–C(ring) and C–Me bond distances are 1.412

(18) Hope, H.; Bernstein, J.; Trueblood, K. N. *Acta. Crystallogr.* **1972**, *B28*, 1733–1743.

(19) (a) Koelle, U.; Fuss, B.; Rajasekharan, M. V.; Ramakrishna, B. L.; Ammeter, J. H.; Boehm, M. C. *J. Am. Chem. Soc.* **1984**, *106*, 4152–4160. (b) Fairhurst, G.; White, C. *J. Chem. Soc., Dalton Trans.* **1979**, 1531–1538. (c) This cobalt complex has also been recently reported elsewhere: Plitzko, K.-D.; Boekelheide, V. *Organometallics* **1988**, *7*, 1573–1582.

**Table II.** $^{13}C$ NMR Data for Ruthenium–Arene Complexes[a]

| | Cp* | Ru–C(arene) | other |
|---|---|---|---|
| $[Cp^*Ru(\eta\text{-}C_6H_6)]^+(OTf^-)$ | 10.9 (q, 129)<br>98.4 (s) | 88.5 (d, 177) | |
| $\{Cp^*Ru[(\eta\text{-}C_6H_5)CH_3]\}^+(OTf^-)$ | 10.6 (q, 129)<br>97.6 (s) | 87.7 (d, 179); 88.4 (d, 177)<br>89.5 (d, 176); 101.8 (s) | 18.7 (q, 128, $CH_3$) |
| $[Cp^*Ru(\eta\text{-}C_6(CH_3)_3H_3)]^+(OTf^-)$ | 10.1 (q, 128)<br>96.1 (s) | 90.0 (d, 172); 101.7 (s) | 18.5 (q, 129, $CH_3$) |
| $\{Cp^*Ru[\eta\text{-}C_6(CH_3)_6]\}^+(OTf^-)$[b] | 9.1 (q, 128)<br>98.6 (s) | 92.1 (s) | 15.5 (q, 129, $CH_3$) |
| $\{Cp^*Ru[(\eta\text{-}C_6H_5)CH{=}O]\}^+(OTf^-)$ | 10.8 (q, 129)<br>100.1 (s) | 87.8 (d, 172); 90.0 (d, 177)<br>90.7 (d, 179); 91.7 (s) | 193.4 (d, 188, CH=O) |
| $\{Cp^*Ru[(\eta\text{-}C_6H_5)CH{=}CH_2]\}^+(OTf^-)$ | 10.5 (q, 129)<br>98.0 (s) | 86.1 (d, 176); 88.6 (d, 183)<br>88.7 (d, 183); 99.2 (s) | 121.4 (dd, 155, 162, $CH_2$)<br>132.6 (d, 160, $CH{=}CH_2$) |
| $[(Cp^*Ru)_2(\eta^6,\eta^6\text{-}[2_2]\text{-}1,4\text{-cyclophane})]^{2+}(OTf^-)_2$[b] | 11.0 (q, 129)<br>95.7 (s) | 86.1 (d, 178)<br>117.5 (s) | 30.6 (t, 138, $CH_2$) |
| $[Cp^*Co(\eta^6\text{-}[2_2]\text{-}1,4\text{-cyclophane})]^{2+}(OTf^-)_2$ | 11.4 (q, 131)<br>109.3 (s) | 99.8 (d, 183); 139.6 (s) | 33.2 (t, 137, $CH_2$); 35.3 (t, 135, $CH_2$)<br>135.7 (d, 160, arene); 141.0 (s, arene) |
| $[Cp^*Ru(\eta^6,\eta^6\text{-}[2_2]\text{-}1,4\text{-cyclophane})CoCp^*]^{3+}(OTf^-)_3$ | 10.9 (q, 129)<br>11.0 (q, 132)<br>98.4 (s); 111.0 (s) | 87.0 (d, 178); 101.2 (d, 184)<br>119.1 (s); 140.3 (s) | 31.8 (t, 136, $CH_2$); 32.4 (t, 136, $CH_2$) |
| $[(\eta^6\text{-}[2_2]\text{-}1,4\text{-cyclophane})_2Ru]^{2+}(OTf^-)_2$ | | 89.2 (d, 184)<br>135.4 (s) | 35.1 (t, 136, $CH_2$); 37.0 (t, 134, $CH_2$)<br>137.4 (d, 159, arene); 142.8 (s, arene) |
| $\{[Cp^*Ru(\eta^6,\eta^6\text{-}[2_2]\text{-}1,4\text{-cyclophane})]_2Ru\}^{4+}(OTf^-)_4$ | 10.9 (q, 129)<br>98.2 (s) | 87.0 (d, 178); 88.8 (d, 185)<br>117.9 (s); 135.1 (s) | 31.5 (t, 139, $CH_2$); 32.5 (t, 141, $CH_2$) |
| $[Cp^*Ru(\eta^6\text{-triptycene})]^+(OTf^-)$ | 10.7 (q, 129)<br>97.8 (s) | 85.5 (d, 176); 85.6 (d, 176)<br>112.8 (s) | 51.8 (d, 145, bridgehead C)<br>125.6 (d, 161, $C_6H_4$)<br>126.3 (d, 161, $C_6H_4$)<br>127.5 (d, 161, $C_6H_4$); 144.3 (s, $C_6H_4$)<br>127.7 (d, 162, $C_6H_4$); 146.2 (s, $C_6H_4$) |
| $[syn\text{-}(Cp^*Ru)_2(\eta^6,\eta^6\text{-triptycene})]^{2+}(OTf^-)_2$ | 10.8 (q, 129)<br>98.5 (s) | 85.7 (d, 179); 86.0 (d, 178)<br>111.9 (s) | 48.7 (d, 149, bridgehead C)<br>127.4 (d, 161, $C_6H_4$)<br>129.2 (d, 164, $C_6H_4$); 140.8 (s, $C_6H_4$) |
| $[anti\text{-}(Cp^*Ru)_2(\eta^6,\eta^6\text{-triptycene})]^{2+}(OTf^-)_2$[c] | 10.7 (q, 129)<br>11.4 (q, 129)<br>98.2 (s); 98.7 (s) | 85.6 (d, 179); 85.8 (d, 177)<br>86.1 (d, 178);[d] 86.7 (d, 178)<br>109.6 (s); 112.0 (s)[d] | 48.6 (d, 149, bridgehead C)[d]<br>126.9 (d, 161, $C_6H_4$)<br>128.6 (d, 162, $C_6H_4$); 144.4 (s, $C_6H_4$) |
| $[(Cp^*Ru)_3(\eta^6,\eta^6,\eta^6\text{-triptycene})]^{3+}(OTf^-)_3$ | 11.6 (q, 129)<br>99.0 (s) | 85.6 (d, 177); 86.7 (d, 179)<br>110.0 (s) | 45.6 (d, 153, bridgehead C) |
| $\{[Cp^*Ru(\eta\text{-}C_6H_5)]_4C\}^{4+}(OTf^-)_4$ | 11.4 (q, 129)<br>100.4 (s) | 86.3 (d, 174); 87.2 (d, 179)<br>89.7 (d, 186); 90.2 (d, 180)<br>108.3 | 57.4 (s, $CPh_4$) |
| $\{[Cp^*Ru(\eta\text{-}C_6H_5)]_4Si\}^{4+}(OTf^-)_4$ | 11.7 (q, 129)<br>100.3 (s) | 88.1 (s); 89.6 (d, 180)<br>90.7 (d, 182); 91.0 (d, 173) | |
| $\{[Cp^*Ru(\eta\text{-}C_6H_5)]_4Ge\}^{4+}(OTf^-)_4$ | 11.8 (q, 129)<br>100.6 (s) | 89.9 (d, 177); 90.7 (d, 181)<br>91.2 (d, 175); 93.0 (s) | |
| $\{[Cp^*Ru(\eta\text{-}C_6H_5)]_4Sn\}^{4+}(OTf^-)_4$ | 11.8 (q, 129)<br>100.4 (s) | 90.2 (d sat, 181, $J_{Sn-C}$ = 38)<br>90.6 (d, 179); 94.8 (s)<br>93.0 (d sat, 175, $J_{Sn-C}$ = 43) | |
| $\{[Cp^*Ru(\eta\text{-}C_6H_5)]_4Pb\}^{4+}(OTf^-)_4$ | 11.8 (q, 129)<br>100.3 (s) | 90.5 (d, 180); 111.4 (s)<br>90.7 (d sat, 180, $J_{Pb-C}$ = 54)<br>93.8 (d sat, 179, $J_{Pb-C}$ = 81) | |
| $\{[Cp^*Ru(\eta\text{-}C_6H_5)]_3(C_6H_5)Sb\}^{4+}(OTf^-)_4$ | 11.5 (q, 129)<br>101.6 (s) | 87.9 (s); 90.8 (d, 182)<br>91.6 (d, 181) | 119.3 (s, Sb-C); 135.1 (d, 171, Ph)<br>136.4 (d, 175, Ph); 138.2 (d, 167, Ph) |
| $\{[Cp^*Ru(\eta\text{-}C_6H_5)]_4B\}^{3+}(OTf^-)_3$ | 11.4 (q, 129)<br>97.0 (s) | 87.5 (br d, 176); 87.9 (d, 177)<br>88.8 (br d, 172); 90.7 (d, 171)<br>117.9 (1:1:1:1 q, $J_{B-C}$ = 52) | |
| $\{[Cp^*Ru(p\text{-}CH_3O\text{-}\eta\text{-}C_6H_4O)]_6C_6\}^{6+}(OTf^-)_6$ | 11.3 (q, 129)<br>98.9 (s) | 74.7 (d, 179); 77.5 (d, 179)<br>131.6 (s); 132.6 (s) | 58.6 (q, 147, $OCH_3$)<br>140.0 (s, $C_6O_6$) |
| $[(Cp^*Ru)_4(\eta^6,\eta^6,\eta^6,\eta^6\text{-}p\text{-quaterphenyl})]^{4+}(OTf^-)_4$ | 10.5 (q, 129)<br>10.8 (q, 129)<br>99.6 (s)<br>100.5 (s) | 85.7 (d, 177); 86.2 (d, 174)<br>86.4 (d, 178); 89.4 (d, 180)<br>90.2 (d, 181); 94.2 (s)<br>96.2 (s); 97.6 (s) | |
| $[(Cp^*Ru)_6(\eta^6,\eta^6,\eta^6,\eta^6,\eta^6,\eta^6\text{-}p\text{-sexiphenyl})]^{6+}(OTf^-)_6$ | 10.5 (q, 129)<br>10.6 (q, 129)<br>10.8 (q, 129)<br>99.6 (s)<br>100.6 (s); 100.7 (s) | 85.6 (d, 182); 86.2 (sh d, 178)<br>86.4 (d, 178); 89.4 (d, 178)<br>90.2 (d, 180); 94.1 (s)<br>96.0 (s); 96.4 (s)<br>96.5 (s); 97.7 (s) | |

[a] Reported in ppm from tetramethylsilane (75.5 MHz at 25 °C) in $CD_3NO_2$ unless indicated otherwise (s = singlet, d = doublet, t = triplet, q = quartet, sh = shoulder, br = broad, sat = satellites); numbers in parentheses are C–H coupling constants (Hz) unless otherwise specified. Small two-bond $^{13}C$–C–H couplings (<8 Hz) which were observed are not reported. Data were obtained from proton decoupled and gated decoupled spectra. All spectra exhibited a quartet at 122.4 (±0.2) assigned to $O_3SCF_3$ ($J_{C-F}$ = 320 ± 2). [b] Spectra recorded in $CD_2Cl_2$. [c] Data reported for this complex were obtained from spectra of the isolated mixture of the syn and anti isomers aided by comparison to the spectrum of the pure syn isomer. [d] Overlapping with syn isomer resonance.

(range 1.391 (8)–1.426 (6) Å) and 1.489 Å (range 1.47 (1)–1.508 (8) Å), respectively. The average Ru–C(ring) bond distance is 2.168 Å with a range of 2.156 (4)–2.183 (4) Å. The distance from the ruthenium atom to the plane of the $\eta$-$C_5Me_5$ ligand is 1.805 (7) Å. The two $\eta$-$C_5Me_5$ rings within the dication adopt a staggered conformation and are separated by a distance of 9.961 Å. Accordingly the Ru–Ru distance is 6.351 (4) Å. The $\eta$-$C_5Me_5$ rings are planar and are essentially parallel (dihedral angle = 2.38 ± 2.35°) to the plane defined by the four carbon atoms of the cyclophane ligand not bonded to the ethylene bridge. The ruthenium atoms are located 1.701 (5) Å from this $C_4$ plane and 1.752 (5) Å from the cyclophane plane defined by all six ring carbon atoms (due to the 12.3° out-of-plane bending of the cyclophane ring). The distance between the two $C_6$ cyclophane planes defined by the average location of all the atoms in the $C_6$ rings is 2.847 Å, whereas that between the internal $C_4$ planes is 2.952 Å. The corresponding distances in $[2_2]$-1,4-cyclophane are 2.78 and 3.09 Å.[18] The long C–C(bridge) bond length of 1.596

**Table III.** Bond Distances for the Cation $Cp^*Ru[\eta\text{-}C_6(CH_3)_6]^+$ (Å)[a]

| bond | length | bond | length | bond | length | bond | length | bond | length | bond | length |
|---|---|---|---|---|---|---|---|---|---|---|---|
| Ru-C1A | 2.18 (2) | Ru-C5A | 2.186 (9) | C1A-C2A | 1.53 (1) | C2B-C3B | 1.53 (1) | C4B-C5B | 1.50 (1) | C12-C22 | 1.503 (9) |
| Ru-C1B | 2.220 (9) | Ru-C5B | 2.202 (9) | C1A-C5A | 1.50 (1) | C2B-C7B | 1.50 (2) | C4B-C9B | 1.51 (2) | C13-C14 | 1.421 (7) |
| Ru-C2A | 2.22 (2) | Ru-C11 | 2.211 (6) | C1A-C6A | 1.55 (2) | C3A-C4A | 1.48 (1) | C5A-C10A | 1.59 (2) | C13-C23 | 1.508 (7) |
| Ru-C2B | 2.226 (8) | Ru-C12 | 2.220 (6) | C1B-C2B | 1.51 (1) | C3A-C8A | 1.55 (2) | C5B-C10B | 1.53 (2) | C14-C15 | 1.368 (8) |
| Ru-C3A | 2.180 (9) | Ru-C13 | 2.218 (4) | C1B-C5B | 1.52 (1) | C3B-C4B | 1.47 (1) | C11-C12 | 1.392 (7) | C14-C24 | 1.513 (9) |
| Ru-C3B | 2.223 (9) | Ru-C14 | 2.227 (6) | C1B-C6B | 1.51 (2) | C3B-C8B | 1.45 (1) | C11-C16 | 1.348 (9) | C15-C16 | 1.277 (9) |
| Ru-C4A | 2.195 (9) | Ru-C15 | 2.236 (6) | C2A-C3A | 1.51 (1) | C4A-C5A | 1.46 (1) | C11-C21 | 1.54 (2) | C15-C25 | 1.53 (1) |
| Ru-C4B | 2.18 (1) | Ru-C16 | 2.250 (7) | C2A-C7A | 1.51 (3) | C4A-C9A | 1.51 (2) | C12-C13 | 1.436 (8) | C16-C26 | 1.53 (2) |

[a] Numbers in parentheses are estimated standard deviations in the least signifcant figure.

**Table IV.** Bond Angles for the Cation $Cp^*Ru[\eta\text{-}C_6(CH_3)_6]^+$ (deg)[a]

| atoms | angle | atoms | angle | atoms | angle | atoms | angle |
|---|---|---|---|---|---|---|---|
| C2A-C1A-C5A | 105.6 (8) | C2A-C3A-C4A | 108.0 (7) | C1A-C5A-C4A | 110.4 (8) | C12-C13-C14 | 116.0 (4) |
| C2A-C1A-C6A | 121 (1) | C2A-C3A-C8A | 136 (1) | C1A-C5A-C10A | 121 (1) | C12-C13-C23 | 122.1 (4) |
| C5A-C1A-C6A | 134 (1) | C4A-C3A-C8A | 115.6 (9) | C4A-C5A-C10A | 129 (2) | C14-C13-C23 | 121.8 (5) |
| C2B-C1B-C5B | 106.3 (7) | C2B-C3B-C4B | 106.9 (7) | C1B-C5B-C4B | 108.1 (7) | C13-C14-C15 | 119.8 (6) |
| C2B-C1B-C6B | 119.5 (8) | C2B-C3B-C8B | 131 (1) | C1B-C5B-C10B | 109.8 (8) | C13-C14-C24 | 120.6 (5) |
| C5B-C1B-C6B | 134.0 (8) | C4B-C3B-C8B | 122 (1) | C4B-C5B-C10B | 143 (1) | C15-C14-C24 | 119.7 (6) |
| C1A-C2A-C3A | 107.4 (8) | C3A-C4A-C5A | 108.6 (7) | C12-C11-C16 | 121.8 (5) | C14-C15-C16 | 123.5 (6) |
| C1A-C2A-C7A | 131 (1) | C3A-C4A-C9A | 124.2 (9) | C12-C11-C21 | 118.9 (6) | C14-C15-C25 | 115.4 (7) |
| C3A-C2A-C7A | 121 (2) | C5A-C4A-C9A | 128 (1) | C16-C11-C21 | 119.4 (6) | C16-C15-C25 | 121.1 (6) |
| C1B-C2B-C3B | 108.8 (7) | C3B-C4B-C3A | 110.0 (8) | C11-C12-C13 | 118.3 (5) | C11-C16-C15 | 120.7 (6) |
| C1B-C2B-C7B | 133.0 (8) | C3B-C4B-C6B | 134 (1) | C11-C12-C22 | 120.6 (6) | C11-C16-C26 | 117.9 (6) |
| C3B-C2B-C7B | 118.3 (8) | C5B-C4B-C7A | 117 (1) | C13-C12-C22 | 121.0 (5) | C15-C16-C26 | 121.4 (6) |

[a] Numbers in parentheses are estimated standard deviations in the least significant figure.

**Table V.** Bond Distances for the Dication $[(Cp^*Ru)_2(\eta^6,\eta^6\text{-}[2_2]\text{-}1,4\text{-cyclophane})]^{2+}$ (Å)[a]

| bond | length | bond | length | bond | length | bond | length | bond | length | bond | length |
|---|---|---|---|---|---|---|---|---|---|---|---|
| Ru-C2 | 2.323 (3) | Ru-C7 | 2.185 (4) | Ru-C14 | 2.163 (4) | C4-C5 | 1.385 (7) | C10-C14 | 1.406 (4) | C12-C17 | 1.47 (1) |
| Ru-C3 | 2.200 (4) | Ru-C10 | 2.156 (4) | C1-C2 | 1.516 (5) | C5-C6 | 1.430 (5) | C10-C15 | 1.480 (8) | C13-C14 | 1.391 (8) |
| Ru-C4 | 2.208 (4) | Ru-C11 | 2.162 (4) | C2-C3 | 1.412 (5) | C5-C8 | 1.525 (6) | C11-C12 | 1.425 (6) | C13-C18 | 1.495 (6) |
| Ru-C5 | 2.340 (4) | Ru-C12 | 2.174 (6) | C2-C7 | 1.383 (7) | C6-C7 | 1.422 (6) | C11-C16 | 1.492 (6) | C14-C19 | 1.508 (8) |
| Ru-C6 | 2.207 (5) | Ru-C13 | 2.183 (4) | C3-C4 | 1.410 (6) | C10-C11 | 1.410 (7) | C12-C13 | 1.426 (6) | | |

[a] Numbers in parentheses are estimated standard deviations in the least significant figure.

**Table VI.** Intramolecular Bond Angles for the Dication $[(Cp^*Ru)_2(\eta^6,\eta^6\text{-}[2_2]\text{-}1,4\text{-cyclophane})]^{2+}$ (deg)[a]

| atoms | angle | atoms | angle | atoms | angle | atoms | angle |
|---|---|---|---|---|---|---|---|
| C2-Ru-C3 | 36.2 (1) | C5-Ru-C7 | 65.4 (1) | Ru-C2-C1 | 146.4 (4) | C11-C10-C14 | 108.1 (5) |
| C2-Ru-C4 | 65.2 (1) | C5-Ru-C10 | 129.2 (2) | Ru-C2-C3 | 67.1 (2) | C11-C10-C15 | 125.1 (3) |
| C2-Ru-C5 | 74.7 (1) | C5-Ru-C11 | 166.0 (2) | Ru-C2-C7 | 66.7 (2) | C14-C10-C15 | 126.9 (5) |
| C2-Ru-C6 | 65.3 (2) | C5-Ru-C12 | 152.3 (1) | C1-C2-C3 | 120.8 (5) | Ru-C11-C10 | 70.8 (3) |
| C2-Ru-C7 | 35.6 (2) | C5-Ru-C13 | 119.8 (1) | C1-C2-C7 | 120.8 (3) | Ru-C11-C12 | 71.4 (3) |
| C2-Ru-C10 | 132.4 (1) | C5-Ru-C14 | 110.3 (2) | C3-C2-C7 | 117.9 (3) | Ru-C11-C16 | 125.6 (4) |
| C2-Ru-C11 | 109.8 (1) | C6-Ru-C7 | 37.8 (1) | Ru-C3-C2 | 76.6 (2) | C10-C11-C12 | 107.5 (3) |
| C2-Ru-C12 | 116.6 (2) | C6-Ru-C10 | 107.7 (2) | Ru-C3-C4 | 71.7 (2) | C10-C11-C16 | 126.1 (5) |
| C2-Ru-C13 | 148.0 (2) | C6-Ru-C11 | 132.1 (2) | C2-C3-C4 | 119.8 (5) | C12-C11-C16 | 126.4 (6) |
| C2-Ru-C14 | 170.4 (1) | C6-Ru-C12 | 170.3 (1) | Ru-C4-C3 | 71.1 (3) | Ru-C12-C11 | 70.3 (4) |
| C3-Ru-C4 | 37.3 (1) | C6-Ru-C13 | 143.7 (2) | Ru-C4-C5 | 77.5 (2) | Ru-C12-C13 | 71.3 (3) |
| C3-Ru-C5 | 64.7 (2) | C6-Ru-C14 | 113.2 (2) | C5-C4-H4 | 121 (4) | Ru-C12-C17 | 125.8 (4) |
| C3-Ru-C6 | 79.0 (2) | C7-Ru-C10 | 109.7 (1) | Ru-C5-C4 | 67.1 (2) | C11-C12-C13 | 107.6 (5) |
| C3-Ru-C7 | 66.2 (2) | C7-Ru-C11 | 109.8 (1) | Ru-C5-C6 | 66.7 (3) | C11-C12-C17 | 126.6 (4) |
| C3-Ru-C10 | 163.7 (1) | C7-Ru-C12 | 138.6 (1) | Ru-C5-C8 | 148.6 (3) | C13-C12-C17 | 125.8 (5) |
| C3-Ru-C11 | 126.8 (2) | C7-Ru-C13 | 172.9 (1) | C4-C5-C6 | 118.2 (4) | Ru-C13-C12 | 70.5 (3) |
| C3-Ru-C12 | 108.1 (2) | C7-Ru-C14 | 138.0 (2) | C4-C5-C8 | 121.8 (3) | Ru-C13-C14 | 70.6 (2) |
| C3-Ru-C13 | 119.9 (2) | C10-Ru-C11 | 38.1 (2) | C6-C5-C8 | 119.2 (4) | Ru-C13-C18 | 126.0 (4) |
| C3-Ru-C14 | 153.3 (1) | C10-Ru-C12 | 63.7 (2) | Ru-C6-C5 | 76.7 (3) | C12-C13-C14 | 107.6 (3) |
| C4-Ru-C5 | 35.3 (2) | C10-Ru-C13 | 63.4 (2) | Ru-C6-C7 | 70.3 (3) | C12-C13-C18 | 126.6 (5) |
| C4-Ru-C6 | 66.4 (2) | C10-Ru-C14 | 38.0 (1) | C5-C6-C7 | 118.3 (3) | C14-C13-C18 | 125.7 (4) |
| C4-Ru-C7 | 78.4 (1) | C11-Ru-C12 | 38.4 (2) | Ru-C7-C2 | 77.7 (2) | Ru-C14-C10 | 70.7 (3) |
| C4-Ru-C10 | 159.0 (1) | C11-Ru-C13 | 63.9 (1) | Ru-C7-C6 | 72.0 (2) | Ru-C14-C13 | 72.1 (2) |
| C4-Ru-C11 | 158.8 (3) | C11-Ru-C14 | 63.6 (2) | C2-C7-C6 | 121.6 (3) | Ru-C14-C19 | 126.6 (5) |
| C4-Ru-C12 | 123.3 (2) | C12-Ru-C13 | 38.3 (2) | Ru-C10-C11 | 71.2 (2) | C10-C14-C13 | 109.3 (4) |
| C4-Ru-C13 | 108.6 (1) | C12-Ru-C14 | 63.2 (2) | Ru-C10-C14 | 71.3 (2) | C10-C14-C19 | 124.6 (5) |
| C4-Ru-C14 | 123.8 (1) | C13-Ru-C14 | 37.3 (2) | Ru-C10-C15 | 129.4 (4) | C13-C14-C19 | 126.0 (3) |
| C5-Ru-C6 | 36.5 (1) | | | | | | |

[a] Numbers in parentheses are estimated standard deviations in the least significant figure.

(7) Å is comparable with other cyclophanes (1.569 Å in $[2_2]$-1,4-cyclophane[18]) and is ascribed to steric interactions between the two $C_6$ rings.

Other rod-like cations with varying degrees of charge along the rod can be synthesized with $[2_2]$-1,4-cyclophane as a linear template. We have prepared a mixed-metal cobalt–ruthenium–cyclophane complex which contains a (2+)-(1+) arrangement of charge down the long axis of the molecule. Reaction of **1** with the complex $[Cp^*Co(\eta^6\text{-}[2_2]\text{-}1,4\text{-cyclophane})]^{2+}(OTf^-)_2$ (synthesized by a variation of the method used by Koelle et al. for

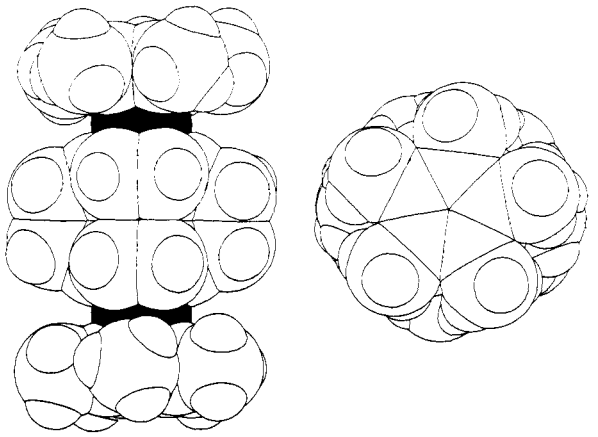

**Figure 3.** Two views of a van der Waals space-filling model of the dication $[(Cp^*Ru)_2(\eta^6,\eta^6\text{-}[2_2]\text{-}1,4\text{-cyclophane})]^{2+}$ constructed from the X-ray structural coordinates.

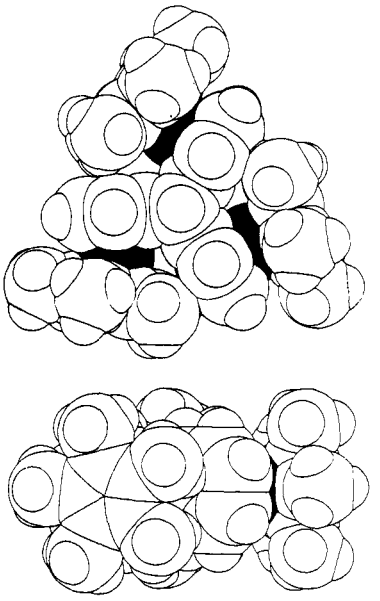

**Figure 4.** Two views of a van der Waals space-filling model of the triangular trication $[(Cp^*Ru)_3(\eta^6,\eta^6,\eta^6\text{-triptycene})]^{3+}$. The Cp*Ru fragments of the model were constructed with structural parameters obtained from the X-ray analysis of $\{[Cp^*Ru(\eta\text{-}C_6H_5)]_4C\}^{4+}$.

the preparation of Cp*Co arene complexes)[19] in $CH_2Cl_2$ precipitates the trication $[Cp^*Ru(\eta^6,\eta^6\text{-}[2_2]\text{-}1,4\text{-cyclophane})\text{-}CoCp^*]^{3+}(OTf^-)_3$ (eq 5). The $^1H$ NMR and $^{13}C$ NMR spectral

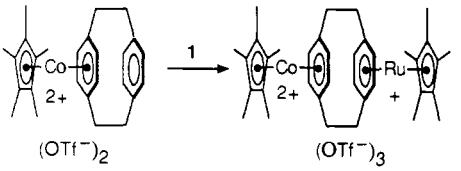

(5)

parameters for this molecule are listed in Tables I and II. Reaction of 2 equiv of **1** with the complex $(\eta^6\text{-}[2_2]\text{-}1,4\text{-cyclophane})_2Ru^{2+}(OTf^-)_2$ (prepared by a minor modification of the procedure reported by Boekelheide and co-workers[10d]) results in the formation of the pale yellow tetracation $\{[Cp^*Ru(\eta^6,\eta^6\text{-}[2_2]\text{-}1,4\text{-cyclophane})]_2Ru\}^{4+}$ isolated as its triflate salt (eq 6) (Tables I and II). This tetracation contains a (1+)-(2+)-(1+) arrangement of charge down the long molecular axis.

**C. Synthesis of a Triangular Trication.** Reaction of **1** with triptycene in $CH_2Cl_2$ progresses sequentially with formation of first the monosubstituted complex $[Cp^*Ru(\eta^6\text{-triptycene})]^+(OTf^-)$, which was isolated (eq 7) (see Tables I and II). The reaction was carried out at 0 °C with an excess of triptycene to avoid formation of the dications *syn*-**4** and *anti*-**4** (vide infra), which were difficult

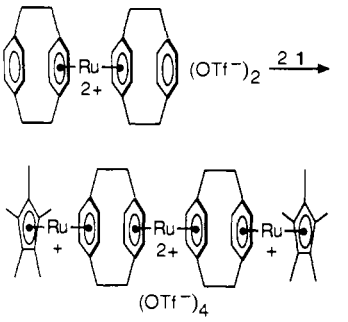

(6)

to separate from the monocation. Only two other monosubstituted triptycene complexes are known.[20]

Addition of 2 equiv of **1** to an equiv of triptycene results in the formation of two isomeric dicationic complexes *syn*-$[(Cp^*Ru)_2(\eta^6,\eta^6\text{-triptycene})]^{2+}(OTf^-)_2$ and *anti*-$[(Cp^*Ru)_2(\eta^6,\eta^6\text{-triptycene})]^{2+}(OTf^-)_2$, which were isolated as the mixture. These dications are assigned the structures *syn*-**4** and *anti*-**4**, respectively (see eq 7), and these assignments are supported by spectroscopic

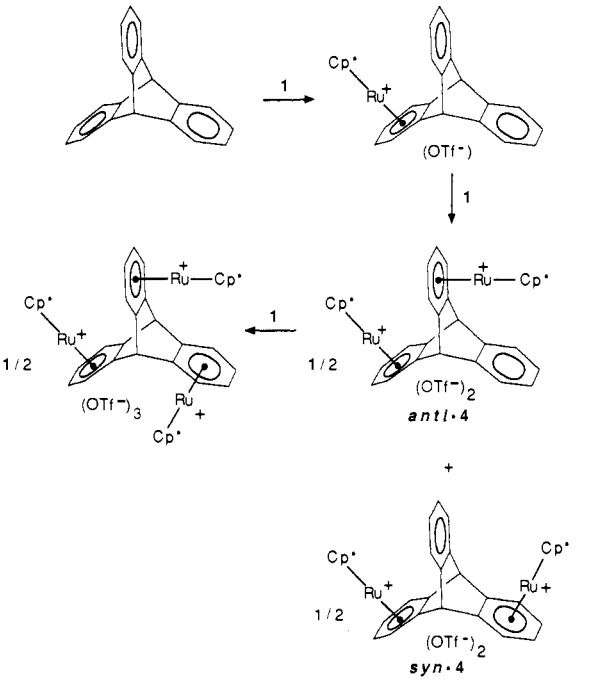

(7)

data (Tables I and II). Note that in *syn*-**4**, the remaining uncoordinated arene ring is inaccessible to further reaction with **1** since it is sterically blocked on both faces by the Cp*Ru groups. Such is not the case for *anti*-**4**, and addition of another equivalent of **1** results in the disappearance of *anti*-**4** and formation of a mixture of *syn*-**4** and the desired triangular trication $[(Cp^*Ru)_3(\eta^6,\eta^6,\eta^6\text{-triptycene})]^{3+}$ as monitored by $^1H$ NMR spectroscopy. The more soluble dication *syn*-**4** can be separated by washing the isolated solid mixture with $CH_2Cl_2$, leaving behind the pure triangular tricationic complex $[(Cp^*Ru)_3(\eta^6,\eta^6,\eta^6\text{-triptycene})]^{3+}(OTf^-)_3$. Pure *syn*-**4** can then be isolated as its triflate salt from the washings (Tables I and II).

A space-filling model of the trication $[(Cp^*Ru)_3(\eta^6,\eta^6,\eta^6\text{-triptycene})]^{3+}$ constructed with parameters obtained from the X-ray structures of the other ruthenium cations reported in this paper (vide infra) is shown in Figure 4. On the basis of this model, the overall shape of this molecule can be seen to approximate a triangular prism.

**D. Synthesis of Tetrahedral Tetracations and Related Species.** Reaction of greater than 4 equiv of **1**, with tetraphenylmethane,

(20) (a) Gancarz, R. A.; Blount, J. F.; Mislow, K. *Organometallics* **1985**, *4*, 2028–2032. (b) Gancarz, R. A.; Baum, M. W.; Hunter, G.; Mislow, K. *Organometallics* **1986**, *5*, 2327–2332. (c) Pohl, R. L.; Willeford, B. R. *J. Organomet. Chem.* **1970**, *23*, C45–C46.

**Table VII.** Interatomic Distances for the tetracation $\{[Cp^*Ru(\eta\text{-}C_6H_5)]_4C\}^{4+}$ (Å)[a]

| atoms | distance | atoms | distance | atoms | distance | atoms | distance | atoms | distance |
|---|---|---|---|---|---|---|---|---|---|
| Ru1–C11′ | 2.194 (12) | Ru2–C21″ | 2.328 (11) | C10–C21″ | 1.565 (13) | C13″–C14″ | 1.382 (15) | C22–C22′ | 1.513 (16) |
| Ru1–C11″ | 2.327 (10) | Ru2–C22′ | 2.225 (12) | C11–C11′ | 1.521 (20) | C14–C14′ | 1.459 (20) | C22′–C23′ | 1.443 (17) |
| Ru1–C12′ | 2.168 (12) | Ru2–C22″ | 2.253 (10) | C11′–C12′ | 1.385 (17) | C14′–C15′ | 1.427 (19) | C22″–C23″ | 1.408 (14) |
| Ru1–C12″ | 2.246 (10) | Ru2–C23′ | 2.185 (12) | C11′–C15′ | 1.406 (18) | C14″–C15″ | 1.433 (15) | C23–C23′ | 1.498 (19) |
| Ru1–C13′ | 2.146 (12) | Ru2–C23″ | 2.196 (10) | C11″–C12″ | 1.440 (14) | C15–C15′ | 1.483 (19) | C23′–C24′ | 1.408 (19) |
| Ru1–C13″ | 2.221 (10) | Ru2–C24′ | 2.167 (12) | C11″–C15″ | 1.419 (13) | C15″–C15″ | 1.409 (14) | C23″–C24″ | 1.374 (15) |
| Ru1–C14′ | 2.176 (13) | Ru2–C24″ | 2.171 (11) | C12–C12′ | 1.493 (19) | C21–C21′ | 1.515 (17) | C24–C24′ | 1.539 (18) |
| Ru1–C14″ | 2.198 (11) | Ru2–C25′ | 2.187 (13) | C12′–C13′ | 1.362 (17) | C21′–C22′ | 1.417 (16) | C24′–C25′ | 1.388 (18) |
| Ru1–C15′ | 2.217 (12) | Ru2–C25″ | 2.171 (11) | C12″–C13″ | 1.405 (14) | C21′–C25′ | 1.405 (16) | C24″–C25″ | 1.406 (15) |
| Ru1–C15″ | 2.223 (10) | Ru2–C26″ | 2.256 (11) | C13–C13′ | 1.509 (19) | C21″–C22″ | 1.428 (14) | C25–C25′ | 1.498 (18) |
| Ru1–C15″ | 2.185 (11) | C10–C11″ | 1.539 (12) | C13′–C14′ | 1.376 (18) | C21″–C26″ | 1.447 (14) | C25″–C26″ | 1.428 (14) |
| Ru2–C21′ | 2.208 (12) | | | | | | | | |

[a] Numbers in parentheses are estimated standard deviations in the least significant figure.

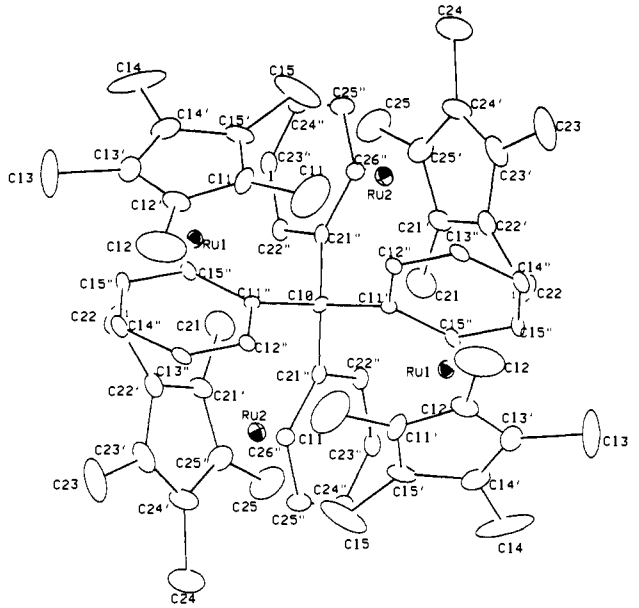

**Figure 5.** ORTEP drawing and numbering scheme for the tetracation $\{[Cp^*Ru(\eta\text{-}C_6H_5)]_4C\}^{4+}$ (H atoms omitted).

-silane, -germane, -stannane, and -plumbane in $CH_2Cl_2$ results in formation of the tetrahedral tetracations **5(C)**$^{4+}$, **5(Si)**$^{4+}$, **5(Ge)**$^{4+}$, **5(Sn)**$^{4+}$, and **5(Pb)**$^{4+}$, which were isolated as the triflate salts (eq 8). The reactions require repeated heating and removal

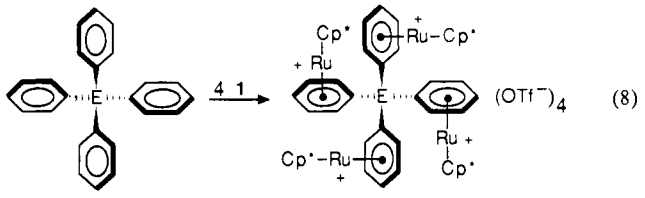

**5(E)**$^{4+}$ (E = C, Si, Ge, Sn, Pb) (8)

of solvent to eliminate the $CH_3CN$ that is generated in order to drive the reactions to completion. For **5(C)**$^{4+}$, the product is sometimes contaminated with <10% of the tricationic complex $\{[Cp^*Ru(\eta\text{-}C_6H_5)]_3(C_6H_5)C\}^{3+}(OTf^-)_3$, which can be removed by fractional crystallization from $CH_3NO_2$/ether. In the cases of **5(Si)**$^{4+}$, **5(Ge)**$^{4+}$, **5(Sn)**$^{4+}$, and **5(Pb)**$^{4+}$, the substitution on all four phenyl groups proceeds to completion more readily, presumably as consequence of the decreased steric congestion in these molecules due to the longer element–phenyl bond lengths (vide infra). The tetracations are very soluble in polar solvents such as $CH_3NO_2$ and $CH_3CN$ and insoluble in THF and ether. The spectroscopic properties of these tetrahedral tetracations are presented in Tables I and II.

The structures of the tetracations **5(C)**$^{4+}$, **5(Si)**$^{4+}$, and **5(Ge)**$^{4+}$ have been determined from single-crystal X-ray structural analyses of the complexes $\{[Cp^*Ru(\eta\text{-}C_6H_5)]_4C\}^{4+}\{C_3[C(CN)_2]_3^-\}_4 \cdot 6CH_3NO_2$, $\{[Cp^*Ru(\eta\text{-}C_6H_5)]_4Si\}^{4+}\{C_3[C(CN)_2]_3^-\}_4 \cdot 4CH_3NO_2$,

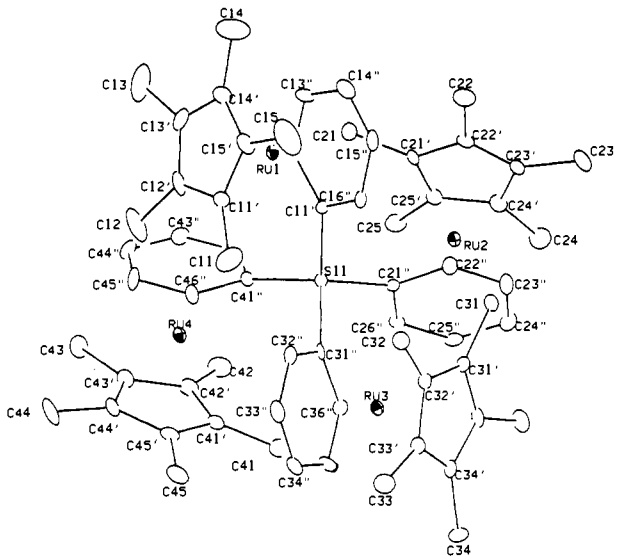

**Figure 6.** ORTEP drawing and numbering scheme for the tetracation $\{[Cp^*Ru(\eta\text{-}C_6H_5)]_4Si\}^{4+}$ (H atoms omitted).

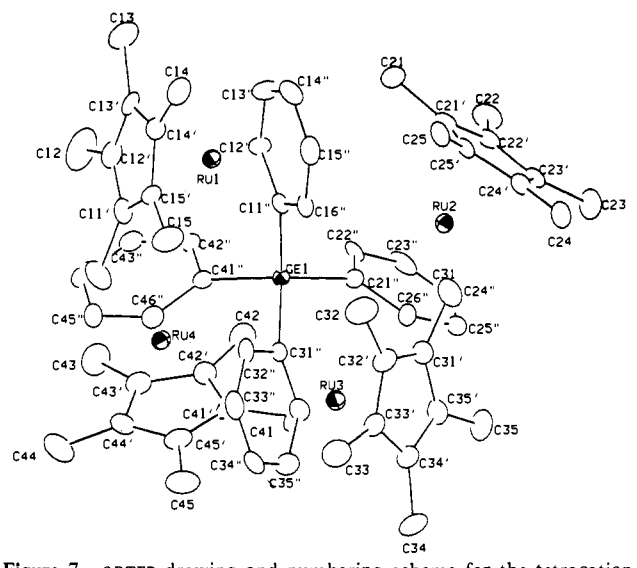

**Figure 7.** ORTEP drawing and numbering scheme for the tetracation $\{[Cp^*Ru(\eta\text{-}C_6H_5)]_4Ge\}^{4+}$ (H atoms omitted).

and $\{[Cp^*Ru(\eta\text{-}C_6H_5)]_4Ge\}^{4+}(OTf^-)_4$, respectively. Experimental aspects of the X-ray analyses and structural details for the anions of the former two complexes are described in the following paper.[1] However, descriptions of the structures of **5(C)**$^{4+}$ and **5(Si)**$^{4+}$ are presented here along with a complete description of the germanium-containing complex.

ORTEP drawings of the tetracations **5(C)**$^{4+}$, **5(Si)**$^{4+}$, and **5(Ge)**$^{4+}$ are presented in Figures 5–7, and stereoviews are presented in

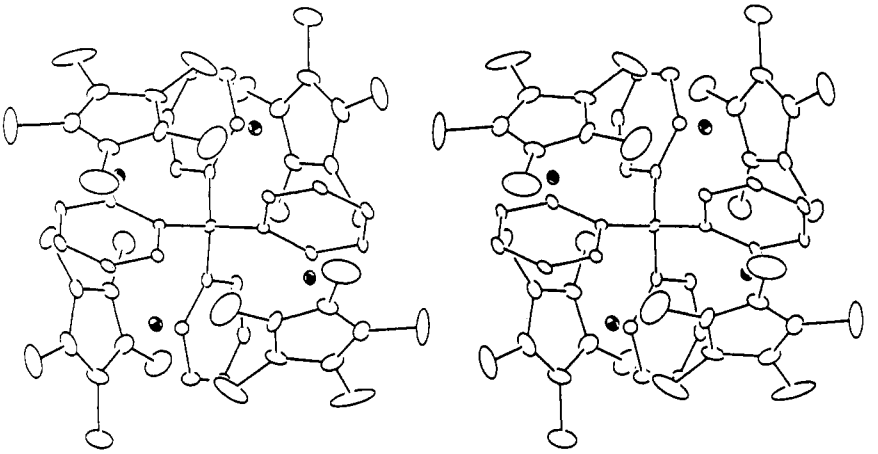

**Figure 8.** Stereoview of the tetracation $\{[Cp^*Ru(\eta\text{-}C_6H_5)]_4C\}^{4+}$.

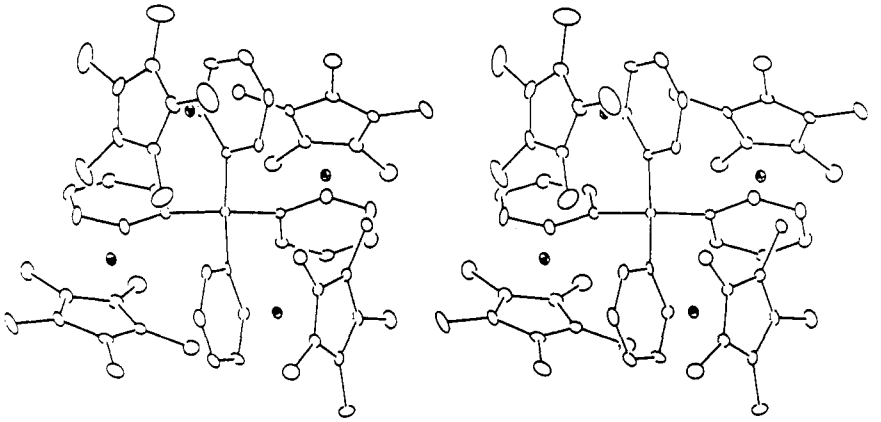

**Figure 9.** Stereoview of the tetracation $\{[Cp^*Ru(\eta\text{-}C_6H_5)]_4Si\}^{4+}$.

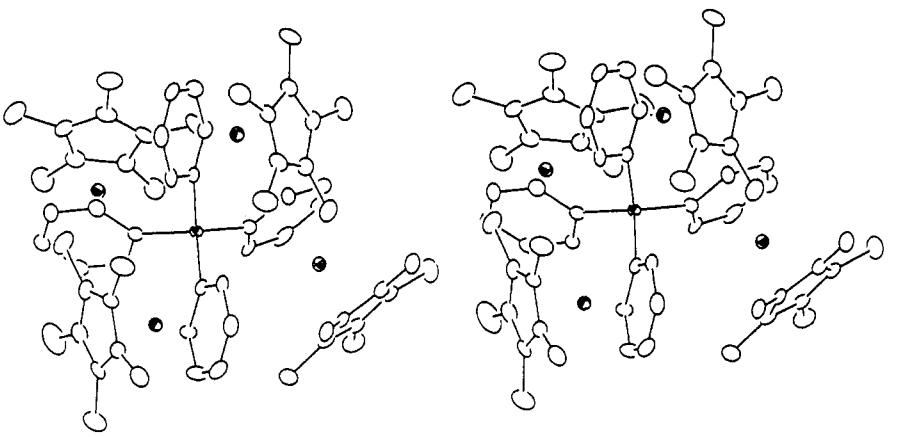

**Figure 10.** Stereoview of the tetracation $\{[Cp^*Ru(\eta\text{-}C_6H_5)]_4Ge\}^{4+}$.

**Table VIII.** Intramolecular Bond Angles for the Tetracation $\{[Cp^*Ru(\eta\text{-}C_6H_5)]_4C\}^{4+}$ (deg)[a]

| atoms | angle | atoms | angle | atoms | angle | atoms | angle |
|---|---|---|---|---|---|---|---|
| C11″–C10–C11″a | 114 (1) | C11″–C12″–C13″ | 121 (1) | C11″–C15″–C15″ | 122 (1) | C22′–C23′–C23 | 125 (2) |
| C11″–C10–C21″ | 106.9 (5) | C12′–C13′–C13 | 127 (2) | C14″–C15″–C15″ | 120 (1) | C22′–C23′–C24′ | 106 (1) |
| C11″–C10–C21″a | 107.7 (5) | C12′–C13′–C14′ | 110 (1) | C21–C21′–C22′ | 125 (1) | C23–C23′–C24′ | 129 (2) |
| C21″–C10–C21″a | 114 (1) | C13–C13′–C14′ | 123 (2) | C21–C21′–C25′ | 124 (1) | C22″–C23″–C24″ | 121 (1) |
| C11–C11′–C12′ | 125 (2) | C12″–C13″–C14″ | 122 (1) | C22′–C21′–C25′ | 110 (1) | C23′–C24′–C24 | 123 (2) |
| C11–C11′–C15′ | 126 (2) | C13′–C14′–C14 | 129 (2) | C10–C21″–C22″ | 120 (1) | C23′–C24′–C25′ | 111 (1) |
| C12′–C11′–C15′ | 108 (1) | C13′–C14′–C15′ | 107 (1) | C10–C21″–C26″ | 121 (1) | C24–C24′–C25′ | 126 (2) |
| C10–C11″–C12″ | 120 (1) | C14–C14′–C15′ | 125 (2) | C22″–C21″–C26″ | 119 (1) | C23″–C24″–C25″ | 120 (1) |
| C10–C11″–C15″ | 123 (1) | C13″–C14″–C15″ | 119 (1) | C21′–C22′–C22 | 125 (1) | C21′–C25′–C24′ | 106 (1) |
| C12″–C11″–C15″ | 117 (1) | C11′–C15′–C14′ | 107 (1) | C21′–C22′–C23′ | 106 (1) | C21′–C25′–C25 | 126 (1) |
| C11′–C12′–C12 | 122 (2) | C11′–C15′–C15 | 126 (2) | C22–C22′–C23′ | 128 (1) | C24′–C25′–C25 | 127 (1) |
| C11′–C12′–C13′ | 108 (1) | C14′–C15′–C15 | 126 (2) | C21″–C22″–C23″ | 120 (1) | C24″–C25″–C26″ | 121 (1) |
| C12–C12′–C13′ | 129 (2) | | | | | C21″–C26″–C25″ | 118 (1) |

[a] Numbers in parentheses are estimated standard deviations in the least significant figure. Atom symmetry operation code a: $1 - X, Y, {}^1/_2 - Z$.

**Table IX.** Interatomic Distances for the Tetracation $\{[Cp^*Ru(\eta\text{-}C_6H_5)]_4Si\}^{4+}$ (Å)[a]

| atoms | distance | atoms | distance | atoms | distance | atoms | distance | atoms | distance |
|---|---|---|---|---|---|---|---|---|---|
| Ru1–C11′ | 2.213 (9) | Ru3–C31″ | 2.303 (8) | Si1–C21″ | 1.875 (8) | C21″–C22″ | 1.437 (11) | C33′–C34′ | 1.457 (12) |
| Ru1–C11″ | 2.301 (8) | Ru3–C32′ | 2.187 (9) | Si1–C31″ | 1.852 (9) | C21″–C26″ | 1.406 (11) | C33″–C34″ | 1.378 (13) |
| Ru1–C12′ | 2.204 (9) | Ru3–C32″ | 2.223 (9) | Si1–C41″ | 1.866 (9) | C22–C22′ | 1.505 (12) | C34–C34′ | 1.496 (12) |
| Ru1–C12″ | 2.234 (8) | Ru3–C33′ | 2.171 (9) | C11–C11′ | 1.459 (13) | C22′–C23′ | 1.384 (12) | C34′–C35′ | 1.417 (12) |
| Ru1–C13′ | 2.168 (9) | Ru3–C33″ | 2.192 (9) | C11′–C12′ | 1.445 (13) | C22″–C23″ | 1.404 (12) | C34″–C35″ | 1.393 (13) |
| Ru1–C13″ | 2.199 (9) | Ru3–C34′ | 2.171 (9) | C11′–C15′ | 1.404 (12) | C23–C23′ | 1.515 (13) | C35–C35′ | 1.494 (12) |
| Ru1–C14′ | 2.174 (10) | Ru3–C34″ | 2.205 (9) | C11″–C12″ | 1.446 (11) | C23′–C24′ | 1.421 (12) | C35″–C36″ | 1.407 (11) |
| Ru–C14″ | 2.199 (9) | Ru3–C35′ | 2.201 (9) | C11″–C16″ | 1.412 (11) | C23″–C24″ | 1.381 (12) | C41–C41′ | 1.489 (13) |
| Ru1–C15′ | 2.184 (9) | Ru3–C35″ | 2.181 (9) | C12–C12′ | 1.470 (13) | C24–C24′ | 1.522 (13) | C41′–C42′ | 1.428 (12) |
| Ru1–C15″ | 2.190 (9) | Ru3–C36″ | 2.224 (8) | C12′–C13′ | 1.410 (13) | C24′–C25′ | 1.410 (12) | C41′–C45′ | 1.409 (12) |
| Ru1–C16″ | 2.223 (8) | Ru4–C41′ | 2.220 (9) | C12″–C13″ | 1.395 (11) | C24″–C25″ | 1.401 (13) | C41″–C42″ | 1.423 (12) |
| Ru2–C21′ | 2.192 (8) | Ru4–C41″ | 2.297 (8) | C13–C13′ | 1.524 (16) | C25–C25′ | 1.507 (12) | C41″–C46″ | 1.427 (11) |
| Ru2–C21″ | 2.269 (8) | Ru4–C42′ | 2.197 (9) | C13′–C14′ | 1.401 (14) | C25″–C26″ | 1.406 (11) | C42–C42′ | 1.488 (13) |
| Ru2–C22′ | 2.163 (8) | Ru4–C42″ | 2.235 (8) | C13″–C14″ | 1.394 (14) | C31–C31′ | 1.492 (11) | C42′–C43′ | 1.425 (12) |
| Ru2–C22″ | 2.206 (8) | Ru4–C43′ | 2.146 (9) | C14–C14′ | 1.468 (14) | C31′–C32′ | 1.434 (11) | C42″–C43″ | 1.412 (12) |
| Ru2–C23′ | 2.178 (9) | Ru4–C43″ | 2.204 (9) | C14′–C15′ | 1.382 (13) | C31′–C35′ | 1.425 (12) | C43–C43′ | 1.523 (13) |
| Ru2–C23″ | 2.181 (9) | Ru4–C44′ | 2.173 (8) | C14″–C15″ | 1.405 (14) | C31″–C32″ | 1.430 (11) | C43′–C44′ | 1.392 (12) |
| Ru2–C24′ | 2.161 (9) | Ru4–C44″ | 2.185 (9) | C15–C15′ | 1.500 (14) | C31″–C36″ | 1.414 (11) | C43″–C44″ | 1.390 (13) |
| Ru2–C24″ | 2.210 (9) | Ru4–C45′ | 2.188 (9) | C15″–C16″ | 1.419 (12) | C32–C32′ | 1.472 (12) | C44–C44′ | 1.505 (13) |
| Ru2–C25′ | 2.173 (9) | Ru4–C45″ | 2.176 (9) | C21–C21′ | 1.505 (12) | C32′–C33′ | 1.419 (11) | C44′–C45′ | 1.445 (12) |
| Ru2–C25″ | 2.200 (9) | Ru4–C46″ | 2.214 (8) | C21′–C22′ | 1.435 (12) | C32″–C33″ | 1.398 (12) | C44″–C45″ | 1.379 (13) |
| Ru2–C26″ | 2.220 (8) | Si1–C11″ | 1.886 (8) | C21′–C25′ | 1.418 (12) | C33–C33′ | 1.506 (12) | C45–C45′ | 1.505 (13) |
| Ru3–C31′ | 2.221 (8) | | | | | | | C45″–C46″ | 1.408 (12) |

[a] Numbers in parentheses are estimated standard deviations in the least significant figure.

**Table X.** Intramolecular Angles for the Tetracation $\{[Cp^*Ru(\eta\text{-}C_6H_5)]_4Si\}^{4+}$ (deg)

| atoms | angle | atoms | angle | atoms | angle | atoms | angle |
|---|---|---|---|---|---|---|---|
| C11″–Si1–C21″ | 109.1 (4) | C12′–C13′–C14′ | 110 (1) | C23′–C24′–C25′ | 108.0 (9) | C31′–C35′–C34′ | 108.2 (8) |
| C11″–Si1–C31″ | 115.2 (4) | C12′–C13′–C13 | 124 (1) | C23′–C24′–C24 | 126 (1) | C31′–C35′–C35 | 125.7 (8) |
| C11″–Si1–C41″ | 105.5 (4) | C13–C13′–C14′ | 126 (1) | C24–C24′–C25′ | 126 (1) | C34′–C35′–C35 | 125.7 (9) |
| C21″–Si1–C31″ | 104.7 (4) | C12″–C13″–C14″ | 120 (1) | C23″–C24″–C25″ | 120.2 (9) | C34″–C35″–C36″ | 120.3 (9) |
| C21″–Si1–C41″ | 115.8 (4) | C13′–C14′–C14 | 126 (1) | C21′–C25′–C24′ | 108.0 (8) | C31″–C36″–C35″ | 121.5 (8) |
| C31″–Si1–C41″ | 107.0 (4) | C13′–C14′–C15′ | 106 (1) | C21′–C25′–C25 | 126.4 (9) | C41–C41′–C42′ | 126.6 (9) |
| Ru1–C11″–Si1 | 144.1 (4) | C14–C14′–C15′ | 127 (1) | C24′–C25′–C25 | 125.4 (9) | C41–C41′–C45′ | 124.9 (9) |
| Ru2–C21″–Si1 | 146.7 (4) | C13″–C14″–C15″ | 121 (1) | C24″–C25″–C26″ | 119.3 (9) | C42′–C41′–C45′ | 108.2 (8) |
| Ru3–C31″–Si1 | 143.6 (4) | C11′–C15′–C14′ | 111 (1) | C21″–C26″–C25″ | 122.3 (8) | C42″–C41″–C46″ | 116.7 (8) |
| Ru4–C41″–Si1 | 145.6 (4) | C11′–C15′–C15 | 125 (1) | C31–C31′–C35′ | 124.5 (8) | C41′–C42′–C43′ | 106.7 (8) |
| Si1–C11″–C16″ | 122.5 (6) | C14′–C15′–C15 | 124 (1) | C31–C31′–C32′ | 126.3 (8) | C41′–C42′–C42 | 127 (1) |
| Si1–C11″–C12″ | 119.4 (6) | C14″–C15″–C16″ | 119 (1) | C32′–C31′–C35′ | 108.6 (8) | C42–C42′–C43′ | 126 (1) |
| Si1–C21″–C26″ | 122.6 (6) | C11″–C16″–C15″ | 121.6 (8) | C32″–C31″–C36″ | 116.3 (8) | C41″–C42″–C43″ | 121.5 (8) |
| Si1–C21″–C22″ | 118.4 (6) | C21–C21′–C25′ | 126.4 (8) | C31′–C32′–C32 | 127.3 (8) | C42′–C43′–C44′ | 110.0 (9) |
| Si1–C31″–C36″ | 120.5 (6) | C21–C21′–C22′ | 126.2 (9) | C31′–C32′–C33′ | 107.6 (8) | C42′–C43′–C43 | 123.9 (9) |
| Si1–C31″–C32″ | 122.1 (7) | C22′–C21′–C25′ | 107.0 (8) | C32–C32′–C33′ | 124.8 (8) | C43–C43′–C44′ | 126 (1) |
| Si1–C41″–C46″ | 117.1 (7) | C22″–C21″–C26″ | 116.7 (8) | C31″–C32″–C33″ | 121.0 (9) | C42″–C43″–C44″ | 119 (1) |
| Si1–C41″–C42″ | 124.5 (7) | C21′–C22′–C23′ | 108.6 (8) | C32′–C33′–C34′ | 107.9 (8) | C43′–C44′–C44 | 127 (1) |
| C11–C11′–C15′ | 127 (1) | C21′–C22′–C22 | 124.3 (9) | C32′–C33′–C33 | 125.9 (8) | C43′–C44′–C45′ | 106.8 (8) |
| C11–C11–C12′ | 127 (1) | C22–C22′–C23′ | 127 (1) | C33–C33′–C34′ | 126.2 (8) | C44–C44′–C45′ | 126 (1) |
| C12′–C11′–C15′ | 105.9 (9) | C21″–C22″–C23″ | 120.5 (8) | C32″–C33″–C34″ | 121 (1) | C43″–C44″–C45″ | 120.8 (9) |
| C12″–C11″–C16″ | 116.9 (8) | C22′–C23′–C23 | 125 (1) | C33′–C34′–C35′ | 107.6 (8) | C41′–C45′–C44′ | 108.3 (8) |
| C11′–C12′–C13′ | 106.4 (9) | C22′–C23′–C24′ | 108.3 (8) | C33′–C34′–C34 | 126.6 (8) | C41′–C45′–C45 | 125 (1) |
| C11′–C12′–C12 | 127 (1) | C23–C23′–C24′ | 126 (1) | C34–C34′–C35′ | 125.7 (9) | C44′–C45′–C45 | 126 (1) |
| C12–C12′–C13′ | 127 (1) | C22″–C23″–C24″ | 120.8 (9) | C33″–C34″–C35″ | 119 (1) | C44″–C45″–C46″ | 120.5 (9) |
| C11″–C12″–C13″ | 121.5 (8) | | | | | C41″–C46″–C45″ | 120.8 (9) |

[a] Numbers in parentheses are estimated standard deviations in the least significant figure.

Figures 8–10. A comparison of the van der Waals space-filling models of the three tetracations is displayed in Figure 11. Tables VII–XII list the bond distances and bond angles for **5(C)**$^{4+}$, **5(Si)**$^{4+}$, and **5(Ge)**$^{4+}$, and Table XIII presents a comparison of the important structural parameters.

The tetracation **5(C)**$^{4+}$ consists of four Cp*Ru groups bound in a $\eta^6$ fashion to the four phenyl groups of the tetraphenylmethane. The tetracation has nearly perfect $S_4$ point group symmetry and resides on a crystallographic $C_2$ axis. The average Cp*(centroid)–Ru distance is 1.834 (13) Å, while the average phenyl(centroid)–Ru distance is 1.726 (11) Å. As can be seen from the space-filling model in Figure 11, the overall structure of this molecule resembles a filled-in tetrahedron.

The sterically crowded nature of the tetracation manifests itself in several of the structural parameters (see Figure 12). The Cp*(centroid)–Ru–phenyl(centroid) angle is 171.2 (6)° with the Cp* ligand being bent away from the central region of the molecule (see Figure 12). Two of the methyl groups of the Cp* ligand are bent out of the plane defined by the five Cp* ring carbon atoms, avoiding the hydrogens of the phenyl groups and the methyls of the other Cp* ligands toward which they point. For example, C15 and C11 are bent out of the $C_5$ ring plane by 8 (1)°. By comparison, the three other methyl carbons C12, C13, and

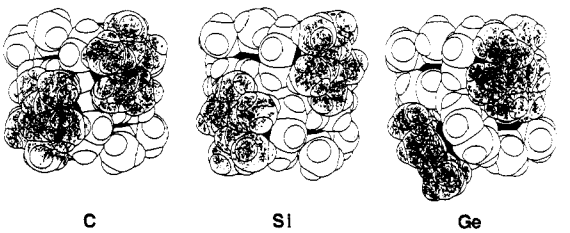


**Figure 11.** Comparison of van der Waals space-filling models of the tetracations **5(C)**$^{4+}$, **5(Si)**$^{4+}$, and **5(Ge)**$^{4+}$ constructed from the X-ray structural coordinates. Shaded Cp*Ru groups are those closest to the viewer.

**Table XI.** Interatomic Distances for the Tetracation $\{[Cp^*Ru(\eta\text{-}C_6H_5)]_4Ge\}^{4+}$ (Å)[a]

| atoms | distance | atoms | distance | atoms | distance | atoms | distance | atoms | distance |
|---|---|---|---|---|---|---|---|---|---|
| Ru1–C11′ | 2.242 (6) | Ru3–C31″ | 2.284 (5) | Ge1–C21″ | 1.968 (5) | C21″–C22″ | 1.409 (8) | C33′–C34′ | 1.447 (8) |
| Ru1–C11″ | 2.274 (5) | Ru3–C32′ | 2.206 (6) | Ge1–C31″ | 1.953 (5) | C21″–C26″ | 1.433 (8) | C33″–C34″ | 1.420 (9) |
| Ru1–C12′ | 2.179 (6) | Ru3–C32″ | 2.239 (6) | Ge1–C41″ | 1.964 (5) | C22–C22′ | 1.503 (8) | C34–C34′ | 1.492 (9) |
| Ru1–C12″ | 2.220 (6) | Ru3–C33′ | 2.168 (6) | C11–C11′ | 1.507 (9) | C22′–C23′ | 1.431 (8) | C34′–C35′ | 1.446 (8) |
| Ru1–C13′ | 2.167 (6) | Ru3–C33″ | 2.194 (6) | C11′–C12′ | 1.430 (9) | C22″–C23″ | 1.415 (8) | C34″–C35″ | 1.399 (9) |
| Ru1–C13″ | 2.201 (6) | Ru3–C34′ | 2.177 (6) | C11′–C15′ | 1.421 (9) | C23–C23′ | 1.488 (8) | C35–C35′ | 1.502 (8) |
| Ru1–C14′ | 2.178 (6) | Ru3–C34″ | 2.210 (6) | C11″–C12″ | 1.408 (8) | C23′–C24′ | 1.425 (8) | C35″–C36″ | 1.403 (8) |
| Ru1–C14″ | 2.201 (6) | Ru3–C35′ | 2.200 (6) | C11″–C16″ | 1.428 (8) | C23″–C24″ | 1.401 (9) | C41–C41′ | 1.506 (8) |
| Ru1–C15′ | 2.204 (6) | Ru3–C35″ | 2.210 (6) | C12–C12′ | 1.504 (10) | C24–C24′ | 1.490 (8) | C41′–C42′ | 1.414 (8) |
| Ru1–C15″ | 2.222 (6) | Ru3–C36″ | 2.214 (6) | C12′–C13′ | 1.415 (9) | C24′–C25′ | 1.437 (8) | C41′–C45′ | 1.429 (9) |
| Ru1–C16″ | 2.246 (5) | Ru4–C41′ | 2.211 (6) | C12″–C13″ | 1.420 (8) | C24″–C25″ | 1.411 (9) | C41″–C42″ | 1.427 (8) |
| Ru2–C21′ | 2.202 (6) | Ru4–C41″ | 2.266 (5) | C13–C13′ | 1.506 (9) | C25–C25′ | 1.486 (8) | C41″–C46″ | 1.419 (8) |
| Ru2–C21″ | 2.294 (6) | Ru4–C42′ | 2.195 (6) | C13′–C14′ | 1.443 (8) | C25″–C26″ | 1.405 (8) | C42–C42′ | 1.504 (9) |
| Ru2–C22′ | 2.181 (6) | Ru4–C42″ | 2.239 (6) | C13″–C14″ | 1.402 (9) | C31–C31′ | 1.499 (9) | C42′–C43′ | 1.441 (8) |
| Ru2–C22″ | 2.213 (5) | Ru4–C43′ | 2.191 (6) | C14–C14′ | 1.495 (8) | C31′–C32′ | 1.418 (8) | C42″–C43″ | 1.412 (8) |
| Ru2–C23′ | 2.184 (6) | Ru4–C43″ | 2.225 (6) | C14′–C15′ | 1.421 (8) | C31′–C35′ | 1.433 (8) | C43–C43′ | 1.486 (8) |
| Ru2–C23″ | 2.195 (6) | Ru4–C44′ | 2.169 (6) | C14″–C15″ | 1.417 (9) | C31″–C32″ | 1.434 (8) | C43′–C44′ | 1.442 (9) |
| Ru2–C24′ | 2.207 (6) | Ru4–C44″ | 2.226 (6) | C15–C15′ | 1.497 (9) | C31″–C36″ | 1.409 (8) | C43″–C44″ | 1.409 (8) |
| Ru2–C24″ | 2.193 (6) | Ru4–C45′ | 2.193 (6) | C15″–C16″ | 1.421 (8) | C32–C32′ | 1.497 (9) | C44–C44′ | 1.498 (9) |
| Ru2–C25′ | 2.237 (6) | Ru4–C45″ | 2.199 (6) | C21–C21′ | 1.493 (8) | C32′–C33′ | 1.434 (8) | C44′–C45′ | 1.435 (8) |
| Ru2–C25″ | 2.213 (6) | Ru4–C46″ | 2.204 (6) | C21′–C22′ | 1.430 (8) | C32″–C33″ | 1.404 (8) | C45–C45′ | 1.478 (9) |
| Ru2–C26″ | 2.244 (6) | Ge1–C11″ | 1.949 (6) | C21′–C25′ | 1.426 (8) | C33–C33′ | 1.488 (9) | C44″–C45″ | 1.422 (8) |
| Ru3–C31′ | 2.212 (6) | | | | | | | C45″–C46″ | 1.400 (8) |

[a] Numbers in parentheses are estimated standard deviations in the least significant figure.

**Table XII.** Intramolecular Angles for the Tetracation $\{[Cp^*Ru(\eta\text{-}C_6H_5)]_4Ge\}^{4+}$ (deg)[a]

| atoms | angle | atoms | angle | atoms | angle | atoms | angle |
|---|---|---|---|---|---|---|---|
| C11″–Ge1–C41″ | 108.1 (2) | C12″–C13″–C14″ | 120.2 (6) | C23″–C24″–C25″ | 120.2 (6) | C34′–C35′–C35 | 125.5 (6) |
| C11″–Ge1–C31″ | 109.4 (2) | C13′–C14′–C15′ | 107.2 (5) | C21′–C25′–C25 | 126.0 (5) | C34″–C35″–C36″ | 119.5 (6) |
| C11″–Ge1–C21″ | 111.4 (2) | C13′–C14′–C14 | 125.9 (5) | C21′–C25′–C24′ | 107.9 (5) | C31″–C36″–C35″ | 123.1 (6) |
| C21″–Ge1–C41″ | 111.7 (2) | C14–C14′–C15′ | 126.8 (6) | C24′–C25′–C25 | 125.5 (5) | C41–C41′–C45′ | 124.6 (6) |
| C21″–Ge1–C31″ | 110.7 (2) | C13″–C14″–C15″ | 120.5 (6) | C24′–C25′–C25 | 125.5 (5) | C41–C41′–C42′ | 125.5 (6) |
| C31″–Ge1–C41″ | 105.3 (2) | C11′–C15′–C14′ | 108.9 (5) | C24″–C25″–C26″ | 119.3 (5) | C42′–C41′–C45′ | 109.7 (5) |
| Ge1–C11″–C12″ | 120.6 (4) | C11′–C15′–C15 | 126.1 (6) | C21″–C26″–C25″ | 121.6 (5) | C42″–C41″–C46″ | 117.3 (5) |
| Ge1–C11″–C16″ | 120.5 (4) | C14′–C15′–C15 | 124.6 (6) | C31–C31′–C32′ | 125.6 (6) | C41′–C42′–C42 | 126.6 (6) |
| Ge1–C21″–C26″ | 118.6 (4) | C14″–C15″–C16″ | 119.0 (6) | C31–C31′–C35′ | 125.1 (6) | C41′–C42′–C43′ | 108.2 (5) |
| Ge1–C21″–C22″ | 123.3 (4) | C11″–C16″–C15″ | 120.9 (5) | C32′–C31′–C35′ | 108.8 (5) | C42–C42′–C43′ | 125.0 (6) |
| Ge1–C31″–C36″ | 122.9 (4) | C21–C21′–C22′ | 124.7 (5) | C32″–C31″–C36″ | 116.6 (5) | C41″–C42″–C43″ | 121.2 (5) |
| Ge1–C31″–C32″ | 119.6 (4) | C21–C21′–C25′ | 127.0 (6) | C31′–C32′–C32 | 126.5 (6) | C42′–C43′–C43 | 126.1 (6) |
| Ge1–C41″–C46″ | 118.2 (4) | C22′–C21′–C25′ | 108.0 (5) | C31′–C32′–C33′ | 108.5 (5) | C42′–C43′–C44′ | 106.5 (5) |
| Ge1–C41″–C42″ | 124.2 (4) | C22″–C21″–C26″ | 117.6 (5) | C32–C32′–C33′ | 124.9 (6) | C43–C43′–C44′ | 127.3 (6) |
| C11–C11′–C12′ | 126.2 (6) | C21′–C22′–C22 | 125.4 (5) | C31″–C32″–C33″ | 120.7 (6) | C42″–C43″–C44″ | 120.6 (5) |
| C11–C11′–C15′ | 125.3 (6) | C21′–C22′–C23′ | 108.0 (5) | C32′–C33′–C34′ | 107.6 (5) | C43′–C44′–C44 | 125.9 (6) |
| C12′–C11′–C15′ | 107.5 (5) | C22–C22′–C23′ | 126.4 (6) | C32′–C33′–C33 | 126.2 (6) | C43′–C44′–C45′ | 109.2 (5) |
| C12″–C11″–C16″ | 118.7 (5) | C21″–C22″–C23″ | 121.0 (5) | C33–C33′–C34′ | 126.1 (6) | C44–C44′–C45′ | 124.8 (6) |
| C11′–C12′–C12 | 125.8 (7) | C22′–C23′–C23 | 126.3 (5) | C32″–C33″–C34″ | 120.7 (6) | C43″–C44″–C45″ | 118.7 (5) |
| C11′–C12′–C13′ | 108.4 (6) | C22′–C23′–C24′ | 108.0 (5) | C33′–C34′–C34 | 126.5 (6) | C41′–C45′–C44′ | 106.4 (5) |
| C12–C12′–C13′ | 125.7 (6) | C23–C23′–C24′ | 125.6 (5) | C33′–C34′–C35′ | 107.6 (5) | C41′–C45′–C45 | 127.3 (6) |
| C11″–C12″–C13″ | 120.6 (5) | C22″–C23″–C24″ | 120.2 (6) | C34–C34′–C35′ | 125.8 (6) | C44′–C45′–C45 | 126.1 (6) |
| C12′–C13′–C14′ | 108.0 (5) | C23′–C24′–C25′ | 107.9 (5) | C33″–C34″–C35″ | 119.2 (6) | C44″–C45″–C46″ | 120.5 (5) |
| C12′–C13′–C13 | 126.1 (6) | C23′–C24′–C24 | 125.3 (5) | C31′–C35′–C34′ | 107.5 (5) | C41″–C46″–C45″ | 121.7 (5) |
| C13–C13′–C14′ | 126.0 (6) | C24–C24′–C25′ | 126.2 (5) | C31′–C35′–C35 | 126.7 (6) | | |

[a] Numbers in parentheses are estimated standard deviations in the least significant figure.

C14 are bent out of the $C_5$ plane by 4 (1), 3 (1), and 4 (1)°, respectively. The phenyl groups are also bent in such a way to allow the Cp*Ru groups to splay away from the central portion of the molecule (see Figure 12); the average phenyl(centroid)–C(ipso)–C10 angles are 169.6 (10)°. No such bending is seen in the structure of the parent molecule tetraphenylmethane.[21] In addition, it can be seen that the Ru to phenyl carbon distances range from 2.171 (11) to 2.328 (11) Å with the largest Ru–C distance being associated with the phenyl carbons attached to the central C10 atom (e.g., Ru1–C11″ = 2.327 (10) Å whereas Ru1–C14″ = 2.198 (11) Å). This again attests to the steric congestion within the molecule.

Looking down the $C_2$ axis of the molecule, the pair of phenyl rings that are related to each other by $C_2$ symmetry are rotated about the C11″–C10 bonds such that the mean plane of each phenyl group twists 35° out of the plane defined by C11″, C10, and C11″. Similarly, the mean planes of the other pair of phenyl groups related by $C_2$ symmetry twist out of the plane defined by C21″, C10, and C21″ by 36°. The same overall conformation

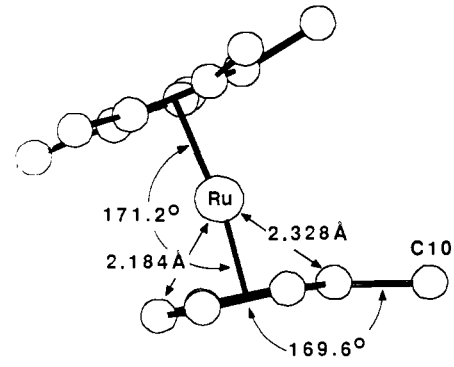


**Figure 12.** View parallel to the phenyl $C_6$ plane showing sterically induced distortions in the tetracation $\{[Cp^*Ru(\eta\text{-}C_6H_5)]_4C\}^{4+}$. Values displayed are the average of the two crystallographically independent $Cp^*Ru(\eta\text{-}C_6H_5)^+$ groups.

(21) Robbins, A.; Jeffrey, G. A.; Chesick, J. P.; Donohue, J.; Cotton, F. A.; Frenz, B. A.; Murillo, C. A. *Acta Crystallogr.* **1975**, *B31*, 2395–2399.

**Table XIII.** Important Structural Parameters for the Tetracation $\{[Cp^*Ru(\eta\text{-}C_6H_5)]_4E\}^{4+}$ (E = C, Si, Ge)[a]

| | E = C | | E = Si | | E = Ge |
|---|---|---|---|---|---|
| | | Distances, Å | | | |
| Cp*(centroid)–Ru1 | 1.831 (13) | | 1.833 (10) | | 1.829 (6) |
| Cp*(centroid)–Ru2 | 1.836 (13) | | 1.810 (10) | | 1.836 (6) |
| Cp*(centroid)–Ru3 | | | 1.821 (10) | | 1.821 (6) |
| Cp*(centroid)–Ru4 | | | 1.821 (10) | | 1.822 (6) |
| average | 1.834 | | 1.821 | | 1.827 |
| phenyl(centroid)–Ru1 | 1.729 (11) | | 1.720 (9) | | 1.720 (6) |
| phenyl(centroid)–Ru2 | 1.724 (11) | | 1.711 (9) | | 1.720 (6) |
| phenyl(centroid)–Ru3 | | | 1.723 (9) | | 1.721 (6) |
| phenyl(centroid)–Ru4 | | | 1.716 (9) | | 1.720 (6) |
| average | 1.726 | | 1.718 | | 1.720 |
| Ru1–Ru1′ | 5.339 (3) | Ru1–Ru2 | 6.801 (2) | Ru1–Ru2 | 6.622 (1) |
| Ru2–Ru2′ | 5.393 (3) | Ru1–Ru3 | 6.033 (2) | Ru1–Ru3 | 5.858 (1) |
| Ru1–Ru2 | 6.295 (3) | Ru1–Ru4 | 6.608 (2) | Ru1–Ru4 | 6.603 (1) |
| Ru1–Ru2′ | 6.334 (3) | Ru2–Ru3 | 6.499 (2) | Ru2–Ru3 | 6.195 (1) |
| Ru2–Ru2′ | 6.295 (3) | Ru2–Ru4 | 6.316 (2) | Ru2–Ru4 | 6.653 (1) |
| Ru1′–Ru2′ | 6.334 (3) | Ru3–Ru4 | 6.609 (2) | Ru3–Ru4 | 6.698 (1) |
| average | 5.998 | | 6.478 | | 6.438 |
| E–Ru1 | 3.670 (10) | | 3.985 (3) | | 3.918 (1) |
| E–Ru2 | 3.697 (10) | | 3.971 (3) | | 4.003 (1) |
| E–Ru3 | | | 3.950 (3) | | 3.995 (1) |
| E–Ru4 | | | 3.979 (3) | | 3.926 (1) |
| average | 3.684 | | 3.971 | | 3.960 |
| E–C(phenyl) (av) | 1.552 | | 1.869 | | 1.958 |
| | | Angles, deg | | | |
| Cp*(centroid)–Ru1–phenyl(centroid) | 171.2 (6) | | 172.4 (4) | | 172.2 (3) |
| Cp*(centroid)–Ru2–phenyl(centroid) | 171.2 (6) | | 174.1 (4) | | 173.6 (3) |
| Cp*(centroid)–Ru3–phenyl(centroid) | | | 173.1 (4) | | 172.8 (3) |
| Cp*(centroid)–Ru4–phenyl(centroid) | | | 173.0 (4) | | 175.2 (3) |
| average | 171.2 | | 173.2 | | 173.5 |
| phenyl(centroid)–C(ipso)–E | 169.5 (10) | | 167.4 (7) | | 174.9 (4) |
| | 169.7 (10) | | 164.1 (7) | | 171.3 (4) |
| | | | 168.0 (7) | | 170.1 (4) |
| | | | 165.4 (7) | | 173.6 (4) |
| average | 169.6 | | 166.2 | | 172.5 |
| | | Mean Plane Angles, deg | | | |
| (C11″–C16″)–(C11″,C10,C11″) | 35.5 | (C11″–C16″)–(C11″,Si1,C31″) | 38.2 | (C11″–C16″)–(C11″,Ge1,C31″) | 25.2 |
| (C21″–C26″)–(C21″,C10,C21″) | 36.0 | (C21″–C26″)–(C21″,Si1,C41″) | 33.0 | (C21″–C26″)–(C21″,Ge1,C41″) | 36.8 |
| | | (C31″–C36″)–(C11″,Si1,C31″) | 30.8 | (C31″–C36″)–(C11″,Ge1,C31″) | 29.0 |
| | | (C41″–C46″)–(C21″,Si1,C41″) | 28.8 | (C41″–C46″)–(C21″,Ge1,C41″) | 42.2 |
| (C11″,C10,C11″)–(C21″,C10,C21″) | 89.5 | (C11″,Si1,C31″)–(C21″,Si1,C41″) | 91.9 | (C11″,Ge1,C31″)–(C21″,Ge1,C41″) | 90.9 |

[a] Numbers in parentheses are estimated standard deviations that were calculated or chosen as the maximum values observed for other representative distances or angles.

of the phenyl groups is observed in the structure of tetraphenylmethane, although the analogous twisting is reportedly somewhat larger (49°).[21] The bonding about the central carbon C10 is most severely distorted from perfect tetrahedral symmetry along the angles defined by C11″–C10–C11″ and C21″–C10–C21″ which are both 114 (1)°. This is consistent with the fact that the two symmetry related Cp*Ru(phenyl) groups approach each other most closely across these angles. The other angles about C10 range from 106.9 (5) to 107.7 (5)°. For tetraphenylmethane the angles about the central quaternary carbon range from 106.7 (2) to 110.9 (2)°.[21] The average C10–C(phenyl) distances of 1.539 (12) and 1.565 (13) Å are identical within experimental error to the value of 1.553 (3) Å reported for tetraphenylmethane.[21] The effect of the twisting of the phenyl groups in $\mathbf{5(C)}^{4+}$ is such that the positively charged ruthenium centers do not define a perfect tetrahedral array but are distorted such that two of the Ru–Ru axes are pulled away from one another as can be seen in Figure 13 (cf. Table XIII).

The structure of the tetracation $\mathbf{5(Si)}^{4+}$ is in all respects quite similar to that of $\mathbf{5(C)}^{4+}$, as can be seen from the entries in Table XIII. Again the tetracation closely approximates $S_4$ point group symmetry, but it does not lie on any crystallographic symmetry axes. Despite the longer C(phenyl)–Si bond lengths of 1.859 (9)–1.886 (8) Å, there are still distortions comparable with those in $\mathbf{5(C)}^{4+}$ caused by unfavorable steric interactions between Cp* ligands and between Cp* ligands and nearby phenyl groups. The C(phenyl)–Si bond lengths are identical within experimental error to the value found in tetraphenylsilane (1.877 (2) Å).[22] Compared to the structure of tetraphenylsilane, the conformation with respect to the observed twisting of the phenyl group mean planes is similar. The reported angle is 37.7° for the twist of the phenyl mean plane with respect to the C–Si–C plane which is within the range of

(22) (a) Gruhnert, V.; Kirfel, A.; Will, G.; Wallrafen, F.; Recker, K. *Z. Kristallogr.* **1983**, *163*, 53–60. (b) Parkanyi, L.; Sasvari, K. *Period. Polytech., Chem. Eng.* **1973**, *17*, 271–276.

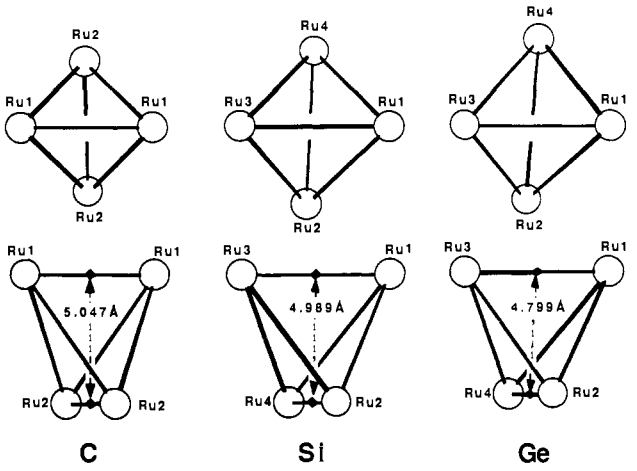


**Figure 13.** Ru atom geometries in the tetracations $\{[Cp^*Ru(\eta\text{-}C_6H_5)]_4E\}^{4+}$ (E = C, Si, Ge).

values found here of 28.8–38.2° (see Table XIII for mean plane angles).[22] As expected, the distances between the positively charged ruthenium centers are lengthened with respect to the corresponding distances in $\mathbf{5(C)}^{4+}$. A comparison of the Ru atom geometry of $\mathbf{5(Si)}^{4+}$ to that of $\mathbf{5(C)}^{4+}$ and $\mathbf{5(Ge)}^{4+}$ is shown in Figure 13, and Ru–Ru distances are compared in Table XIII.

Inspection of the structure of $\mathbf{5(Ge)}^{4+}$ shows that it deviates substantially from that of $\mathbf{5(C)}^{4+}$ and $\mathbf{5(Si)}^{4+}$. There is slightly less steric congestion in the molecule as reflected in the structural parameters. The phenyl(centroid)–C(ipso)–Ge1 angles of 170.1 (4)–174.9 (4)° (cf. $\mathbf{5(Si)}^{4+}$: 164.1 (7)–168.0 (7)°) are comparatively closer to the ideal angle of 180° which is found in the structure of tetraphenylgermane.[23] The angles about the central Ge atom are nearer to perfect tetrahedral geometry. The twisting of the phenyl groups about the central germanium atom is more random (see Table XIII), presumably reflecting the greater rotational freedom about the longer phenyl–germanium bonds. Thus, while the phenyl group conformations in the $S_4$ symmetry C and Si analogues are as shown by **A**, for the case of Ge the conformation is closer to that shown by **B**. This conformation also differs from that found in the structure of tetraphenylgermane

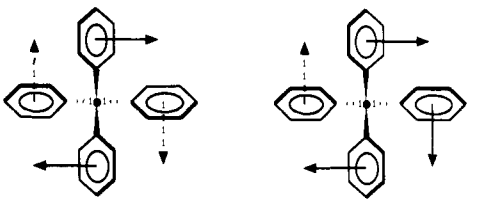


in which the molecule adopts the $S_4$ point group symmetry also observed in tetraphenylmethane and tetraphenylsilane.[24] The C(phenyl)–Ge bond distances of 1.946 (6)–1.968 (5) Å in $\mathbf{5(Ge)}^{4+}$ are not significantly different from that found for tetraphenylgermane (1.9537 (5) Å).[22]

The average Ru–Ru distance in the germanium derivative $\mathbf{5(Ge)}^{4+}$ is 6.438 Å, which is not significantly different than the average Ru–Ru distance in the silicon derivative $\mathbf{5(Si)}^{4+}$ (6.478 Å). This apparent anomaly can be explained by noticing that the phenyl–germanium bond distances are only 0.09 Å longer on average relative to the phenyl–Si bond distances, and at the same time the relief of steric congestion in the molecule allows the phenyl(centroid)–C(ipso)–Ge1 angle to become larger. Therefore, the distances between Ru atoms and the distances of the Ru atoms from the central Si and Ge atoms are similar.

With the purpose of preparing molecules with the same overall shape as $\mathbf{5(C)}^{4+}$ and $\mathbf{5(Si)}^{4+}$ but with different net charge, we have carried out reactions with sodium tetraphenylborate and tetraphenylantimonium trifluoromethanesulfonate. Reacting **1** with sodium tetraphenylborate in a manner similar to that described for $\mathbf{5(C)}^{4+}$ yields the tetrahedral trication $\{[Cp^*Ru(\eta\text{-}C_6H_5)]_4B\}^{3+}$, which was isolated as its triflate salt (Table I and II) (eq 9). As

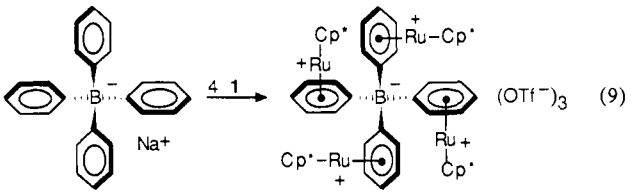


in the cases of $\mathbf{5(C)}^{4+}$ and $\mathbf{5(Si)}^{4+}$, all four phenyl groups of the tetraphenylborate group can be coordinated to a $Cp^*Ru^+$ fragment. Spectral characterization data can be found in Tables I and II. The monosubstituted tetraphenylborate complex $(\eta\text{-}C_5H_5)Ru(\eta\text{-}C_6H_5)B(C_6H_5)_3$ has been reported previously,[25] and the related anion $[(\eta\text{-}C_5H_5)Fe(\eta^5\text{-}C_5H_4)]_4B^-$ is also known.[26]

Reaction of tetraphenylantimonium triflate with **1** results in formation of the tetracationic complex $\{[Cp^*Ru(\eta\text{-}C_6H_5)]_3(C_6H_5)Sb\}^{4+}(OTf^-)_4$ (Tables I and II) in which only three of the available phenyl groups of the tetraphenylantimonium group react with the ruthenium reagent (eq 10). Even with an excess of the

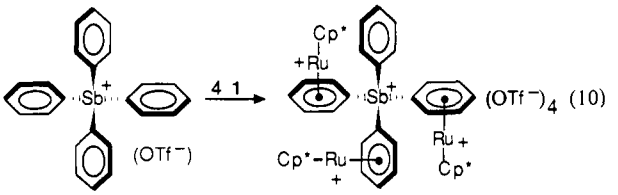


ruthenium reagent **1**, we have not been able to substitute $Cp^*Ru^+$ onto the remaining phenyl group. Presumably, the positive charge on antimony along with the three other positively charged $Cp^*Ru(\eta\text{-}C_6H_5)$ substituents precludes substitution of a fourth positively charged $Cp^*Ru^+$ group due to electrostatic repulsion.

Referring to the $^1H$ and $^{13}C$ NMR data in Tables I and II for the tetracations $\mathbf{5(E)}^{4+}$ (E = C, Si, Ge, Sn, Pb) and $\{[Cp^*Ru(\eta\text{-}C_6H_5)]_4B\}^{3+}$, there is evidence for hindered rotation about the phenyl–C bonds in $\mathbf{5(C)}^{4+}$ since there are four separate $^1H$ NMR resonances (two overlapping) and five $^{13}C$ NMR resonances (two overlapping) for the phenyl groups (25 °C, 300 MHz). This suggests that the conformation of $\mathbf{5(C)}^{4+}$ in solution is similar to that observed in the solid state. This is in contrast to $\mathbf{5(Si)}^{4+}$ for which just three $^1H$ NMR resonances and four $^{13}C$ NMR resonances are observed for the phenyl groups in the room temperature spectra. For $\{[Cp^*Ru(\eta\text{-}C_6H_5)]_4B\}^{3+}$ the room temperature resonances are broadened, suggesting a fluxional process, and we are currently studying the variable-temperature NMR behavior of these complexes to further quantify this process. Hindered rotation about phenyl–element bonds in tetraarylmethane derivatives has previously been studied by Mislow et al.[27]

**E. Synthesis of an Octahedral Hexacation.** For the synthesis of an octahedral array of positively charged ruthenium atoms, we have chosen to use as the template hexakis(*p*-methoxyphenoxy)benzene. From a previous X-ray analysis of this class of aromatic compounds, it was determined that three of the arene moieties are splayed away from one face of the central benzene ring, while the other three point in the opposite direction approximating a trigonal antiprismatic arrangement of the six arene groups.[28] Reaction of slightly greater than 6 equiv of **1** with

(23) Chieh, P. C. *J. Chem. Soc., A* **1971**, 3243–3245.
(24) Schlotter, N. E.; Hudson, B. *J. Phys. Chem.* **1982**, *76*, 4844–4856.
(25) Haines, R. J.; Du Preez, A. L. *J. Organomet. Chem.* **1975**, *84*, 357.
(26) Cowan, D. O.; Shu, P.; Hedberg, F. L.; Rossi, M.; Kistenmacher, T. J. *J. Am. Chem. Soc.* **1979**, *101*, 1138–1142.
(27) (a) Nourse, J. G.; Mislow, K. *J. Am. Chem. Soc.* **1975**, *97*, 4571–4578. (b) Hutchings, M. G.; Andose, J. D.; Mislow, K. *J. Am. Chem. Soc.* **1975**, *97*, 4562–4570. (c) Hutchings, M. G.; Andose, J. D.; Mislow, K. *J. Am. Chem. Soc.* **1975**, *97*, 4553–4561. (d) Hutchings, M. G.; Nourse, J. G.; Mislow, K. *Tetrahedron* **1974**, *30*, 1535–1549. (e) Hutchings, M. G.; Maryanoff, C. A.; Mislow, K. *J. Am. Chem. Soc.* **1973**, *95*, 7158–7159.

**Table XIV.** Interatomic Distances for $\{[Cp^*Ru(p\text{-}CH_3O\text{-}\eta\text{-}C_6H_4\text{-}O)]_6C_6\}^{6+}$ (Å)[a]

| atoms | distance | atoms | distance | atoms | distance | atoms | distance | atoms | distance |
|---|---|---|---|---|---|---|---|---|---|
| Ru1-C11′ | 2.194 (10) | Ru2-C25″ | 2.214 (8) | O24″-C24″ | 1.338 (11) | C13″-C14″ | 1.416 (13) | C24″-C25″ | 1.399 (13) |
| Ru1C11″ | 2.275 (8) | Ru2-C26″ | 2.213 (9) | O24″-C27″ | 1.435 (13) | C14-C14′ | 1.469 (13) | C25-C25′ | 1.519 (14) |
| Ru1-C12′ | 2.179 (9) | Ru3-C31′ | 2.189 (10) | O31″-C3″ | 1.381 (9) | C14′-C15′ | 1.439 (13) | C25″-C26″ | 1.431 (12) |
| Ru1-C12″ | 2.228 (9) | Ru3-C31″ | 2.283 (9) | O31″-C31″ | 1.399 (10) | C14″-C15″ | 1.404 (12) | C31-C31′ | 1.498 (14) |
| Ru1-C13′ | 2.184 (9) | Ru3-C32′ | 2.180 (10) | O34″-C34″ | 1.353 (11) | C15-C15′ | 1.510 (13) | C31′-C32′ | 1.414 (14) |
| Ru1-C13″ | 2.197 (9) | Ru3-C32″ | 2.222 (9) | O34″-C37″ | 1.429 (13) | C15″-C16″ | 1.426 (12) | C31′-C35′ | 1.440 (13) |
| Ru1-C14′ | 2.200 (9) | Ru3-C33′ | 2.167 (10) | C1″-C2″ | 1.384 (11) | C21-C21′ | 1.505 (16) | C31″-C32″ | 1.416 (12) |
| Ru1-C14″ | 2.241 (10) | Ru3-C33″ | 2.196 (9) | C1″-C3″a | 1.394 (11) | C21′-C22′ | 1.371 (15) | C31″-C36″ | 1.407 (11) |
| Ru1-C15′ | 2.187 (10) | Ru3-C34′ | 2.185 (10) | C2″-C3″ | 1.385 (11) | C21′-C25′ | 1.458 (15) | C32-C32′ | 1.506 (14) |
| Ru1-C15″ | 2.206 (9) | Ru3-C34″ | 2.262 (9) | C11-C11′ | 1.494 (14) | C21″-C22″ | 1.453 (12) | C32′-C33′ | 1.382 (14) |
| Ru1-C16″ | 2.213 (9) | Ru3-C35′ | 2.182 (10) | C11′-C12′ | 1.478 (13) | C21″-C26″ | 1.387 (11) | C32″-C33″ | 1.371 (12) |
| Ru2-C21′ | 2.178 (11) | Ru3-C35″ | 2.206 (9) | C11′-C15′ | 1.388 (14) | C22-C22′ | 1.540 (15) | C33-C33′ | 1.521 (15) |
| Ru2-C21″ | 2.312 (8) | Ru3-C36″ | 2.239 (9) | C11″-C12″ | 1.390 (12) | C22′-C23′ | 1.383 (15) | C33′-C34′ | 1.436 (14) |
| Ru2-C22′ | 2.190 (10) | O11″-C1″ | 1.383 (9) | C11″-C16″ | 1.422 (12) | C22″-C23″ | 1.414 (13) | C33″-C34″ | 1.413 (12) |
| Ru2-C22″ | 2.245 (9) | O11″-C11″ | 1.413 (10) | C12-C12′ | 1.492 (14) | C23-C23′ | 1.543 (15) | C34-C34′ | 1.499 (14) |
| Ru2-C23′ | 2.183 (9) | O14″-C14″ | 1.366 (10) | C12′-C13′ | 1.434 (13) | C23′-C24′ | 1.416 (14) | C34′-C35′ | 1.417 (13) |
| Ru2-C23″ | 2.193 (10) | O14″-C17″ | 1.414 (11) | C12″-C13″ | 1.404 (12) | C23″-C24″ | 1.417 (13) | C34″-C35″ | 1.407 (13) |
| Ru2-C24′ | 2.167 (9) | O21″-C2″ | 1.388 (9) | C13-C13′ | 1.502 (13) | C24-C24′ | 1.461 (16) | C35-C35′ | 1.508 (13) |
| Ru2-C24″ | 2.259 (10) | O21″-C21″ | 1.389 (10) | C13′-C14′ | 1.427 (13) | C24′-C25′ | 1.423 (15) | C35″-C36″ | 1.405 (13) |
| Ru2-C25′ | 2.144 (10) | | | | | | | | |

[a] Numbers in parentheses are estimated standard deviations in the least significant figure.

hexakis(*p*-methoxyphenoxy)benzene in $CH_2Cl_2$ results in complete substitution of six Cp*Ru groups onto the six *p*-methoxyarene moieties to yield the complex $\{[Cp^*Ru(p\text{-}CH_3O\text{-}\eta\text{-}C_6H_4\text{-}O)]_6C_6\}^{6+}(OTf^-)_6$ (eq 11). The spectral properties of this complex are listed in Tables I and II.

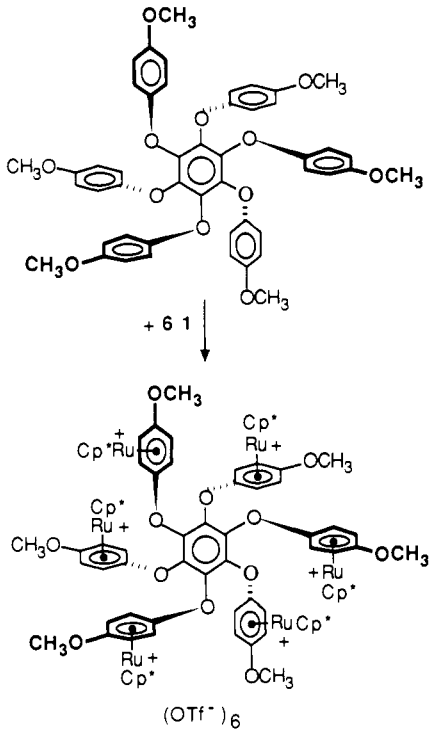


(11)

A single-crystal X-ray analysis was performed on $\{[Cp^*Ru(p\text{-}CH_3O\text{-}\eta\text{-}C_6H_4\text{-}O)]_6C_6\}(OTf)_6\cdot 6CH_3NO_2$. ORTEP drawings of two views of the hexacation are shown in Figures 14 and 15. A stereoview is shown in Figure 16, and bond distances and bond angles for the complex are listed in Tables XIV and XV, respectively. Other important structural parameters are given in Table XVI.

The hexacation is composed of six Cp*Ru groups bound in a $\eta^6$ fashion to the six outer arene moieties of the hexakis(*p*-methoxyphenoxy)benzene. The molecule has an inversion center that is coincident with the centroid of the hexasubstituted benzene ring. The Cp*(centroid)–Ru distances of the three crystallographically unique ruthenium atoms are 1.818 (10), 1.811 (10), and 1.817 (10) Å. The average arene(centroid)–Ru distances are 1.724 (10), 1.736 (10), and 1.741 (10) Å. There is only slight bending of the Cp* ligands with the average Cp*(centroid)–Ru–arene(centroid) angle being 176.7 (5)°. The atoms of the central $C_6O_6$ core of the molecule are essentially coplanar, with the largest deviation from planarity being C2″, which is 0.032 Å from the mean plane defined by the $C_6O_6$ atoms. As expected, the phenoxy groups are oriented such that three alternate phenoxy groups lie on one side of the $C_6O_6$ plane and the other three on the opposite side. Each phenoxy group is twisted away from the $C_6O_6$ plane as measured by the twist of C11″, C21″, and C31″ out of the $C_6O_6$ plane (C11′–O11″–C1″–C3″, C21″–O21″–C2″–C1″, and C31″–O31″–C3″–C1″ torsional angles are 53.5 (10)°, 58.4 (10)°, and 53.2 (10)°, respectively). The twists of the arene rings about the carbon(phenyl)–oxygen($C_6O_6$) bonds are measured by the C16″–C11″–O11″–C1″, C22″–C21″–O21″–C2″, and C32″–C31″–O31″–C3″ torsional angles, which are 36.0 (10)°, 21.2 (10)°, and 28.7 (10)°, respectively. Interestingly, the *p*-methoxy groups are nearly coplanar with the arene ring planes with the dihedral angles C17″–O14″–C14″–C15″, C27″–O24″–C24″–C25″, and C37″–O34″–C34″–C35″ being 2.0 (10)°, 2.3 (10)°, and 2.2 (10)°, respectively. The typical arene

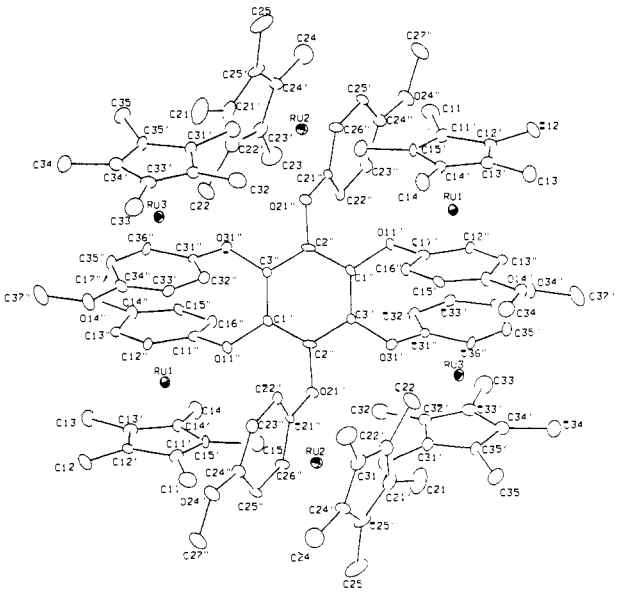

**Figure 14.** ORTEP drawing of the hexacation $\{[Cp^*Ru(p\text{-}CH_3O\text{-}\eta\text{-}C_6H_4\text{-}O]_6C_6\}^{6+}$ looking perpendicular to the central $C_6O_6$ plane (H atoms omitted).

(28) Gilmore, C. J.; MacNicol, D. D.; Murphy, A.; Russell, M. A. *Tetrahedron Lett.* **1983**, *24*, 3269–3272.

Table XV. Intramolecular Angles for $\{[Cp^*Ru(p\text{-}CH_3O\text{-}\eta\text{-}C_6H_4\text{-}O)]_6C_6\}^{6+}$ (deg)[a]

| atoms | angle | atoms | angle | atoms | angle | atoms | angle |
|---|---|---|---|---|---|---|---|
| C1″–O11″–C11″ | 116.8 (6) | O34″–C34″–C33″ | 117.8 (9) | C14′–C15′–C15 | 125 (1) | C24″–C25″–C26″ | 119.3 (8) |
| C14″–O14″–C17″ | 117.4 (8) | C2″–C1″–C3″a | 119.3 (7) | C14″–C15″–C16″ | 118.7 (8) | C21″–C26″–C25″ | 120.8 (9) |
| C2″–O21″–C21″ | 117.9 (7) | C1″–C2″–C3″ | 120.6 (8) | C11″–C16″–C15″ | 119.1 (8) | C31–C31′–C32′ | 124 (1) |
| C24″–O24″–C27″ | 119 (1) | C1″a–C3″–C2″ | 119.9 (8) | C21–C21′–C25′ | 126 (1) | C31–C31′–C35′ | 128 (1) |
| C3″–O31″–C31″ | 117.7 (6) | C11–C11′–C12′ | 122 (1) | C21–C21′–C22′ | 127 (1) | C32′–C31′–C35′ | 108 (1) |
| C34″–O34″–C37″ | 118.3 (8) | C11–C11′–C15′ | 130 (1) | C22′–C21′–C25′ | 107 (1) | C32″–C31″–C36″ | 120.7 (8) |
| O11″–C1″–C3″a | 122.3 (8) | C12′–C11′–C15′ | 107.6 (9) | C22″–C21″–C26″ | 120.0 (8) | C31′–C32′–C32 | 124 (1) |
| O11″–C1″–C2″ | 118.4 (7) | C12″–C11″–C16″ | 121.4 (8) | C21′–C22′–C22 | 124 (1) | C31′–C32′–C33 | 108 (1) |
| O21″–C2″–C1″ | 121.9 (8) | C11′–C12′–C13′ | 106.4 (9) | C21′–C22′–C23′ | 110 (1) | C32–C32′–C33′ | 127 (1) |
| O21″–C2″–C3″ | 117.3 (8) | C11′–C12′–C12 | 126 (1) | C22–C22′–C23′ | 125 (1) | C31″–C32″–C33″ | 119.0 (8) |
| O31″–C3″–C1″a | 122.3 (7) | C12–C12′–C13′ | 127 (1) | C21″–C22″–C23″ | 117.6 (8) | C32′–C33′–C33 | 127 (1) |
| O31″–C3″–C2″ | 117.7 (7) | C11″–C12″–C13″ | 118.9 (8) | C22′–C23′–C24′ | 109 (1) | C32′–C33′–C34′ | 109 (1) |
| O11″–C11″–C16″ | 119.4 (8) | C12′–C13′–C13 | 123 (1) | C22′–C23′–C23 | 128 (1) | C33–C33′–C34′ | 124 (1) |
| O11″–C11″–C12″ | 118.9 (8) | C12′–C13′–C14′ | 108.9 (9) | C23–C23′–C24′ | 124 (1) | C32″–C33″–C34″ | 121.9 (8) |
| O14″–C14″–C13″ | 115.8 (8) | C13–C13′–C14′ | 128 (1) | C22″–C23″–C24″ | 121.5 (9) | C33′–C34′–C35′ | 107 (1) |
| O14″–C14″–C15″ | 123.5 (9) | C12″–C13″–C14″ | 120.5 (8) | C23′–C24′–C24 | 127 (1) | C33′–C34′–C34 | 129 (1) |
| O21″–C21″–C22″ | 122.5 (7) | C13′–C14′–C14 | 125.5 (9) | C23′–C24′–C25′ | 107 (1) | C34–C34′–C35′ | 124 (1) |
| O21″–C21″–C26″ | 117.4 (8) | C13′–C14′–C15′ | 107.1 (9) | C24–C24′–C25′ | 126 (1) | C33″–C34″–C35″ | 118 (1) |
| O24″–C24″–C25″ | 124.1 (9) | C14–C14′–C15′ | 127 (1) | C23″–C24″–C25″ | 119.7 (9) | C31′–C35′–C35 | 127 (1) |
| O24″–C24″–C23″ | 116 (1) | C13″–C14″–C15″ | 120.6 (8) | C21′–C25′–C24′ | 107.0 (9) | C31′–C35′–C34′ | 107.4 (9) |
| O31″–C31″–C36″ | 115.3 (7) | C11′–C15′–C14′ | 110.0 (8) | C21′–C25′–C25 | 127 (1) | C34′–C35′–C35 | 125 (1) |
| O31″–C31″–C32″ | 124.0 (8) | C11′–C15′–C15 | 125 (1) | C24′–C25′–C25 | 126 (1) | C34″–C35″–C36″ | 121.1 (9) |
| O34″–C34″–C35″ | 124 (1) | | | | | C31″–C36″–C35″ | 118.5 (8) |

[a] Numbers in parentheses are estimated standard deviations in the least significant figure.

carbon to methoxy oxygen distance is ca. 0.05 Å shorter than the typical arene carbon to $C_6O_6$ group oxygen distance (e.g., C34″–O34″ = 1.353 (11) Å whereas C31″–O31″ = 1.399 (10) Å). Also, for example, the angle C34″–O34″–C37″ is 118.3 (8)°. These structural parameters presumably reflect some contribution of the resonance structure **C** shown below.

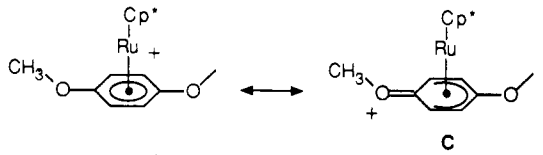


**C**

An unexpected structural feature of this hexacation is that the Ru–Cp*(centroid) vectors are arranged as shown below by the structure **D** rather than the propeller type arrangements as in

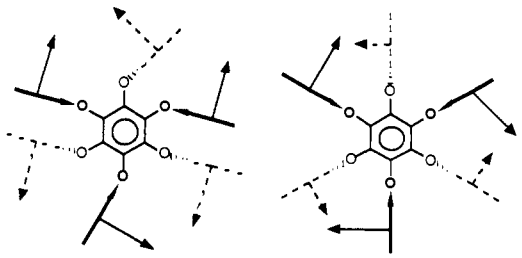

**D** **E**

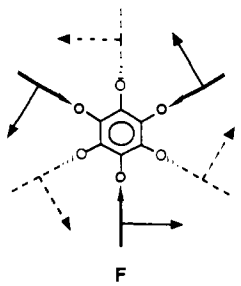

**F**

structures **E** and **F**. The reason for this is not clear since there are no obvious steric difficulties with either arrangements **E** or **F**. It is possible this hexacation prefers conformation **D** because a more efficient packing of the Cp*Ru groups results. It is worth noting that by $^1H$ NMR spectroscopy, all six Cp* ligands are chemically equivalent, indicating that in solution this molecule is conformationally flexible. Nevertheless, the six Ru atoms are arranged in a distorted octahedral array as shown in Figure 17.

**F. Attachment of Cp*Ru on Polyphenyls.** The reaction of **1** with *p*-quaterphenyl and *p*-sexiphenyl proceeds as shown in eq 12 and 13. Full substitution on all of the arene rings occurs to

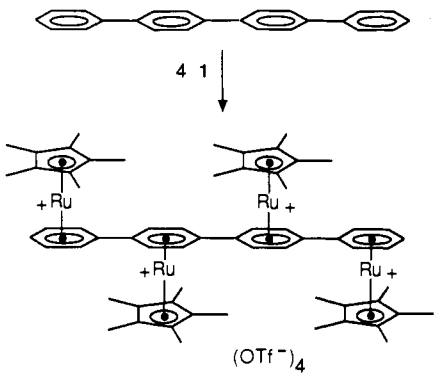


(12)

produce the tetracation $[(Cp^*Ru)_4(\eta^6,\eta^6,\eta^6,\eta^6\text{-}p\text{-quaterphenyl})]^{4+}$ and the hexacation $[(Cp^*Ru)_6(\eta^6,\eta^6,\eta^6,\eta^6,\eta^6,\eta^6\text{-}p\text{-sexiphenyl})]^{6+}$, respectively, which are isolated as their triflate salts. While insoluble in $CH_2Cl_2$, both are very soluble in $CH_3NO_2$ and are readily isolated by precipitation with diethyl ether. Spectral characterization data are presented in Tables I and II.

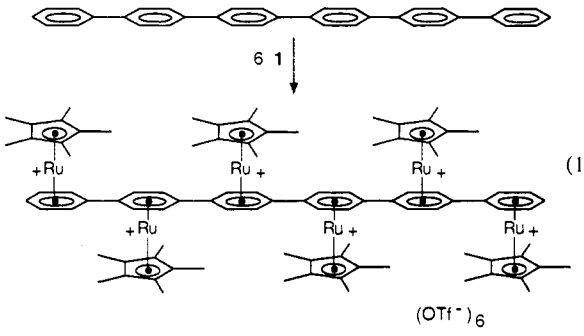


(13)

The structure of the *p*-quaterphenyl derivative has been determined by a single-crystal X-ray structural analysis of the complex $[(Cp^*Ru)_4(\eta^6,\eta^6,\eta^6,\eta^6\text{-}p\text{-quaterphenyl})]^{4+}(OTf^-)_4$. An ORTEP drawing of the tetracation is shown in Figure 18, and a van der Waals space-filling model is depicted in Figure 19. Bond distances and bond angles are listed in Tables XVII and XVIII. Other important structural parameters are listed in Table XIX.

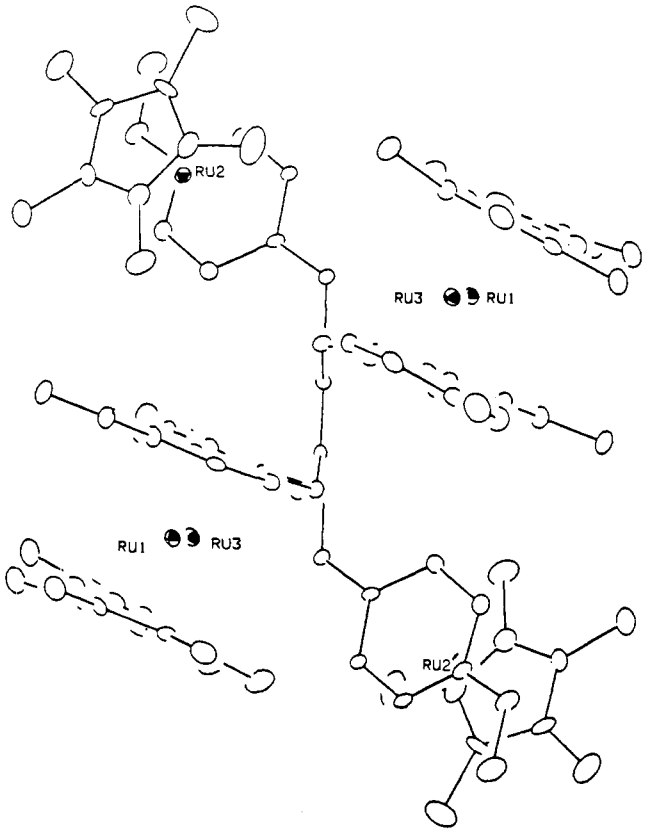


**Figure 15.** ORTEP drawing of the hexacation $\{[Cp^*Ru(p\text{-}CH_3O\text{-}\eta\text{-}C_6H_4\text{-}O]_6C_6\}^{6+}$ looking parallel to the central $C_6O_6$ plane (H atoms omitted).

The tetracation consists of four Cp*Ru groups bound in a $\eta^6$ fashion to each of the arene rings of the *p*-quaterphenyl nucleus. The molecule has an inversion center located at the midpoint of the bond C10′–C10′ connecting the two central arene rings. The two unique Cp*(centroid)–Ru distances are 1.819 (4) and 1.809 (4) Å for Ru(1) and Ru(2), respectively. For the corresponding arene(centroid)–Ru distances, the values are 1.706 (4) and 1.714 (4) Å. No bending of the Cp* ligand is observed with the Cp*(centroid)–Ru–arene(centroid) angles being 179.0 (2)° and 178.5 (2)°. These values are similar to the other values reported for sterically uncrowded molecules in this paper. While the end phenyl ring mean plane is twisted by 27.5° with respect to the mean plane of the adjacent central arene ring, the two central arene ring mean planes are coplanar (0.0°) with respect to one another. Along the molecular axis of the *p*-quaterphenyl group there is little bending with the phenyl(centroid)–C20′–C13′ angle being 179.1 (3)°, and the central arene(centroid)–C10′–C10′ angle being 176.3 (4)°. In the structure of the parent *p*-quaterphenyl molecule, the average torsional angle between internal rings is 22.7°, and between the external and internal rings the angle is 17.1°.[29]

It can been seen that the Cp*Ru groups attached to the two central arene rings are on opposite sides of the *p*-quaterphenyl nucleus. Referring to the space-filling model in Figure 19, it is apparent that the bulky Cp* ligands cannot lie adjacent to one another. Thus the molecule adopts a zigzag arrangement of positively charged ruthenium centers. It is quite likely that the *p*-sexiphenyl derivative has a similar structural arrangement.

## Discussion

The propensity of the $Cp^*Ru^+$ fragment to form adducts with a variety of arene compounds in high yield under relatively mild conditions appears to be unparalled by any other transition-metal fragment. The reagent $Cp^*Ru(CH_3CN)_3^+OTf^-$ reported here is especially useful as it can be prepared in large quantities. The use of the triflate counterion and the well-known solubilizing power of the Cp* ligand[30] are the keys to preparing *soluble* highly charged species such as the tetrahedral tetracation $\{[Cp^*Ru(\eta\text{-}C_6H_5)]_4C\}^{4+}$, the octahedral hexacation $\{[Cp^*Ru(p\text{-}CH_3O\text{-}\eta\text{-}C_6H_4\text{-}O)]_6C_6\}^{6+}$, and the *p*-sexiphenyl hexacationic derivative $[(Cp^*Ru)_6(\eta^6,\eta^6,\eta^6,\eta^6,\eta^6,\eta^6\text{-}p\text{-sexiphenyl})]^{6+}$.

The strength of the ruthenium–arene interaction can be appreciated from the synthesis and the structural determination of the tetraphenylmethane derivative $\{[Cp^*Ru(\eta\text{-}C_6H_5)]_4C\}^{4+}$. This molecule can be prepared despite extensive steric congestion between Cp* ligands and between Cp* ligands and the phenyl groups. Also, four positively charged centers are being placed within the same molecule. In retrospect, the strength of this interaction may not be surprising since Ru(II) is an excellent $\pi$-donor, and the electron-donating Cp* ligand[31] should enhance this ability. As we have reported elsewhere, the substitution of $Cp^*Ru^+$ fragments onto the phenyl groups of 5,6,11,12-tetraphenylnaphthacene (rubrene) was observed to twist the naphthacene functionality into a helical shape;[32] this again emphasizes the strong ruthenium to phenyl interaction.

We tend to view the positive charge in the molecules reported here as being primarily localized on the ruthenium atom. This is supported to some extent by the preparation of the *p*-quaterphenyl and *p*-sexiphenyl derivatives $[(Cp^*Ru)_4(\eta^6,\eta^6,\eta^6,\eta^6\text{-}p\text{-quaterphenyl})]^{4+}$ and $[(Cp^*Ru)_6(\eta^6,\eta^6,\eta^6,\eta^6,\eta^6,\eta^6\text{-}p\text{-sexiphenyl})]^{6+}$ in which the positively charged Cp*Ru fragments are bound to adjacent arene rings. If substantial positive charge were delocalized onto the arene carbon atoms and taking into consideration that the central arene rings in these molecules are coplanar, then formation of these stable highly substituted molecules would be unlikely to occur.

Using the $Cp^*Ru^+$ fragment as a positive charge carrier and aromatic organic molecules as geometric templates has allowed us to prepare a variety of rigid molecules with particular arrangements and distributions of charge such as those illustrated in Scheme I. Thus reaction of **1** with a simple arene gives the trivial "zero-dimensional" case of one positive charge contained within a molecule. Use of [2$_2$]-1,4-cyclophane as a linear template allows the preparation of "one-dimensional" molecules with a $(1^+)$-$(1^+)$, $(1^+)$-$(2^+)$, and $(1^+)$-$(2^+)$-$(1^+)$ linear array of charges down the molecular axis as illustrated by the preparation of the complexes $[(Cp^*Ru)_2(\eta^6,\eta^6\text{-}[2_2]\text{-}1,4\text{-cyclophane})]^{2+}(OTf^-)_2$, $[Cp^*Ru(\eta^6,\eta^6\text{-}[2_2]\text{-}1,4\text{-cyclophane})CoCp^*]^{3+}(OTf^-)_3$, and $\{[Cp^*Ru(\eta^6,\eta^6\text{-}[2_2]\text{-}1,4\text{-cyclophane})]_2Ru\}^{4+}(OTf^-)_4$, respectively. In principle, many other extended linear arrays of charge should be obtainable using this or related approaches. These molecules offer the opportunity to examine the effect in extended one-dimensional molecular solids of changes in the magnitude and distances between charges along the molecular axis. Progressing to the "two-dimensional" cases, we have been able to prepare one example, namely the triangular trication $[(Cp^*Ru)_3(\eta^6,\eta^6,\eta^6\text{-triptycene})]^{3+}$ with triptycene as the template. Clearly, other two-dimensional geometries of charge (square tetracation, pentagonal pentacation, etc.) should be accessible with use of the appropriate arene precursor.

Finally, we come to the "three-dimensional" charge arrangements as represented by the preparation of the tetrahedral tetracations $\{[Cp^*Ru(\eta\text{-}C_6H_5)]_4E\}^{4+}$ (E = C, Si, Ge, Sn, Pb) and the octahedral hexacation $\{[Cp^*Ru(p\text{-}CH_3O\text{-}\eta\text{-}C_6H_4\text{-}O)]_6C_6\}^{6+}$. The tetrahedral tetracations are an intriguing set since the distance between the positively charged ruthenium centers can be varied on changing the central atom from carbon to silicon. In preparing solid-state compounds, it is intended that this should provide a means to vary systematically the lattice parameters by switching from the carbon tetracation to the silicon analogue and observe

(29) (a) Baudour, J. L.; Delugeard, Y.; Rivet, P. *Acta. Crystallogr.* **1978**, *B34*, 625–628. (b) Delugeard, Y.; Deusche, J.; Baudour, J. L. *Acta. Crystallogr.* **1976**, *B32*, 702–705.

(30) Manriquez, J. M.; Fagan, P. J.; Schertz, L. D.; Marks, T. J. *Inorg. Synth.* **1982**, *21*, 181–185.

(31) Bordwell, F. G.; Bausch, M. J. *J. Am. Chem. Soc.* **1983**, *105*, 6188–6189.

(32) Fagan, P. J.; Ward, M. D.; Caspar, J. V.; Calabrese, J. C.; Krusic, P. J. *J. Am. Chem. Soc.* **1988**, *110*, 2981–2983.

Table XVI. Important Structural Parameters for the Hexacation $\{[Cp^*Ru(p\text{-}CH_3O\text{-}\eta\text{-}C_6H_4\text{-}O]_6C_6\}^{6+}$ [a]

| parameter | value | parameter | value |
|---|---|---|---|
| | | Distances, Å | |
| Cp*(centroid)-Ru1 | 1.818 (10) | Ru2-Ru3 | 8.142 (4) |
| Cp*(centroid)-Ru2 | 1.811 (10) | Ru2-Ru2′ | 11.005 (4) |
| Cp*(centroid)-Ru3 | 1.817 (10) | Ru2-Ru3′ | 8.417 (4) |
| | | Ru3-Ru3′ | 11.148 (4) |
| Ru1-Ru2 | 7.354 (4) | | |
| Ru1-Ru3 | 8.474 (4) | arene(centroid)-Ru1 | 1.724 (10) |
| Ru1-Ru1′ | 11.092 (4) | arene(centroid)-Ru2 | 1.736 (10) |
| Ru1-Ru2′ | 8.246 (4) | arene(centroid)-Ru3 | 1.741 (10) |
| Ru1-Ru3′ | 7.200 (4) | | |
| | | $C_6O_6$(centroid)-Ru1 | 5.546 (9) |
| | | $C_6O_6$(centroid)-Ru2 | 5.502 (9) |
| | | $C_6O_6$(centroid)-Ru3 | 5.574 (9) |
| | | Angles, deg | |
| C11″-O11″-C1″-C3″ | 53.5 | Cp*(centroid)-Ru1-arene(centroid) | 177.3 (5) |
| C21″-O21″-C2″-C1″ | 58.4 | Cp*(centroid)-Ru2-arene(centroid) | 177.0 (5) |
| C31″-O31″-C3″-C1″ | 53.2 | Cp*(centroid)-Ru3-arene(centroid) | 176.0 (5) |
| C17″-O14″-C14″-C15″ | 2.0 | C16″-C11″-O11″-C1″ | 36.0 |
| C27″-O24″-C24″-C25″ | 2.3 | C22″-C21″-O21″-C2″ | 21.2 |
| C37″-O34″-C34″-C35″ | 2.2 | C32″-C31″-O31″-C3″ | 28.7 |

[a] Numbers in parentheses are estimated standard deviations that were calculated or were chosen as the maximum values observed for other representative distances or angles.

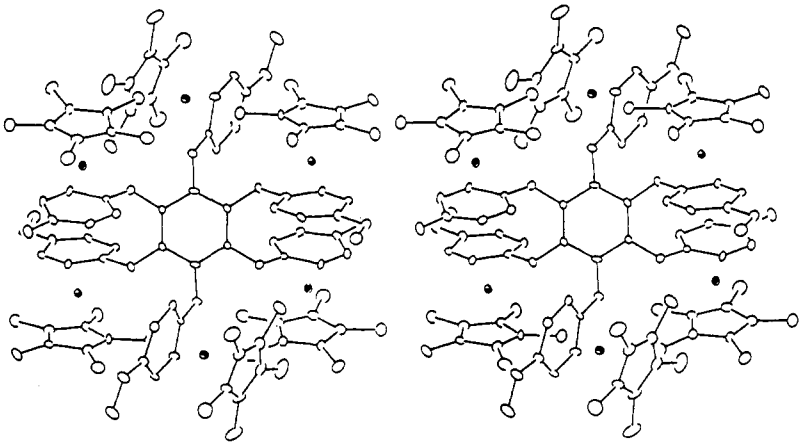

Figure 16. Stereoview of the hexacation $\{[Cp^*Ru(p\text{-}CH_3O\text{-}\eta\text{-}C_6H_4\text{-}O]_6C_6\}^{6+}$.

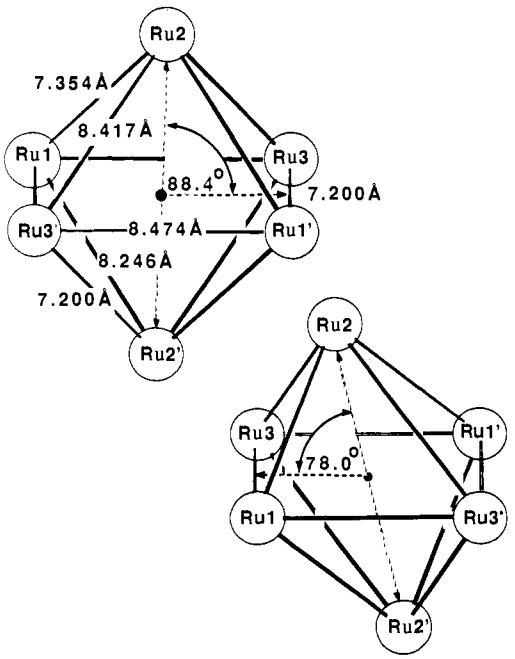


Figure 17. Ru atom geometry in the hexacation $\{[Cp^*Ru(p\text{-}CH_3O\text{-}\eta\text{-}C_6H_4\text{-}O]_6C_6\}^{6+}$

any changes in physical properties. Progressing from silicon to germanium does not on average increase the distance between positively charged ruthenium centers in this particular series because of the special steric demands of these molecules (vide supra). The synthesis of the tetrahedral trication $\{[Cp^*Ru(\eta\text{-}C_6H_5)]_4B\}^{3+}$ which has the same overall shape as the carbon and silicon analogues, but differs in charge by one unit, brings about the possibility of using this molecule as a "dopant" by partial substitution into a growing lattice built up from the tetrahedral tetracations. (This would be a molecular analogue of using boron as a p-dopant in elemental silicon.)

Our initial efforts to apply and demonstrate the concepts outlined in this paper for controlling crystallization of molecular constituents are presented in the following paper.[1] Crystallization of some of the ruthenium cations reported here with planar organic polycyanoanions is described. Although in these particular anions the negative charge is delocalized over the molecular framework,

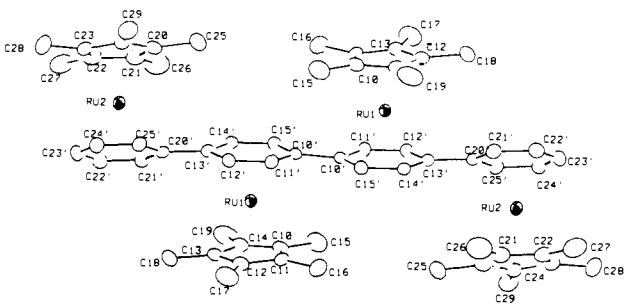

Figure 18. ORTEP drawing and numbering scheme for the tetracation $[(Cp^*Ru)_4(\eta^6,\eta^6,\eta^6,\eta^6\text{-}p\text{-quaterphenyl})^{4+}$ (H atoms omitted).

**Table XVII.** Interatomic Distances for $[(Cp^*Ru)_4(\eta^6,\eta^6,\eta^6,\eta^6\text{-}p\text{-quaterphenyl})]^{4+}$ (Å)[a]

| atoms | distance | atoms | distance | atoms | distance | atoms | distance | atoms | distance |
|---|---|---|---|---|---|---|---|---|---|
| Ru1–C10 | 2.183 (4) | Ru2–C20′ | 2.238 (3) | C10–C14 | 1.430 (6) | C13–C14 | 1.426 (5) | C21–C22 | 1.434 (6) |
| Ru1–C10′ | 2.218 (3) | Ru2–C21 | 2.176 (4) | C10–C15 | 1.498 (6) | C13–C18 | 1.495 (6) | C21–C26 | 1.498 (7) |
| Ru1–C11 | 2.178 (4) | Ru2–C21′ | 2.209 (4) | C10′–C10′a | 1.488 (7) | C13′–C14′ | 1.416 (5) | C21′–C22′ | 1.404 (5) |
| Ru1–C11′ | 2.212 (4) | Ru2–C22 | 2.180 (4) | C10′–C11′ | 1.420 (5) | C13′–C20′ | 1.488 (5) | C22–C23 | 1.427 (6) |
| Ru1–C12 | 2.190 (4) | Ru2–C22′ | 2.214 (4) | C10′–C15′ | 1.426 (5) | C14–C19 | 1.487 (6) | C22–C27 | 1.492 (6) |
| Ru1–C12′ | 2.226 (4) | Ru2–C23 | 2.172 (4) | C11–C12 | 1.433 (6) | C14′–C15′ | 1.414 (5) | C22′–C23′ | 1.409 (6) |
| Ru1–C13 | 2.193 (4) | Ru2–C23′ | 2.216 (4) | C11–C16 | 1.497 (6) | C20–C21 | 1.419 (6) | C23–C24 | 1.428 (6) |
| Ru1–C13′ | 2.242 (4) | Ru2–C24 | 2.182 (4) | C11′–C12′ | 1.416 (5) | C20–C24 | 1.428 (6) | C23–C28 | 1.493 (6) |
| Ru1–C14 | 2.189 (4) | Ru2–C24′ | 2.218 (4) | C12–C13 | 1.427 (5) | C20–C25 | 1.503 (6) | C23′–C24′ | 1.399 (6) |
| Ru1–C14′ | 2.211 (3) | Ru2–C25′ | 2.225 (4) | C12–C17 | 1.505 (6) | C20′–C21′ | 1.423 (5) | C24–C29 | 1.507 (6) |
| Ru1–C15′ | 2.203 (4) | C10–C11 | 1.421 (6) | C12′–C13′ | 1.418 (5) | C20′–C25′ | 1.420 (5) | C24′–C25′ | 1.408 (5) |
| Ru2–C20 | 2.180 (4) | | | | | | | | |

[a] Numbers in parentheses are estimated standard deviations in the least significant figure.

**Table XVIII.** Intramolecular Bond Angles for $[(Cp^*Ru)_4(\eta^6,\eta^6,\eta^6,\eta^6\text{-}p\text{-quaterphenyl})]^{4+}$ (deg)[a]

| atoms | angle | atoms | angle | atoms | angle | atoms | angle |
|---|---|---|---|---|---|---|---|
| C11–C10–C14 | 108.2 (4) | C13–C12–C17 | 126.1 (4) | C10′–C15′–C14′ | 120.9 (3) | C21–C22–C27 | 125.7 (5) |
| C11–C10–C15 | 126.1 (5) | C11′–C12′–C13′ | 121.1 (3) | C21–C20–C24 | 108.7 (4) | C23–C22–C27 | 126.2 (5) |
| C14–C10–C15 | 125.6 (5) | C12–C13–C14 | 108.5 (3) | C21–C20–C25 | 125.4 (4) | C21′–C22′–C23′ | 120.1 (4) |
| C10′a–C10′–C11′ | 122.0 (4) | C12–C13–C18 | 126.0 (4) | C24–C20–C25 | 125.9 (4) | C22–C23–C24 | 108.1 (4) |
| C10′a–C10′–C15′ | 120.2 (4) | C14–C13–C18 | 125.4 (4) | C13′–C20′–C21′ | 120.6 (3) | C22–C23–C28 | 125.8 (4) |
| C11′–C10′–C15′ | 117.7 (3) | C12′–C13′–C14′ | 117.8 (3) | C13′–C20′–C25′ | 120.5 (3) | C24–C23–C28 | 126.1 (4) |
| C10–C11–C12 | 108.2 (4) | C12′–C13′–C20′ | 120.2 (3) | C21′–C20′–C25′ | 118.9 (3) | C22′–C23′–C24′ | 119.8 (4) |
| C10–C11–C16 | 126.9 (4) | C14′–C13′–C20′ | 121.9 (3) | C20–C21–C22 | 107.6 (4) | C20–C24–C23 | 107.6 (4) |
| C12–C11–C16 | 124.7 (4) | C10–C14–C13 | 107.6 (4) | C20–C21–C26 | 127.3 (4) | C20–C24–C29 | 126.3 (4) |
| C10′–C11′–C12′ | 121.1 (3) | C10–C14–C19 | 124.7 (4) | C22–C21–C26 | 125.0 (4) | C23–C24–C29 | 126.1 (4) |
| C11–C12–C13 | 107.5 (4) | C13–C14–C19 | 127.6 (4) | C20′–C21′–C22′ | 120.5 (4) | C23′–C24′–C25′ | 120.9 (4) |
| C11–C12–C17 | 126.4 (4) | C13′–C14′–C15′ | 121.4 (3) | C21–C22–C23 | 108.0 (4) | C20′–C25′–C24′ | 119.8 (4) |

[a] Numbers in parentheses are estimated standard deviations in the least significant figure.

**Table XIX.** Important Structural Parameters for the Tetracation $[(Cp^*Ru)_4(\eta^6,\eta^6,\eta^6,\eta^6\text{-}p\text{-quaterphenyl})]^{4+}$ [a]

| distance | value, Å | angle | value, deg |
|---|---|---|---|
| Cp*(centroid)–Ru1 | 1.819 (4) | Cp*(centroid)–Ru1–phenyl(centroid) | 179.0 (2) |
| Cp*(centroid)–Ru2 | 1.809 (4) | Cp*(centroid)–Ru2–arene(centroid) | 178.5 (2) |
| phenyl(centroid)–Ru1 | 1.706 (4) | phenyl(centroid)–C20′–C13′ | 179.1 (3) |
| arene(centroid)–Ru2 | 1.714 (4) | arene(centroid)–C10′–C10′ | 176.3 (4) |
| | | arene(centroid)–C20′–C13′ | 176.8 (3) |
| Ru1–Ru2 | 5.463 (1) | | |
| Ru2–Ru2′ | 5.448 (1) | phenyl(plane)–arene(plane) | 27.5 |
| Ru1–Ru2′ | 8.822 (1) | | |
| Ru1–Ru1′ | 13.626 (1) | arene(plane)–arene′(plane) | 0.0 |

[a] Numbers in parentheses are estimated standard deviations which were calculated or were chosen as the maximum values observed for other representative distances or angles.

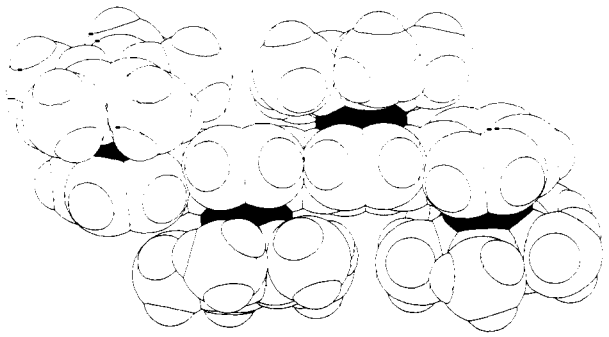

**Figure 19.** A van der Waals space-filling model of the tetracation $[(Cp^*Ru)_4(\eta^6,\eta^6,\eta^6,\eta^6\text{-}p\text{-quaterphenyl})]^{4+}$ constructed from the X-ray structural coordinates.

the propensity of these anions to align in one-dimensional stacks due to $\pi$–$\pi$ interactions in the solid helps to limit the number of lattice geometries possible. We show that the charge geometry of some of the ruthenium complexes reported here can influence the stacking motif of these flattened anionic cyanohydrocarbons. Specifically, the linear rod-like dication $[(Cp^*Ru)_2(\eta^6,\eta^6\text{-}[2_2]\text{-}1,4\text{-cyclophane})]^{2+}$ is used to promote the formation of "one-dimensional" stacks of the anions in the solid state. In the case of the tetrahedral tetracations $\{[Cp^*Ru(\eta\text{-}C_6H_5)]_4E\}^{4+}$ (E = C, Si) (in which two perpendicular axes of dipositive charge exist (Figure 13)), it was thought that crystallization with planar cyanohydrocarbons would lead to solid phases which contain cyanohydrocarbon stacks that are mutually perpendicular. This has in fact been realized.[1]

## Conclusion

In summary, use of the $Cp^*Ru^+$ fragment allows the preparation of molecules with particular shapes and geometries of localized positive charge. This will allow us to test the concept of whether geometric control over localized electrostatic forces can lead to predictable construction of three-dimensional solid-state molecular lattices; our initial efforts in this regard are encouraging. Although we have been using organometallic reagents, the possibility of using organic, main group, or inorganic coordination complexes as the charge carriers also exists. There is very little fundamental knowledge and understanding of how to control molecular packing, or as we are attempting here, to build in a predictable manner solid lattices starting from a basic precept. Such knowledge should ultimately aid in designing molecular solids with desirable physical properties.

## Experimental Section

All procedures were carried out in a glovebox equipped with a constant nitrogen flush, or in Schlenk-type glassware interfaced to a high-vacuum ($10^{-4}$–$10^{-5}$ Torr) line. Solvents were dried and distilled under dinitrogen

before use by employing the following drying agents: tetrahydrofuran (THF) and diethyl ether (Na dispersion); $CH_2Cl_2$ ($CaH_2$); $CH_3NO_2$ (vacuum transfer from $P_2O_5$); $CH_3CN$ ($P_2O_5$). (Note: THF or ether should not be distilled from Na/benzophenone ketyl. This leads to contamination of these solvents by trace amounts of benzene which reacts with **1** forming the cation $Cp^*Ru(\eta\text{-}C_6H_6)^+$; this can contaminate the final product in certain cases.) The following chemicals were purchased from commercial sources and used without further purification: Aldrich, Alfa: [2$_2$]-1,4-cyclophane, tetraphenylmethane, tetraphenylsilane, tetraphenylgermane, tetraphenylstannane, tetraphenylplumbane, triptycene, tetraphenylantimonium chloride, *p*-quaterphenyl, sodium tetraphenylborate, triethylborohydride (1 M in THF). K&K: *p*-sexiphenyl. The compound $Cp^*RuCl_2$ was prepared by scaling up and following the literature procedure of Tilley et al.[11a] (40.00 g of $RuCl_3\cdot 3H_2O$ was dissolved in 800 mL of $CH_3OH$ and filtered into a flask containing 55.0 mL of $(CH_3)_5C_5H$; this was refluxed for 3 h under $N_2$; the volume was reduced to 700 mL in vacuo; the crystalline dark precipitate was isolated by filtration, was washed with methanol and hexane, and was dried thoroughly under high vacuum. Yield: 43.18 g (92%)). The compound $Cp^*CoCl_2$ was prepared by the procedure of Koelle et al.[33] The compound hexakis(*p*-methoxyphenoxy)benzene was prepared from *p*-methoxyphenoxide by using the procedures reported by MacNicol et al.[28] We thank Dr. Wilson Tam for generously providing us with a sample of this compound. The complex ($\eta^4$-1,3-cyclohexadiene)Ru($\eta^6$-[2$_2$]-1,4-cyclophane) was prepared according to the literature procedure.[10d] For all of the filtration steps in the procedures below, medium porosity fritted glass apparati were used.

Some of the complexes reported below (especially the more highly charged species which were recrystallized from $CH_3NO_2$/ether) tended to contain varying amounts of $CH_3NO_2$ of crystallization. For analytical purposes, the majority of this was removed by heating under high vacuum.

**[Cp*Ru($\mu_3$-Cl)]$_4$.** A 300-mL round-bottomed flask was charged with 20.28 g (66.01 mmol) of $Cp^*RuCl_2$ and 113 mL of THF. Then 66.0 mL of 1 M lithium triethylborohydride in THF (66.0 mmol) were added all at once to the solution via syringe. The reaction mixture turned a dark blue-green color initially during the addition, and gas evolution was observed. After 45 min of stirring, the crystalline orange precipitate which formed was isolated by filtration and was rinsed twice with small amounts (ca. 5 mL) of THF. It was then dried in vacuo to yield 14.18 g of crystalline orange $[Cp^*Ru(\mu_3\text{-}Cl)]_4$ (79%). Anal. Calcd for $C_{40}H_{60}Ru_4Cl_4$: C, 44.20; H, 5.56, Cl, 13.05. Found: C, 44.55; H, 5.61; Cl, 12.80. $^1$H NMR (300 MHz, THF-$d_8$, 25 °C): $\delta$ 1.56 (s, Cp*).

**[Cp*Ru(CH$_3$CN)$_3^+$]OTf$^-$ (1).** A 300-mL round-bottomed flash was charged with 30.00 g (27.60 mmol) of $[Cp^*Ru(\mu_3\text{-}Cl)]_4$ and 200 mL of acetonitrile. The mixture was refluxed for 1 h and then allowed to cool to room temperature. To the stirred mixture were added 28.359 g (110.4 mmol) of silver trifluoromethanesulfonate whereupon a white precipitate of AgCl formed. After 1 h of stirring, the solution was filtered, and solvent was removed from the filtrate in vacuo. Diethyl ether (100 mL) was added to the residue, and the orange-yellow crystalline solid was collected by filtration, washed twice with 20-mL portions of diethyl ether, and dried in vacuo to yield 53.43 g of **1** (95%). Anal. Calcd for $C_{17}H_{24}F_3N_3O_3SRu$: C, 40.15; H, 4.76; N, 8.26. Found: C, 40.16; H, 4.75; N, 8.10. $^1$H NMR (300 MHz, THF-$d_8$, 25 °C): $\delta$ 1.61 (s, 15 H, Cp*); 2.39 (slightly broad s, 9 H, $CH_3CN$).

**[Cp*Ru($\eta$-C$_6$H$_6$)]$^+$OTf$^-$ (3a).** A 25-mL flask was charged with 0.300 g (0.590 mmol) of **1** and 20 mL of $CH_2Cl_2$. Benzene (100 $\mu$L, 1.12 mmol) was then added, and the solution was stirred at room temperature for 3 h. The solution was then filtered, and 20 mL of diethyl ether were added to the filtrate. The white solid which precipitated was isolated by filtration, rinsed twice with 2-mL portions of diethyl ether, and dried in vacuo to yield 0.201 g of a white crystalline solid. Another 0.050 g was obtained by addition of 30 mL of diethyl ether to the filtrate and isolating the white solid which formed by filtration. Total yield: 0.251 g (92%). Anal. Calcd for $C_{17}H_{21}F_3O_3SRu$: C, 44.06; H, 4.57. Found: C, 43.78; H, 4.54.

**[Cp*Ru($\eta$-C$_6$H$_5$CH$_3$)]$^+$OTf$^-$ (3b).** A 25-mL flask was charged with 0.300 g (0.590 mmol) of **1** and 20 mL of $CH_2Cl_2$. Toluene (100 $\mu$L, 0.941 mmol) was added, and the solution was stirred at room temperature for 3 h. The solution was then filtered, and 60 mL of diethyl ether were added to the filtrate. The white solid which precipitated was isolated by filtration, rinsed twice with 2-mL portions of diethyl ether, and dried in vacuo to yield 0.226 g of a white solid. Another 0.026 g was obtained by adding 30 mL of diethyl ether to the filtrate and isolating the white solid which formed by filtration. Total yield: 0.252 g (89%). Anal. Calcd for $C_{18}H_{23}F_3O_3SRu$: C, 45.28; H, 4.86. Found: C, 45.26; H, 4.71.

**[Cp*Ru($\eta$-C$_6$(CH$_3$)$_3$H$_3$)]$^+$OTf$^-$ (3c).** A 100-mL flask was charged with 0.600 g (1.18 mmol) of **1** and 400 $\mu$L (2.88 mmol) of mesitylene. After addition of 40 mL of THF, the mixture was refluxed for 15 min. The solution was filtered, and solvent was removed from the filtrate in vacuo. Diethyl ether (30 mL) was added to the residue. The white solid was isolated by filtration, washed twice with 5-mL portions of diethyl ether, and then dried in vacuo. Yield: 0.548 g (92%). Anal. Calcd for $C_{20}H_{27}F_3O_3SRu$: C, 47.52; H, 5.38. Found: C, 47.14; H, 5.25.

**{Cp*Ru[$\eta$-C$_6$(CH$_3$)$_6$]}$^+$OTf$^-$ (3d).** A 100-mL flask was charged with 0.600 g (1.18 mmol) of **1** and 0.323 g (1.99 mmol) of hexamethylbenzene. After addition of 40 mL of THF, the mixture was refluxed for 5 h. Solvent was removed in vacuo. The residue was dissolved in 20 mL of $CH_2Cl_2$ and was filtered. Addition of 10 mL of THF to the filtrate formed a white precipitate which was collected by filtration, washed twice with 2-mL portions of THF and twice with 5-mL portions of diethyl ether, and then dried in vacuo. Yield: 0.570 g (88%). Anal. Calcd for $C_{23}H_{33}F_3O_3SRu$: C, 50.44; H, 6.07. Found: C, 50.20; H, 5.96.

**[Cp*Ru($\eta$-C$_6$H$_5$CH=O)]$^+$OTf$^-$ (3e).** A 25-mL flask was charged with 0.300 g (0.590 mmol) of **1** and 20 mL of $CH_2Cl_2$. Benzaldehyde (100 $\mu$L, 0.984 mmol) was added, and the solution was stirred at room temperature for 3 h. The solution was then filtered, and 60 mL of diethyl ether were added to the filtrate. The white solid which precipitated was isolated by filtration, rinsed twice with 2-mL portions of diethyl ether, and dried in vacuo to yield 0.246 g (85%) of a white solid. Anal. Calcd for $C_{18}H_{21}F_3O_4SRu$: C, 43.99; H, 4.31. Found: C, 43.56; H, 4.16.

**[Cp*Ru($\eta$-C$_6$H$_5$CH=CH$_2$)]$^+$OTf$^-$ (3f).** A 100-mL round-bottomed flask equipped with a Teflon stopcock and magnetic stirring bar was charged with 0.800 g (1.57 mmol) of **1** and 400 $\mu$L (3.49 mmol) of styrene. After 10 mL of $CH_2Cl_2$ were added to the flask, the stopcock was sealed and the flask was placed in an oil bath maintained at 60 °C behind a safety shield. After being stirred for 1.5 h, the solution was filtered, and 50 mL of diethyl ether were added to the filtrate. The white precipitate which formed was collected by filtration, washed with small amounts of diethyl ether, and dried in vacuo. Yield: 0.716 g (93%). Anal. Calcd for $C_{19}H_{23}F_3O_3SRu$: C, 46.62; H, 4.74. Found: C, 46.54; H, 4.72.

**[(Cp*Ru)$_2$($\eta^6$,$\eta^6$-[2$_2$]-1,4-cyclophane)]$^{2+}$(OTf$^-$)$_2$.** A 100-mL round-bottom flask was charged with 0.600 g (1.18 mmol) of **1**, 0.122 g (0.586 mmol) of [2$_2$]-1,4-cyclophane, and 20 mL of THF. The reaction mixture was refluxed for 1 h, and was then cooled to room temperature. The white precipitate which was present was collected by filtration, washed three times with 2-mL portions of THF, and dried in vacuo to yield 0.543 g of product. The solid was dissolved in 10 mL of $CH_2Cl_2$, and this solution was filtered. Solvent was removed from the filtrate in vacuo, and 10 mL of THF were added to the residue. The white solid was isolated by filtration, rinsed twice with 2-mL portions of THF and once with 10 mL of diethyl ether, and dried in vacuo. Yield: 0.520 g (91%). Anal. Calcd for $C_{38}H_{46}F_6O_6S_2Ru_2$: C, 46.62; H, 4.74. Found: C, 46.80; H, 4.70.

**[(Cp*Co)($\eta^6$-[2$_2$]-1,4-cyclophane)]$^{2+}$(OTf$^-$)$_2$.** A 100-mL round-bottomed flask was charged with 0.500 g (1.89 mmol) of $Cp^*CoCl_2$ and 20 mL of acetone. Then 0.969 g (3.77 mmol) of $AgO_3SCF_3$ were added to the flask, and after 20 min of stirring, the solution was filtered from precipitated AgCl. Solvent was removed from the filtrate in vacuo. Then, 0.420 g (2.02 mmol) of [2$_2$]-1,4-cyclophane and 20 mL of $CH_2Cl_2$ were added to the residue. After addition of 1.00 mL of trifluoromethanesulfonic acid, the mixture was warmed for 10 min in a 50 °C oil bath. After the mixture was cooled to room temperature, 70 mL of diethyl ether were added slowly to the flask. The crude product was collected by filtration, washed twice with 20-mL portions of diethyl ether, and dried in vacuo. The product was dissolved in 25 mL of acetonitrile, and this solution was filtered. Slow addition of 75 mL of diethyl ether to the filtrate precipitated orange crystals that were collected by filtration, washed twice with 10-mL portions of diethyl ether, and dried in vacuo. Yield: 0.633 g (48%). Anal. Calcd for $C_{28}H_{31}F_6O_6S_2Co$: C, 48.00; H, 4.46. Found: C, 47.90; H, 4.48.

**[Cp*Ru($\eta^6$,$\eta^6$-[2$_2$]-1,4-cyclophane)CoCp*]$^{3+}$(OTf$^-$)$_3$.** A 25-mL flask was charged with 0.250 g (0.357 mmol) of [(Cp*Co)($\eta^6$-[2$_2$]-1,4-cyclophane)]$^{2+}$(OTf$^-$)$_2$, 0.185 g (0.364 mmol) of **1**, and 10 mL of $CH_2Cl_2$. The mixture was warmed in an oil bath maintained at 60 °C for 10 min. An orange precipitate was observed, and after the flask was allowed to cool to room temperature, the solid was collected by filtration, washed twice with 1-mL portions of $CH_2Cl_2$, and dried in vacuo. Yield: 0.330 g (85%). Anal. Calcd for $C_{39}H_{46}F_9O_9S_3CoRu$: C, 43.14; H, 4.27. Found: C, 42.57; H, 4.03.

**[($\eta^6$-[2$_2$]-1,4-cyclophane)$_2$Ru]$^{2+}$(OTf$^-$)$_2$.** A 300-mL round-bottomed flask equipped with a reflux condenser was charged with 0.900 g (2.31 mmol) of ($\eta^4$-1,3-cyclohexadiene)Ru($\eta^6$-[2$_2$]-1,4-cyclophane), 0.700 g (3.36 mmol) of [2$_2$]-1,4-cyclophane, and 20 mL of acetone. Then 1.2 mL (13.6 mmol) of trifluoromethanesulfonic acid were added carefully

(33) (a) Koelle, U.; Fuss, B. *Chem. Ber.* **1984**, *117*, 743–752. (b) Koelle, U.; Fuss, B. *Chem. Ber.* **1984**, *117*, 753–762.

with stirring. The solution was refluxed, and then an additional 0.6 mL (6.8 mmol) of trifluoromethanesulfonic acid were added slowly and carefully to the reaction mixture. After refluxing for 1 h, the solution was cooled, and 250 mL of diethyl ether were added to the flask. The solid in the flask was collected by filtration, washed three times with 10-mL portions of ether, and dried. The solid was dissolved in ca. 20 mL of $CH_3NO_2$, and this solution was filtered. Addition of diethyl ether precipitated the product which was then collected by filtration, washed with ether, and dried in vacuo. Yield: 1.1 g (58%). Anal. Calcd for $C_{34}H_{32}F_6O_6S_2Ru$: C, 50.06; H, 3.95. Found: C, 49.61; H, 3.86.

**{[Cp*Ru($\eta^6$,$\eta^6$-[2$_2$]-1,4-cyclophane)]$_2$Ru}$^{4+}$(OTf$^-$)$_4$.** A 25-mL flask equipped with a Teflon stopcock and magnetic stirring bar was charged with 0.200 g (0.245 mmol) of [($\eta^6$-[2$_2$]-1,4-cyclophane)$_2$Ru]$^{2+}$(OTf$^-$)$_2$ and 0.249 g (0.490 mmol) of **1**. After addition of 20 mL of $CH_2Cl_2$, the Teflon stopcock was sealed. The reaction mixture was stirred at room temperature for 30 min and was then warmed to 60 °C in an oil bath behind a safety shield. Solvent was then removed in vacuo. The residue was dissolved in 15 mL of $CH_3NO_2$ and was filtered. Diethyl ether (30 mL) was added to the filtrate which precipitated a pale yellow solid. This was collected by filtration, rinsed with diethyl ether, and dried in vacuo. Yield: 0.363 g (93%). Anal. Calcd for $C_{56}H_{62}F_{12}O_{12}S_4Ru_3$: C, 42.40; H, 3.94. Found: C, 42.65; H, 3.82.

**[Cp*Ru($\eta^6$-triptycene)]$^+$OTf$^-$.** A 100-mL round-bottomed flask was charged with 0.300 g (1.18 mmol) of triptycene and 30 mL of $CH_2Cl_2$. The flask was cooled to 0 °C in an ice–water bath, and a solution of 0.300 g (0.590 mmol) of **1** in 20 mL of $CH_2Cl_2$ was added dropwise to the stirred solution. The mixture was stirred for 4.3 h at 0 °C and was then allowed to warm to room temperature. Solvent was removed in vacuo. THF (20 mL) was added to the residue, and the solution was filtered. Addition of 45 mL of diethyl ether to the filtrate precipitated a white solid that was isolated by filtration and washed twice with 10 mL of ether to yield 0.307 g of product after drying. The solid was dissolved in 5 mL of $CH_3NO_2$ and was filtered. Addition of 80 mL of ether precipitated a white product that was isolated by filtration, washed twice with 5-mL portions of diethyl ether, and dried in vacuo. Yield: 0.190 g (51%). Anal. Calcd for $C_{31}H_{29}F_3O_3SRu$: C, 58.21; H, 4.57. Found: C, 58.72; H, 4.43.

**Mixture of [*syn*-(Cp*Ru)$_2$($\eta^6$,$\eta^6$-triptycene)]$^{2+}$(OTf$^-$)$_2$ (*syn*-4) and [*anti*-(Cp*Ru)$_2$($\eta^6$,$\eta^6$-triptycene)]$^{2+}$(OTf$^-$)$_2$ (*anti*-4).** A 100-mL round-bottomed flask equipped with a Teflon stopcock and magnetic stirring bar was charged with 0.600 g (1.18 mmol) of **1** and 0.150 g (0.590 mmol) of triptycene. After adding 20 mL of $CH_2Cl_2$ to the flask, the stopcock was sealed and the flask was placed in an oil bath maintained at 60 °C behind a safety shield. After 1 h of stirring at 60 °C, solvent was removed and the residue was dried in vacuo. Then, 20 mL of $CH_2Cl_2$ were added to the flask and this was heated at 60 °C for 1 h. Solvent was removed in vacuo, the residue was dissolved in 10 mL of $CH_3NO_2$, and this solution was filtered. Addition of 40 mL of diethyl ether to the filtrate precipitated a white solid. The solid was collected by filtration, rinsed twice with 2-mL portions of diethyl ether, and dried in vacuo. Yield: 0.575 g (95%). Anal. Calcd for $C_{42}H_{44}F_6O_6S_2Ru_2$: C, 49.21; H, 4.33. Found: C, 49.35; H, 4.38.

**[(Cp*Ru)$_3$($\eta^6$,$\eta^6$,$\eta^6$-triptycene)]$^{3+}$(OTf$^-$)$_3$ and [*syn*-(Cp*Ru)$_2$($\eta^6$,$\eta^6$-triptycene)]$^{2+}$(OTf$^-$)$_2$ (*syn*-4).** A 100-mL round-bottomed flask equipped with a Teflon stopcock and magnetic stirring bar was charged with 0.180 g (0.708 mmol) of triptycene and 1.300 g (2.56 mmol) of **1**. After adding 40 mL of $CH_2Cl_2$ to the flask, the stopcock was sealed and the flask was placed in an oil bath maintained at 60 °C behind a safety shield. After the mixture was stirred for 1 h at 60 °C, solvent was removed and the residue was dried in vacuo. Then, 40 mL of $CH_2Cl_2$ were added to the flask and this was heated at 60 °C for 1 h. Solvent was removed in vacuo. The addition of 40 mL of $CH_2Cl_2$, heating for 1 h at 60 °C, and removal of solvent steps were repeated once more. After addition of 10 mL of THF to the residue, the insoluble material was collected by filtration and washed twice with 5-mL portions of tetrahydrofuran. The solid was then washed three times with 1-mL portions of $CH_2Cl_2$ and finally twice with 5-mL portions of diethyl ether. The combined tetrahydrofuran, $CH_2Cl_2$, and diethyl ether filtrate and washings (which contain the dication [*syn*-(Cp*Ru)$_2$($\eta^6$,$\eta^6$-triptycene)]$^{2+}$(OTf$^-$)$_2$) were retained. The isolated solid was taken up in 10 mL of $CH_3NO_2$ and was filtered. Diethyl ether (80 mL) was added to the filtrate which precipitated a white solid. This was collected by filtration, washed two times with 5-mL portions of ether, and dried in vacuo to yield 0.305 g (31%) of [(Cp*Ru)$_3$($\eta^6$,$\eta^6$,$\eta^6$-triptycene)]$^{3+}$(OTf$^-$)$_3$. Anal. Calcd for $C_{53}H_{59}F_9O_9S_3Ru_3$: C, 45.13; H, 4.22. Found: C, 44.73; H, 4.04.

Solvent was removed in vacuo from the combined tetrahydrofuran, $CH_2Cl_2$, and diethyl ether filtrate and washings that were retained above. The residue was dissolved in 10 mL of $CH_2Cl_2$, and then 8 mL of diethyl ether were added to this solution. This was filtered, and 10 mL of diethyl ether were added to the filtrate which precipitated a white solid. The solid was collected by filtration, washed twice with 10-mL portions of THF and then twice with 5-mL portions of diethyl ether, and dried. This yields 0.350 g (48%) of the dicationic complex [*syn*-(Cp*Ru)$_2$($\eta^6$,$\eta^6$-triptycene)]$^{2+}$(OTf$^-$)$_2$. Anal. Calcd for $C_{42}H_{44}F_6O_6S_2Ru_2$: C, 49.21; H, 4.33. Found: C, 48.47; H, 4.17.

**{[Cp*Ru($\eta$-C$_6$H$_5$)]$_4$C}$^{4+}$(OTf$^-$)$_4$ (5(C)$^{4+}$(OTf$^-$)$_4$).** A 100-mL round-bottomed flask equipped with a Teflon stopcock and magnetic stirring bar was charged with 0.161 g (0.502 mmol) of tetraphenylmethane and 1.200 g (2.360 mmol) of **1**. After 20 mL of $CH_2Cl_2$ were added to the flask, the stopcock was sealed and the flask was placed in an oil bath maintained at 60 °C behind a safety shield. After the mixture was stirred for 1 h, solvent was removed and the residue was dried in vacuo. Then, another 20 mL of $CH_2Cl_2$ were added to the flask and this was heated at 60 °C for 1 h. Solvent was removed in vacuo. The addition of 20 mL of $CH_2Cl_2$, heating for 1 h at 60 °C, and removal of solvent steps were repeated once more. After addition of 20 mL of $CH_2Cl_2$, the white solid was collected by filtration, rinsed twice with 2 mL of $CH_2Cl_2$, and dried in vacuo to yield 0.882 g. This was recrystallized by dissolving the solid in 15 mL of $CH_3NO_2$, filtering the solution, and adding 40 mL of diethyl ether to the filtrate. The white precipitate was collected by filtration, rinsed with diethyl ether, and dried in vacuo. Yield: 0.700 g (75%). Anal. Calcd for $C_{69}H_{80}F_{12}O_{12}S_4Ru_4$: C, 44.51; H, 4.33. Found: C, 43.55; H, 4.27.

**{[Cp*Ru($\eta$-C$_6$H$_5$)]$_4$Si}$^{4+}$(OTf$^-$)$_4$ (5(Si)$^{4+}$(OTf$^-$)$_4$).** A 100-mL round-bottomed flask equipped with a Teflon stopcock and magnetic stirring bar was charged with 0.168 g (0.499 mmol) of tetraphenylsilane and 1.200 g (2.360 mmol) of **1**. After 20 mL of $CH_2Cl_2$ were added to the flask, the stopcock was sealed and the flask was placed in an oil bath maintained at 60 °C behind a safety shield. After 1 h of stirring, solvent was removed and the residue was dried in vacuo. Then, another 20 mL of $CH_2Cl_2$ were added to the flask and this was heated at 60 °C for 1 h. Solvent was removed in vacuo. The addition of 20 mL of $CH_2Cl_2$, heating for 1 h at 60 °C, and removal of solvent steps were repeated once more. Then, 20 mL of $CH_2Cl_2$ were added to the residue. The insoluble material was collected by filtration, rinsed twice with 2 mL of $CH_2Cl_2$, and dried in vacuo to yield 0.908 g of a white solid. This was recrystallized by dissolving the solid in 15 mL of $CH_3NO_2$, filtering the solution, and adding 50 mL of diethyl ether to the filtrate. The white precipitate which formed was collected by filtration, rinsed with diethyl ether, and dried in vacuo. Yield: 0.775 g (83%). Anal. Calcd for $C_{68}H_{80}F_{12}O_{12}S_4SiRu_4$: C, 43.49; H, 4.29. Found: C, 43.38; H, 4.36.

**{[Cp*Ru($\eta$-C$_6$H$_5$)]$_4$Ge}$^{4+}$(OTf$^-$)$_4$ (5(Ge)$^{4+}$(OTf$^-$)$_4$).** A 100-mL round-bottomed flask equipped with a Teflon stopcock and magnetic stirring bar was charged with 0.095 g (0.25 mmol) of tetraphenylgermane and 0.600 g (1.18 mmol) of **1**. After adding 20 mL of $CH_2Cl_2$ to the flask, the stopcock was sealed and the flask was placed in an oil bath maintained at 60 °C behind a safety shield. After 1 h of stirring, solvent was removed and the residue was dried in vacuo. Then, 20 mL of $CH_2Cl_2$ were added to the flask and this was heated at 60 °C for 1 h. The reaction mixture was cooled, and the white precipitate which was observed was collected by filtration, rinsed with small amounts of $CH_2Cl_2$, and dried in vacuo. The solid was taken up in $CH_3NO_2$, and this solution was filtered. Diethyl ether was added to the filtrate to precipitate a white solid which was collected by filtration and dried in vacuo. Yield: 0.309 g (64%). Anal. Calcd for $C_{68}H_{80}F_{12}GeO_{12}S_4Ru_4$: C, 42.48; H, 4.19. Found: C, 42.61; H, 4.02.

**{[Cp*Ru($\eta$-C$_6$H$_5$)]$_4$Sn}$^{4+}$(OTf$^-$)$_4$ (5(Sn)$^{4+}$(OTf$^-$)$_4$).** A 100-mL round-bottomed flask equipped with a Teflon stopcock and magnetic stirring bar was charged with 0.107 g (0.251 mmol) of tetraphenylstannane and 0.600 g (1.18 mmol) of **1**. After adding 20 mL of $CH_2Cl_2$ to the flask, the solution was stirred for 1 h at room temperature. Solvent was removed in vacuo. Then, $CH_2Cl_2$ (20 mL) was added to the residue, and the reaction mixture was stirred for 1 h at room temperature. Solvent was removed in vacuo, and 20 mL of $CH_2Cl_2$ were added to the residue. The stopcock was sealed, the flask was placed in an oil bath maintained at 60 °C for 1 h, and then solvent was removed in vacuo. The residue was taken up in $CH_3NO_2$ (ca. 5–10 mL), and this was filtered. Addition of diethyl ether precipitated a white solid which was isolated by filtration, rinsed with ether, and dried in vacuo. Yield: 0.404 g (82%). Anal. Calcd for $C_{68}H_{80}F_{12}O_{12}S_4SnRu_4$: C, 41.49; H, 4.10. Found: C, 40.94; H, 4.15.

**{[Cp*Ru($\eta$-C$_6$H$_5$)]$_4$Pb}$^{4+}$(OTf$^-$)$_4$ (5(Pb)$^{4+}$(OTf$^-$)$_4$).** The complex {[Cp*Ru($\eta$-C$_6$H$_5$)]$_4$Pb}$^{4+}$(OTf$^-$)$_4$ was synthesized and isolated by a procedure identical with that for {[Cp*Ru($\eta$-C$_6$H$_5$)]$_4$Sn}$^{4+}$(OTf$^-$)$_4$ using 0.129 g (0.250 mmol) of tetraphenylplumbane and 0.600 g (1.18 mmol) of **1**. Yield: 0.499 g (97%). Anal. Calcd for $C_{68}H_{80}F_{12}O_{12}S_4PbRu_4$: C, 39.70; H, 3.92. Found: C, 39.33; H, 3.77.

**{[Cp*Ru($\eta$-C$_6$H$_5$)]$_3$(C$_6$H$_5$)Sb}$^{4+}$(OTf$^-$)$_4$.** A 25-mL flask was charged with 0.500 g (0.980 mmol) of tetraphenylantimonium bromide and 10 mL of acetonitrile. To the stirred solution were added 0.252 g of Ag-

$O_3SCF_3$ (0.980 mmol). After 10 min, the solution was filtered from precipitated AgBr, and 80 mL of diethyl ether were added to the filtrate to precipitate a white crystalline product. The product was collected by filtration, rinsed with diethyl ether, and dried in vacuo to yield 0.399 g (70%) of tetraphenylantimonium trifluoromethanesulfonate.

A 100-mL round-bottomed flask equipped with a Teflon stopcock and magnetic stirring bar was charged with 0.085 g (0.15 mmol) of tetraphenylantimonium trifluoromethanesulfonate and 0.400 g (0.787 mmol) of **1**. After adding 20 mL of $CH_2Cl_2$ to the flask, the stopcock was sealed and the flask was placed in an oil bath maintained at 60 °C behind a safety shield. After 1 h of stirring, solvent was removed and the residue was dried in vacuo. Then, another 20 mL of $CH_2Cl_2$ were added to the flask and this was heated for 1 h. Solvent was removed in vacuo. The addition of 20 mL of $CH_2Cl_2$, heating for 1 h, and removal of solvent steps were repeated twice more. Then, $CH_2Cl_2$ (20 mL) was added to the residue. The insoluble material was collected by filtration, rinsed twice with 2 mL of $CH_2Cl_2$, and dried in vacuo to yield 0.210 g of an off-white solid. This was dissolved in $CH_3NO_2$ (ca. 10 mL) and filtered. Diethyl ether was added to the filtrate to precipitate a white solid which was collected by filtration, rinsed with diethyl ether, and dried in vacuo. Yield: 0.185 g (71%). Anal. Calcd for $C_{58}H_{65}F_{12}O_{12}S_4SbRu_3$: C, 40.14; H, 3.78. Found: C, 39.78; H, 3.72.

**{[Cp*Ru($\eta$-$C_6H_5$)]$_4$B}$^{3+}$(OTf$^-$)$_3$.** A 100-mL round-bottomed flask equipped with a Teflon stopcock and magnetic stirring bar was charged with 0.050 g (0.15 mmol) of sodium tetraphenylborate and 0.305 g (0.600 mmol) of **1**. After 10 mL of $CH_2Cl_2$ were added to the flask, the stopcock was sealed and the flask was placed in an oil bath maintained at 60 °C behind a safety shield. After 1 h of stirring, solvent was removed and the residue was dried in vacuo. Then, another 10 mL of $CH_2Cl_2$ were added to the flask and this was heated at 60 °C for 1 h. Solvent was removed in vacuo. The addition of 10 mL of $CH_2Cl_2$, heating for 1 h, and removal of solvent steps were repeated twice more. Then, $CH_2Cl_2$ (10 mL) was added to the residue, and the insoluble material was collected by filtration, rinsed twice with 2 mL of $CH_2Cl_2$, and dried in vacuo to yield 0.280 g of a white solid. This was recrystallized by dissolving the filtrate in 5 mL of $CH_3NO_2$, filtering the solution, and adding 15 mL of diethyl ether to the filtrate. The white precipitate was collected by filtration, rinsed with diethyl ether, and dried in vacuo with warming (ca. 40 °C). Yield: 0.219 g (85%). Anal. Calcd for $C_{67}H_{80}BF_9O_9S_3Ru_4$: C, 47.02; H, 4.71. Found: C, 46.35; H, 4.34.

**{[Cp*Ru(*p*-$CH_3O$-$\eta$-$C_6H_4$-O)]$_6$C$_6$}$^{6+}$(OTf$^-$)$_6$.** A 100-mL round-bottomed flask equipped with a Teflon stopcock and magnetic stirring bar was charged with 0.100 g (0.123 mmol) of hexakis(*p*-methoxyphenoxy)benzene and 0.442 g (0.869 mmol) of **1**. After adding 20 mL of $CH_2Cl_2$ to the flask, the stopcock was sealed and the flask was placed in an oil bath maintained at 60 °C behind a safety shield. After 1 h of stirring, solvent was removed in vacuo, and 20 mL of $CH_2Cl_2$ were added to the residue. The reaction was heated at 60 °C for 1 h, and then solvent was removed in vacuo. After addition of $CH_2Cl_2$ (20 mL) and 1 h of heating at 60 °C, solvent was removed in vacuo. The residue was dissolved in 5 mL of $CH_3NO_2$ and filtered. THF (200 mL) was added to the filtrate, and then 100 mL of diethyl ether were added. The white precipitate which formed was collected by filtration, rinsed with ether, and dried in vacuo. Yield: 0.145 g (40%). Anal. Calcd for $C_{114}H_{132}F_{18}O_{30}S_6Ru_6$: C, 43.84; H, 4.26. Found: C, 43.95; H, 4.34.

**[(Cp*Ru)$_4$($\eta^6$,$\eta^6$,$\eta^6$,$\eta^6$-*p*-quaterphenyl)]$^{4+}$(OTf$^-$)$_4$.** A 100-mL round-bottomed flask equipped with a Teflon stopcock and magnetic stirring bar was charged with 0.114 g (0.372 mmol) of *p*-quaterphenyl and 0.900 g (1.77 mmol) of **1**. After 20 mL of $CH_2Cl_2$ were added to the flask, the stopcock was sealed and the flask was placed in an oil bath maintained at 60 °C behind a safety shield. After 1 h of stirring, solvent was removed in vacuo, and 20 mL of $CH_2Cl_2$ were added to the residue. The reaction was heated at 60 °C for 1 h, and then solvent was removed in vacuo. Then, 20 mL of $CH_2Cl_2$ were added. After 1 h of heating at 60 °C, the white precipitate which was observed was isolated by filtration and dried in vacuo to yield 0.630 g of a white solid. The solid was dissolved in 20 mL of $CH_3NO_2$, and this was filtered. Diethyl ether (80 mL) was added to the filtrate, and the white precipitate which formed was collected by filtration, rinsed with diethyl ether, and dried in vacuo. Yield: 0.575 g (84%). Anal. Calcd for $C_{68}H_{78}F_{12}O_{12}S_4Ru_4$: C, 44.20; H, 4.25. Found: C, 43.54; H, 4.15.

**[(Cp*Ru)$_6$($\eta^6$,$\eta^6$,$\eta^6$,$\eta^6$,$\eta^6$,$\eta^6$-*p*-sexiphenyl)]$^{6+}$(OTf$^-$)$_6$.** A 100-mL round-bottomed flask equipped with a Teflon stopcock and magnetic stirring bar was charged with 0.100 g (0.218 mmol) of *p*-sexiphenyl and 0.783 g (1.54 mmol) of **1**. After 20 mL of $CH_2Cl_2$ were added to the flask, the stopcock was sealed and the flask was placed in an oil bath maintained at 60 °C behind a safety shield. After 1 h of stirring, solvent was removed and the residue was dried in vacuo. Then, another 20 mL of $CH_2Cl_2$ were added to the flask and this was heated for 1 h. Solvent was removed in vacuo. The addition of 20 mL of $CH_2Cl_2$, heating for 1 h, and removal of solvent steps were repeated twice more. After addition of 20 mL of $CH_2Cl_2$ to the residue, the insoluble material was collected by filtration, rinsed twice with 2 mL of $CH_2Cl_2$, and dried in vacuo to yield 0.528 g of an off-white solid. This was dissolved in 35 mL of $CH_3NO_2$ and filtered. Slow addition of 35 mL of diethyl ether precipitated an off-white solid which was collected by filtration, rinsed three times with 10 mL portions of diethyl ether, and dried in vacuo with warming (ca. 40 °C). Yield: 0.357 g (59%). Anal. Calcd for $C_{102}H_{116}F_{18}O_{18}S_6Ru_6$: C, 44.22; H, 4.22. Found: C, 43.53; H, 4.22.

**X-ray Structural Analysis of {[Cp*Ru($\eta$-$C_6H_5$)]$_4$Ge}(OTf)$_4$.** Colorless blocks of {[Cp*Ru($\eta$-$C_6H_5$)]$_4$Ge}(OTf)$_4$ ($C_{68}H_{80}F_{12}GeO_{12}S_4Ru_4$) with approximate dimensions of 0.35 × 0.24 × 0.36 mm were grown by slow diffusion of gaseous diethyl ether into a nitromethane solution (monoclinic-*b*, $P2_1/c$ (No. 14); $a$ = 22.633 (3) Å, $b$ = 12.826 (2) Å, $c$ = 24.944 (3) Å, $\beta$ = 93.49 (1)°, from 25 reflections; $V$ = 7227.6 Å$^3$, $Z$ = 4, FW = 1922.62, $D_c$ = 1.767 g/cm$^3$, $\mu$(Mo) = 14.06 cm$^{-1}$). Data were collected on a Syntex R3 diffractometer at −100 °C (graphite monochromator, Mo K$\alpha$ radiation, 12 228 data collected with 4.0° ≤ 2$\theta$ ≤ 48.0°, maximum $h,k,l$ = 25,14,28, data octants = +−+, +−−, $\omega$ scan method, scan width = 1.00° $\omega$, scan speed = 2.00–14.60 °/min, typical half-height width = 0.29° $\omega$, 3 standards collected 66 times, and adjusted for a 6% decrease in intensity; 8.4% variation in azimuth scan; corrected for absorption (DIFABS), range of transmission factors = 0.52–0.76, 225 duplicates, 1.5% R-merge, 7990 unique reflections with $I \geq 3.0\,\sigma(I)$). The structure was solved by automated Patterson analysis (PHASE). The structure was refined by full-matrix least squares on $F$ using scattering factors from the International Tables for X-ray Crystallography, Vol. IV,[34] including anomalous terms for Ru, Ge, and S, and weights $\propto [\sigma^2(I) + 0.0009I^2]^{-1/2}$. With use of 910 parameters, all non-hydrogen atoms were refined anisotropically; all hydrogen atoms were fixed. The final $R$ was 0.035 ($R_w$ = 0.038) with the error of fit being 1.39 and maximum $\Delta/\sigma$ = 0.56. (Although the largest shift on the last cycle was relatively high for atom O2, the average shift/error was 0.07 and the refinement was deemed adequate.) The largest residual density was 1.23 e/Å$^3$ (near S1).

**X-ray Structural Analysis of {[Cp*Ru(*p*-$CH_3O$-$\eta$-$C_6H_4$-O)]$_6$C$_6$}(OTf)$_6$·6$CH_3NO_2$.** Colorless parallelopipeds of {[Cp*Ru(*p*-$CH_3O$-$\eta$-$C_6H_4$-O)]$_6$C$_6$}(OTf)$_6$·6$CH_3NO_2$ ($C_{120}H_{150}F_{18}N_6O_{42}S_6Ru_6$) with approximate dimensions of 0.34 × 0.15 × 0.50 mm were grown by slow diffusion of gaseous diethyl ether into a nitromethane solution (triclinic, $P\bar{1}$ (No. 2); $a$ = 15.784 (3) Å, $b$ = 16.539 (4) Å, $c$ = 17.817 (3) Å, $\alpha$ = 65.47 (2)°, $\beta$ = 61.82 (2)°, $\gamma$ = 63.86 (3)°, from 23 reflections; $V$ = 3552.2 Å$^3$, $Z$ = 1, FW = 3489.50, $D_c$ = 1.631 g/cm$^3$, $\mu$(Mo) = 7.95 cm$^{-1}$). Data were collected on an Enraf-Nonius CAD4 diffractometer at −70 °C (graphite monochromator, Mo K$\alpha$ radiation, 11582 data collected with 2.7° ≤ 2$\theta$ ≤ 48.0°, maximum $h,k,l$ = 18,18,20, data octants = +++, +−+, −++, −−+, $\omega$ scan method, scan width = 1.20–1.50° $\omega$, scan speed = 1.70–5.00 deg/min, typical half-height peak width = 0.16° $\omega$, 2 standards collected 79 times, 4% fluctuation, no absorption correction, 409 duplicates, 5.1% R-merge, 6485 unique reflections with $I \geq 3.0\sigma(I)$). The structure was solved by automated Patterson analysis (PHASE). The asymmetric unit consists of half the hexacation on an inversion center, three triflate anions, and at least three $CH_3NO_2$ solvate molecules. The structure was refined by full-matrix least squares on $F$ using scattering factors from the International Tables for X-ray Crystallography, Vol. IV,[34] including anomalous terms for Ru and S, and weight $\propto [\sigma^2(I) + 0.0009I^2]^{-1/2}$. With use of 905 parameters, Ru, S, F, O, and N were refined anisotropically; F atoms on disordered triflates were refined isotropically; all hydrogen atoms were fixed. The final $R$ was 0.058 ($R_w$ = 0.054) with the error of fit being 1.59 and maximum $\Delta/\sigma$ = 0.30. One of the triflate anions was disordered and was modeled with a translational 0.8/0.2 occupancy of indicated partial occupancies of 0.5 and 0.7. A fourth potential solvent site was indicated on the final difference Fourier map and was not included. The largest residual density was 1.05 e/Å$^3$ near an inversion center (possibly solvent).

**X-ray Structural Analysis of [(Cp*Ru)$_4$($\eta^6$,$\eta^6$,$\eta^6$,$\eta^6$-*p*-quaterphenyl)](OTf)$_4$.** Colorless parallelopipeds of [(Cp*Ru)$_4$($\eta^6$,$\eta^6$,$\eta^6$,$\eta^6$-*p*-quaterphenyl)](OTf)$_4$ ($C_{68}H_{78}F_{12}O_{12}S_4Ru_4$) with approximate dimensions of 0.23 × 0.21 × 0.40 mm were grown by slow diffusion of gaseous diethyl ether into a nitromethane solution (triclinic, $P\bar{1}$ (No. 2); $a$ = 12.897 (3) Å, $b$ = 13.630 (2) Å, $c$ = 11.906 (2) Å, $\alpha$ = 108.31 (1)°, $\beta$ = 107.39 (2)°, $\gamma$ = 100.38 (1)°, from 25 reflections; $V$ = 1807.3 Å$^3$, $Z$ = 1, FW = 1848.02, $D_c$ = 1.698 g/cm$^3$ $\mu$(Mo) = 10.02 cm$^{-1}$). Data were collected on an Enraf-Nonius CAD4 diffractometer at −70 °C (graphite monochromator, Mo K$\alpha$ radiation, 11 582 data collected with 3.3° ≤ 2$\theta$ ≤ 55.0°, maximum $h,k,l$ = 16,17,15, data octants = +++, +−+, −++, −−+, $\omega$ scan method, scan width = 1.20–1.70° $\omega$, scan speed = 1.50–5.00

(34) *International Tables for X-ray Crystallography*; Kynoch Press: Birmingham, England, 1974; Vol. 4.

deg/min, typical half-height peak width = 0.14° $\omega$, 3 standards collected 41 times, 3% fluctuation, 1% variation in azimuth scan, no absorption correction, 398 duplicates, 2.0% R-merge, 5930 unique reflections with $I \geq 3.0\sigma(I)$). The structure was solved by automated Patterson analysis (PHASE). The asymmetric unit consists of half a tetracation lying on an inversion center together with two triflate anions. The structure was refined by full-matrix least squares on $F$ using scattering factors from the International Tables for X-ray Crystallography, Vol. IV,[34] including anomalous terms for Ru and S, and weights $\propto [\sigma^2(I) + 0.0009I^2]^{-1/2}$. With use of 451 parameters, C, Ru, S, F, and O were refined anisotropically; all hydrogen atoms were fixed. The final $R$ was 0.035 ($R_w$ = 0.038) with the error of fit being 1.40 and maximum $\Delta/\sigma$ = 0.13. The largest residual density was 1.52 e/Å$^3$ near Ru1.

**Acknowledgment.** We thank Ronald J. Davis and William Marshall for capable technical assistance.

**Registry No. 1**, 113860-02-9; **2**, 113860-07-4; **3a**, 99617-73-9; **3b**, 118397-71-0; **3c**, 118397-72-1; **3d**, 118397-73-2; **3e**, 118397-75-4; **3f**, 118397-77-6; *syn*-**4**, 118397-89-0; *anti*-**4**, 118456-61-4; **5** $(C)^{4+}(OTf^-)_4$, 118397-93-6; **5** $(Si)^{4+}(OTf^-)_4$, 118397-95-8; **5** $(Ge)^{4+}(OTf^-)_4$, 118417-84-8; **5** $(Sn)^{4+}(OTf^-)_4$, 118417-86-0; **5** $(Pb)^{4+}(OTf^-)_4$, 118417-88-2; $Cp^*RuCl_2$, 92390-47-1; $AgO_3SCF_3$, 2923-28-6; $[(Cp^*Ru)_2(\eta^6,\eta^6\text{-}[2_2]\text{-}1,4\text{-cyclophane})]^{2+}(OTf^-)_2$, 118397-79-8; $[(Cp^*Co)(\eta^6\text{-}[2_2]\text{-}1,4\text{-cyclophane})]^{2+}(OTf^-)_2$, 118397-80-1; $Cp^*CoCl_2$, 118397-98-1; $[(Cp^*Ru)(\eta^6,\eta^6\text{-}[2_2]\text{-}1,4\text{-cyclophane})CoCp^*]^{3+}(OTf^-)_3$, 118397-82-3; $[(\eta^6\text{-}[2_2]\text{-}1,4\text{-cyclophane})_2Ru]^{2+}(OTf^-)_2$, 118397-83-4; $\{[Cp^*Ru(\eta^6,\eta^6\text{-}[2_2]\text{-}1,4\text{-cyclophane})]_2Ru\}^{4+}(OTf^-)_4$, 118397-85-6; $[Cp^*Ru(\eta^6\text{-triptycene})]^+OTf^-$, 118397-87-8; $[(Cp^*Ru)_3(\eta^6,\eta^6,\eta^6\text{-triptycene})]^{3+}(OTf^-)_3$, 118397-91-4; $\{[Cp^*Ru(\eta\text{-}C_6H_5)]_3(C_6H_5)Sb\}^{4+}(OTf^-)_4$, 118417-92-8; $\{[Cp^*Ru(\eta\text{-}C_6H_5)]_4B\}^{3+}(OTf^-)_3$, 118397-97-0; $\{[Cp^*Ru(p\text{-}CH_3O\text{-}\eta\text{-}C_6H_4\text{-}O)]_6C_6\}^{6+}(OTf^-)_6$, 118681-49-5; $[(Cp^*Ru)_4(\eta^6,\eta^6,\eta^6,\eta^6\text{-}p\text{-quaterphenyl})]^{4+}(OTf^-)_4$, 118417-90-6; $[(Cp^*Ru)_6(\eta^6,\eta^6,\eta^6,\eta^6,\eta^6,\eta^6\text{-}p\text{-sexiphenyl})]^{6+}(OTf^-)_6$, 118681-50-8; $(\eta^4\text{-}1,3\text{-cyclohexadiene})Ru(\eta^6\text{-}[2_2]\text{-}1,4\text{-cyclophane})$, 90590-75-3; trifluoromethanesulfonic acid, 1493-13-6; tetraphenylantimonium bromide, 21450-52-2; tetraphenylantimonium trifluoromethanesulfonate, 104316-49-6; sodium tetraphenylborate, 143-66-8.

**Supplementary Material Available:** X-ray data (tables of atomic positional parameters, thermal parameters, H atom fixed fractional coordinates, intra- and intermolecular non-bonding distances, bond distances and bond angles involving H atoms, bond distances and bond angles for the $O_3SCF_3$ anions and $CH_3NO_2$ solvates) (19 pages); observed and calculated structure factors for the complexes $\{[Cp^*Ru(\eta\text{-}C_6H_5)]_4Ge\}^{4+}(OTf^-)_4$, $\{[Cp^*Ru(p\text{-}CH_3O\text{-}\eta\text{-}C_6H_4\text{-}O)]_6C_6\}(OTf)_6\cdot 6CH_3NO_2$, and $[(Cp^*Ru)_4(\eta^6,\eta^6,\eta^6,\eta^6\text{-}p\text{-quaterphenyl})]^{4+}(OTf^-)_4$ (37 pages). Ordering information is given on any current masthead page.

# Electrostatic Structural Enforcement in Low-Dimensional Solids: Synthesis, Structure, and Electronic Properties of Polycationic Ruthenium Complexes with Polycyanoanions

**Michael D. Ward,* Paul J. Fagan,* Joseph C. Calabrese, and David C. Johnson†**

*Contribution No. 4748 from the Central Research and Development Department, Experimental Station 328, E. I. du Pont de Nemours & Co., Wilmington, Delaware 19880-0328.*
*Received May 24, 1988*

**Abstract:** New low-dimensional solids prepared from polycyanoanions and $Cp^*Ru(\eta\text{-}C_6Me_6)^+$ ($D^+$: $Cp^* = C_5Me_5$), $(Cp^*Ru)_2(\eta^6,\eta^6\text{-}[2_2](1,4)\text{cyclophane})^{2+}$ ($D^+\text{-}D^+$), and $[Cp^*Ru(\eta\text{-}C_6H_5)]_4E^{4+}$ ($(D^+)_4E$: E = C, Si) demonstrate that the polycations structurally enforce the solid-state structure, with anions adopting stacking motifs that reflect the spatial distribution of charge in the polycations. The mononuclear $D^+$ cation forms dimorphs with $TCNQ^-$ (TCNQ = tetracyanoquinodimethane) with the empirical formula $[D^+][TCNQ^-]$. One of these (**1**) crystallizes with 1-D mixed stacks of cations and $TCNQ^-$ anions, whereas the other phase (**2**) possesses discrete $D^+A^-A^-D^+$ units with a $(TCNQ)_2^{2-}$ $\pi$-dimer situated between two cations. Segregated stacking motifs that are rather common for the $TCNQ^-$ anion are not observed. However, structural enforcement provided by the ruthenium centers in the rod-shaped $D^+\text{-}D^+$ dication affords different structural motifs in $[D^+\text{-}D^+][(TCNQ)_x^{2-}]$ (**3**, $x$ = 2; 4, $x$ = 4). Nonconducting **3**, prepared by electrochemical reduction of TCNQ in the presence of the dication at −0.1 V (vs. Ag/AgCl), possesses mixed stack linear chains with alternating cations and $(TCNQ)_2^{2-}$ $\pi$-dimers, i.e., a $...D^+\text{-}D^+A^-A^-D^+\text{-}D^+A^-A^-...$ motif. In contrast, **4** crystallizes as conductive black parallelepipeds by slow electrochemical reduction of TCNQ in the presence of the dication at potentials more positive than $E^\circ_{(TCNQ/TCNQ^-)}$ and possesses two crystallographically unique TCNQ stacks parallel to the long axes of the cations. The distance between cationic Ru sites in $D^+\text{-}D^+$ accommodates four TCNQ molecules with an overall (2−) charge; the resultant mixed valent $\rho$ = 0.5 stacks afford a room temperature conductivity of 0.2 $\Omega^{-1}$ cm$^{-1}$. The solid-state structures of the nonconducting charge-transfer salts $[D^+\text{-}D^+]\{C_3[C(CN)_2]_3^-\}_2$ (**5**) and $[(D^+)_4E]\{C_3[C(CN)_2]_3^-\}_4\cdot x MeNO_2$ (**6**, E = C, $x$ = 6; **7**, E = Si, $x$ = 4) exhibit linear chains of $C_3[C(CN)_2]_3^-$ anions. For **5**, the anion stacking axis is parallel to the dications, whereas **6** and **7** possess mutually orthogonal anion stacks that are aligned parallel to the orthogonal axes defined by two pairs of cationic centers in the tetracations. Magnetic susceptibility and EPR data for **4** indicate the presence of an energetically accessible triplet state 0.08 eV above the singlet ground state with zero field splitting constants $|D|$ = 66 G and $|E|$ = 11 G. The EPR spectra of **5**–**7** also indicate the presence of energetically accessible triplet species. However, magnetic susceptibility measurements indicate strong antiferromagnetic coupling of the anion spins, suggesting that these triplet species are due to impurities or crystalline defects.

The design and synthesis of low-dimensional molecular solids[1] with desirable electronic properties requires understanding of the factors that affect the formation of different structural phases, coupled with elucidation of the structure–function relationships in these materials. Whereas numerous organic charge transfer solids have been reported,[2] we have been investigating new materials derived from organometallic reagents with emphasis on

* Author to whom correspondence should be addressed.
† Present Address: Department of Chemistry, University of Oregon, Eugene, OR 97403.

(1) *Extended Linear Chain Compounds*; Miller, J. S., Ed.; Plenum Press: New York, 1981–83; Vol. 1–3.
(2) Herbstein, F. H. *Perspectives in Structural Chemistry*; Dunitz, J. D., Ibers, J. A.; Eds.; John Wiley and Sons: New York, 1971; Vol. IV, p 166.

0002-7863/89/1511-1719$01.50/0 